THE UNIVERSITY OF CALGARY

DYNAMIC RESPONSE OF SPHERICAL SHELLS UNDER LARGE DEFORMATIONS

by

PAK-KIN CHAN

A THESIS

SUBMITTED TO THE FACULTY OF GRADUATE STUDIES

IN PARTIAL FULFILLMENT OF THE REQUIREMENT FOR THE

DEGREE OF MASTER OF SCIENCE IN ENGINEERING

DEPARTMENT OF MECHANICAL ENGINEERING

CALGARY, ALBERTA

MAY, 1986

ISBN Ø-315-32691-3

THE UNIVERSITY OF CALGARY

FACULTY OF GRADUATE STUDIES

The undersigned certify that they have read, and recommend to the Faculty of Graduate Studies for acceptance, a thesis entitled "Dynamic Response of Spherical Shells Under Large Deformations", submitted by Pak-Kin Chan in partial fulfillment of the requirements for the degree of Master of Science in Engineering.

Dr. S.A. Lukasiewicz (Supervisor)
Department of Mechanical Engineering

Dr. P.G. Glockner
Department of Mechanical Engineering

Dr. M.C. Singh
Department of Mechanical Engineering

Dr. R.B. Streets
Department of Electrical Engineering

May 1986

ABSTRACT

The subject of the thesis is to study the nonlinear dynamic responses of vibrating spherical shells, under a concentrated load applied at the apex. Effects of concentrated loading on shells with various thicknesses, radii of curvatures, and geometrical parameters are examined. A number of particular cases of shells with simple geometry are treated as applications. Using Pogorelov's geometrical approach and assumptions, the governing equations of motion for vibrating spherical shells are derived from Hamilton's variational principle. Free vibrations, forced vibrations, and the linearized governing equation of motion of the shell are analyzed using Runge-Kutta and Adam-Moulton numerical methods. The nonlinear softening behaviour is obtained from the relationship of load and deflection and from the forced response curves with an excitation of constant amplitude at varying frequency. The theoretical model correctly describes the nonlinear behaviour of the shell and the results of analysis obtained are confirmed by two numerical methods.

ACKNOWLEDGEMENTS

The author is grateful for the guidance and support of Dr. S.A. Lukasiewicz under whose supervision the investigation was carried out.

Acknowledgements are due to the staff of the Department of Mechanical Engineering for their fruitful suggestions and inspiring discussions. Also, thanks are due to the author's various colleagues for their advice and cooperation. The helpful suggestions and assistance of Dr. R.C. Huntsinger of the Department of Computer Science and Dr. R.B. Streets of the Department of Electrical Engineering are sincerely appreciated. Thanks are extended to Miss Nancy Richards and Miss Wendy Penner for their help in typing the manuscript.

The financial assistance provided by the Department of Mechanical Engineering of the University of Calgary, and the National Science and Engineering Research Council of Canada is gratefully acknowledged.

TABLE OF CONTENTS

LIST OF TABLES

LIST OF FIGURES

NOMENCLATURE

LETTERS

A, A_1, A_2	Numerical constants
a	Base radius of spherical shells
B, B'	Numerical constants
c	Constant coefficient
D	Bending stiffness; Numerical constant
E	Young's modulus; Numerical constant
f	Half of the total deflection from the apex
f_s	Static deflection
f_o	Dimensionless static deflection
F	Numerical constant
G	Gaussian curvature; Numerical constant
g	Gravitational constant
H	Mean curvature; Depth of the shell
h	Thickness
I	Total energy functional
K	Numerical constant
K'	Numerical constant
k_{eq}	Equivalent stiffness of the shell
$\bar{k}$	Curvature vector
L	Numerical constant; Lagrangian
M, M'	Numerical constant; Mass at the apex
M_o	Arbitrary mass
N	Number of data point
$\vec{n}$	Normal vector
P	Applied concentrated force
P_m	Applied static force
$\vec{p}$	Principle normal
P_{cr}	Critical load
p	Input variable

R	Radius of curvature
R_1, R_2	Principal radii of curvature
r	Radial coordinate
$\vec{r}$	Position vector
$S(f)$	Complex function in frequency domain
$s(t)$	Real function in time domain
T	Total kinetic energy
t	Time; tangential vector
u	Total strain energy
$\vec{u}, \vec{v}, \vec{w}$	unit vectors
V	External work done by applied force
W	Vertical deflection from the apex
W_{max}	Maximum depth of depression
x	Vertical apex deflection; Cartesian coordinate
$\dot{x}$	Velocity
$\ddot{x}$	Acceleration
y	Dimensionless vertical apex deflection; Cartesian coordinate
z	Cartesian coordinate

Greek Letters

α	Curvilinear coordinates; dynamic load factor
β	Curvilinear coordinates
δ	Variational operator
ε_y	Yield strain
κ	Curvature
κ_n	Normal curvature
κ_t	Tangential curvature
$\Delta\kappa_1$	Change of curvature of the middle surface
κ_1	Curvature of the original surface
κ_1'	Curvature of the surface after deformation

ϕ	Meridianal angle
ρ	Polar angle
π	Total potential energy; constant
γ	Unit mass of the shell
σ_{pl}	Yield strength of the shell
θ	Circumferential angle; angle between the coordinate curves
λ	Geometrical parameters of central displacements
ν	Poisson's ratio; real component of the root of the characteristic equation

Abbreviations

CDC	Control Data Corporation
CSSL-IV	Continuous System Simulation Language - Version IV
DFT	Discrete Fourier Transform
FFT	Fast Fourier Transform
IMSL	International Mathematical and Statistical Libraries
NOS	Network Operating System
IGP	Interactive Graphic Package

CHAPTER 1

INTRODUCTION

1.1 INTRODUCTION

A study of very large deflections and dynamic response of spherical thin shells under a concentrated load applied at the apex is the subject of the thesis. The effects of wall thicknesses, radii of curvatures, and the load magnitudes on the dynamic response of the shell will be investigated. The governing equations of motion describing the nonlinear behaviour of the shell are derived, and the deflection response and frequency response are analyzed.

In this thesis, a non-classical geometrical method of analysis based on Pogorelov's nonlinear theory of shells [1.1]* is used. The theory can be applied to very large deflections of the order of 100 times the thickness of the shell such that

$$W \leqq 100 \cdot h$$

where W is the deflection of the shell from the apex, and h is the thickness of the shell. For the thin shells being considered here, the ratio of thickness to the radius of curvature is

$$\frac{h}{R} \leqq \frac{1}{100}.$$

where R is the radius of curvature of the shell. There is no restriction imposed on the supporting conditions or on the slope of the

---

* Numbers in square brackets are listed under References.

shell. The clamped edge condition is used throughout the thesis. As a result, the analysis is applicable to deep and shallow spherical shells. The governing equations of motion for the vibrating spherical shells derived from Hamilton's variational principle are obtained in terms of the only unknown vertical apex deflection. It is assumed that the shell deflects symmetrically with respect to the axis of revolution. Therefore, the resulting equations of motion can be considered as a dynamic problem of one degree-of-freedom. Furthermore, the equations of static equilibrium are also obtained from the principle of Stationary Total Potential Energy. The principle states that the total potential energy assumes an extremum position for a system to be in static equilibrium. The first variation of the total potential energy must be zero.

The governing equations of motion obtained are nonlinear differential equations and are treated as an initial value problem. In order to find numerical solutions for the unknown vertical displacement and its derivatives with respect to time, the initial value problem is solved by two different numerical methods, using the Runge-Kutta method and the Adam-Moulton predictor corrector method. Both free vibrations and forced vibrations of the shell are investigated. As a result, the deflection responses and phase plane diagrams are obtained for various wall thicknesses, radii of curvatures and applied load magnitudes. Moreover, the technique of fast Fourier transform (FFT) is used to analyze the frequency response. The frequency of vibration of the system is identified in the results. The numerical work was carried out on the Honeywell Multics and CDC Cyber computer system.

A general review of the historical background will be given in the next section of this chapter. The review concerning the action of concentrated load on the spherical shells is discussed. A comprehensive bibliography of major references on the subject of large deflection and nonlinear behaviour of the shell is also provided in the survey. Finally, the studies of the stability and dynamic responses of the shell under uniform pressure are given. It is hoped that the literature review provides insights into the current study of spherical shells subjected to the applied concentrated force.

1.2 HISTORICAL AND LITERATURE REVIEW

Fundamental theories concerning the vibrations and deformations and the equations of equilibrium of thin shells were first investigated by Euler, Lamb, Rayleigh, and Love [1.2]. The motivation was based on a desire to search for the basic geometrical parameters underlying the design of bells which were being constructed for various cathedrals in the world. The first treatment of dynamic theory of shells attempted to deduce the mode of vibration of bells. Prior to the discovery of the general equations of Elasticity, the earliest work on the subject, as mentioned by Love [1.2, p. 5 and p. 28], was due to Euler (1766), who proposed a model of a bell subdivided into thin annuli which behaved like a curved bar and formulated a theory of resistance of a curved bar due to bending. Later on, James Bernoulli assumed a shell consisting of double sheets of curved bars, being placed at right angle parallels and meridians. He reduced the shell to a plate and developed the first equation of vibration, which is now known to be incorrect.

The formulation of curved plates and shells from the viewpoint of the general equations of Elasticity was first given by Aron (1874). He defined the geometry of the middle surface by two parameters and derived the potential energy for a strained shell. Mathieu (1883) mentioned that the modes of vibration of a shell are not characterized by normal and tangential displacements, and he developed the equations of motion by retaining only the terms dependent on the stretching of middle surface in the equation of potential energy obtained previously by Aron. Afterward, the formulation of the extensional vibrations of closed spherical shells was first presented by Lamb.

Rayleigh (1882) proposed a different theory with the assumption that the middle surface of a vibrating shell remains unstretched and established fundamental theories for the inextensional vibrations of thin shells. Love (1888) first derived the basic equations for the free vibrations and deformations of thin elastic shells. Fundamental theories of bending and extensional vibrations of the shell, together with the assumptions, were formulated and are now referred to as Love's first approximation. It was shown in the problem of vibrating shells that the extensional strain was confined to a narrow region close to the edge of the shell, while the remaining part of the shell vibrated according to the inextensional vibrations presented by Rayleigh. Since then, the investigation of vibrations of shells received little attention until the second decade of the twentieth century.

1.2.1 REVIEW OF SPHERICAL SHELLS UNDER CONCENTRATED LOADS

The problem of a concentrated load applied at the apex of spherical shells has been of increasing interest during the last twenty years. Many papers concerned with solutions for stresses and displacements due to a normal force, a tangential force, and a bending moment were published based on the linear theory of thin shells. This area has been explored very thoroughly.

Reissner [1.3] obtained the solutions for a normal concentrated force at the apex of shallow spherical shells, using the classical theory of shallow shells. Later on, Flügge and Conrad [1.4], and Kalnins and Naghdi [1.5] also examined similar problems.

Furthermore, Leckie [1.6] determined the bending stresses and displacements in a spherical shell subjected to concentrated loads using the simplified theory developed by Havers, and found an asymptotic solution in spherical polar coordinates. Lukasiewicz [1.7] analyzed similar problems and presented a closed form solution using the modified Fourier integrals for the stresses and displacements in the shell. The results were similar to those of Reissner and Flügge.

In view of Leckie's results, several characteristics of the spherical shells under concentrated loads at the apex were observed.

1) The concentrated loads on the surface of the shell usually produce a concentration of stresses at the point of the application of the load. However, it is assumed that this point is very small and that the stresses and displacements in the local area are negligible.

2) The stresses caused by concentrated loads can be considered separately from those resulting from the influence of boundary conditions.

3) The bending effects are highly localized in the spherical shells. The influence of boundary conditions will not affect the state of stresses and displacements near the loading point if this point is far from the edge.

1.2.2 REVIEW OF LARGE DEFLECTIONS OF SPHERICAL SHELLS UNDER CONCENTRATED LOADS

Problems concerned with the large deflections and non-linear behaviour of spherical shells under concentrated loads have not been completely solved, such as nonlinear vibrations and elasto-plastic behaviour of shells. The problem has been the subject of many papers. Biezeno [1.8] was the first one to investigate a freely supported shallow spherical shell subjected to a concentrated load at the apex. He considered the problem as a nonlinear one and assumed the central displacement of the shell as an approximate expression of two arbitrary constants. The expression was then substituted into the nonlinear differential equations in terms of the arbitrary constants. The constant could be determined by equating the central displacements and edge rotations of the initial assumed solutions. For shallow shell, the geometrical parameter for the central displacements λ is proportional to the ratio of the depth to thickness of the shell.

$$\lambda^2 = 2\ [3(1-\nu^2)]^{\frac{1}{4}} \left(\frac{H}{h} \right)^{\frac{1}{2}} . \tag{1.1}$$

where H is the depth of the shell and ν is Poisson's ratio. Biezeno found that, for $\lambda > 4$, the buckling load increases with λ.

Chien and Hu [1.9] considered a spherical shell with a ring load around the apex using a potential energy method. Two simultaneous nonlinear differential equations were found and a one-term expression was assumed for the vertical displacement. The results for the case of zero ring radius were in good agreement with the analytical results by Biezeno.

Ashwell [1.10] presented the following assumption from his experimental observations in a point-loaded shell.

1) When the inward concentrated load is applied to the apex of a thin shell, a dimple of reverse curvature is formed at the apex, with the boundary radius increasing with the load.

2) The membrane strains of inverted shells are equal to those of the original shells. Hence, the same linear differential equations can be used for the inverted shells.

He then solved the nonlinear large deflection problem by assuming two linear small deflection solutions for the point-loaded shell, one for the inverted dimple region and the other for the external undistorted region. The equilibrium of forces and the conditions of continuity of deflections were satisfied at the boundary between the two regions. With increasing values of the applied load and allowing the boundary radius to vary, the solutions were obtained, and the analytical results were compared and agreed well with those of Biezeno and his experiments.

Archer [1.11] studied the freely supported shell using Reissner's nonlinear equations and finite difference methods and reduced the problem to a set of three algebraic equations. His results were in good agreement with those of Biezeno, Chien, and Ashwell up to a point at $\lambda = 5$. However, the results were significantly lower for larger values of λ at which the procedure failed to converge. A local maximum had been reached before the true maximum, which would be the critical load for axisymmetric snap buckling. The asymmetric deformation could occur at the local maximum before symmetric snap buckling. The results were confirmed by Fitch [1.12].

Similar problems of freely supported spherical shells were also investigated by Mescall [1.13] using Reissner's formulation and a Newton-Raphson method. He confirmed Archer's results for values of $\lambda \leqq 6$. For larger values of λ, his results continued to rise and the true maximum load did occur beyond the point where Archer's procedure failed to converge. His results were in reasonable agreement with Ashwell's calculations and experimental critical loads predicted by Evan-Iwanowski [1.14] for $\lambda < 10$.

Moreover, Bushnell [1.15] analyzed the bifurcation phenomena of the shell, performed the eigenvalue calculations to predict bifurcation, but provided no information for the stability of the bifurcations. He obtained results similar to Mescall's and found that the freely supported shell deformed symmetrically for $\lambda < 9.5$. Bifurcation into two circumferential waves and symmetric collapse occurred almost at the same time in the range of $9.5 < \lambda < 10.3$. He predicted that the postbuckling behaviour was stable, and there was no sharp transition from symmetric to asymmetric mode of deformation. However, no test data were presented for $\lambda > 10.3$.

Extensive experimental investigations with analytical results of freely supported shells were also conducted by Evan-Iwanowski [1.14]. He observed the shells to deform and buckle symmetrically for $\lambda \leqq 10.2$. However, for large values of λ, the shell deformed asymmetrically, and the deformation pattern became asymmetric as predicted by Bushnell. The postbuckling loads were also presented for values of $\lambda \geqq 10.7$ at which an asymmetric mode of deformation changed into another asymmetric mode.

In additon, Bushnell's results for the clamped spherical shells were similar to those of freely supported shells except for the buckling characteristic. From the eignevalue calcuations, he found bifurcation occurred for $\lambda > 10.3$, but there was no bifurcation into three waves until $\lambda = 12.5$. For larger values of λ, bifurcation into four waves occurred first before the occurrance of bifurcation into three waves with increasing load. For values of $\lambda \geqq 15.6$, bifurcation into three, four, and five waves was found, but no symmetric snap buckling was predicted. The theoretical predictions of the clamped spherical shells were in good agreement with the experimental and theoretical investigation by Penning and Thurston [1.16].

Penning and Thurston obtained no buckling from symmetric modes calculations for the clamped shallow spherical shell, but the calculations indicated a minimum in the stability determinant at the points corresponding to a flattening in the load deflection curve. They also performed eigenvalue calculations to predict bifurcation into an aysmmetric mode. The existence of such a bifurcation could not be confirmed, but the calculations showed that high circumferential stresses concentrated at the edge of the dimple and that the occurrance of an asymmetric shape was likely. Furthermore, Penning [1.17-1.18] measured the step displacement and the change in shape of the shell under a constant applied force. He observed that a circular dimple under the load developed into three, four, and five-node waves in sequence. The development of the initial dimple, associated with a flattening of the load deflection curve and the gradual transition between the node waves, showed a gentle rise of the curve followed by a steepening. After the jump for $\lambda \geqq 12.0$, the shell retained its load carrying capacity. If the shell was unloaded, it would snap back to its earlier shape at a lower load. He proposed that the gradual transition between the node waves was a function of the amount of asymmetry in the initial shape and that the early portions of the curve identified the load character of the displacements.

Fitch [1.12] studied the buckling and initial post buckling behaviour of the clamped shallow spherical shells using Koiter's stability analysis. He predicted bifurcation into asymmetric snap buckling for $9.2 < \lambda < 10.0$. He obtained that, for values of $\lambda < 7.8$, there was no bifurcation or symmetric snap buckling. For $7.8 < \lambda < 9.2$, a local maximum on the load deflection occurred, and for $\lambda > 9.2$, asymmetric bifurcation started before symmetric snap buckling. As values of λ increased, the critical load approached a limiting value of 10.8 which could be considered as the buckling load. For such λ, the deformation was found in the region near the apex.

Among all the significant researchers, Pogorelov [1.1] presented a different approach. He proposed a geometrical method to obtain a nonlinear load deflection relation. When the spherical shell is subjected to an inward concentrated load, the shell deflects elastically in isometric transformation, having a circular dimple of reverse curvature, formed and spread concentrically from the load at the apex. The most simple form of isometric transformation of a surface is similar to a symmetric deflection pattern as a mirror reflection of the initial surface -- the so-called inverted dimple region. The shape of the deformed surface is predicted from the Gaussian curvature of the isometrically transformed surface which is equal to the curvature of the initial surface. Therefore, the curvature of the deformed surface must be equal to the reverse curvature of the initial surface. Pogorelov divided the shell into three regions: I) the central region of the dimple; II) the ridge region including the inner strip and the outer strip; and III) the outer undistorted region. He then calculated the total strain energy for each of these regions and used a variational principle to minimize the total strain energy with respect to the vertical deflection. A relationship between the load and deflection was obtained, and the results were compared with Penning's experimental results for clamped shallow spherical shells

[1.7, 1.18]. The numerical results for the initial part of the load deflection curve were in good agreement with those calculated from the small deflection theory and those of experimental results for the small values of load. For relatively thin shell, asymmetric buckling mode appeared. Pogorelov's results deviated considerably from Penning's results and did not predict the buckling load.

1.2.3 REVIEW OF STABILITY AND DYNAMIC RESPONSE OF SPHERICAL SHELLS UNDER UNIFORM PRESSURE

The problem of stability and buckling of shallow spherical shells, clamped along its boundary and subjected to a uniform pressure, has been a popular topic for many researchers in the 1930's. There were two separate approaches adopted in the analysis of deformations of the shell. The stability analysis concerned with static deflections and buckling of the shell is used to develop and analyze the equations of equilibrium and the buckling loads. As an alternative, the dynamic analysis interested in the vibrations, modes of deformation, deflection response, and natural frequencies of the shell is adopted to derive and analyze the equations of motion using the related energy principles.

In the classical work of the stability of spherical shells, von Kármán and Tsien [1.19] demonstrated the importance of nonlinear effects in the snap-through stability analysis of shells. They included nonlinear finite displacements in their calculations and found that the stiffness of the shell decreased with increasing displacements.

Budiansky [1.20], Thurston [1.21] and Weinitschke [1.22] obtained similar critical loads from the nonlinear shallow shell equations under the assumptions that the deformed shape is symmetric. The theoretical critical loads found have been a factor of two or more above the experimental values and are referred to as the symmetrical buckling loads.

Thereafter, Parmerter [1.23] presented a new set of experimental data showing that these data were much higher than previous results and suggested the influence of asymmetric modes in the theoretical calculations could lower the theoretical buckling values. Huang [1.24] published an accurate theoretical analysis of asymmetric modes that was in good agreement with the new experiment conducted by Parmerter. The first asymmetric mode of Huang is now referred to as the asymmetric bifurcation load or asymmetric buckling load. Theoretical results have been confirmed by Weinitschke [1.25] and supported by experiments performed by Evan-Iwanowski [1.26]. Recently, the stability of shells has been studied by Gol'denveizer [1.27] using a geometrical theory to investigate the effects of bending and deformations in the middle surface. The results were compared with those obtained from the geometrical method by Pogorelov [1.1].

On the other hand, Federfhofer [1.28, 1.29] analyzed the linear vibrations of shallow spherical shells from the viewpoint of dynamic analysis. He derived a system of differential equations of motions for spherical shells and assumed an approximate solution of Legendre functions for the free axisymmetric vibration equations; but there was no successful effort in obtaining the exact solution.

Reissner [1.30] studied the transverse and longitudinal vibrations problem of similar shells and obtained an approximate solution for the lowest transverse frequency. In 1955, he neglected the longitudinal inertia and modified the frequency response with an exact solution. His work has been taken as a base for future investigation and comparison in shell vibrations.

Extensive theoretical investigations in vibrations of shallow spherical shells and exact solutions to the linear equations of motion have been developed by Naghdi [1.31]. The equations of motion consisted of two independent equations in terms of a transverse displacement and stress function, from the theory of shallow shells. Assuming the longitudinal inertia was negligibly small in the axisymmetric vibration, Naghdi and Kalnins [1.32] provided exact solutions to the equations of motion. The results were in good agreement with Reissner's. Later on, Kalnins [1.33] classified the vibration problems for spherical shells using an energy approach. The following results were summarized from his studies:

1) It was shown that the longitudinal vibrations were independent of thickness but that the transverse vibrations depended on the ratio of the thickness to radius of curvature.

2) From the energy approach, the transverse vibrations were included in the bending energy and longitudinal vibrations in the extensional energy in general.

3) The effect of longitudinal inertia was small in shallow shells but was considerable in nonshallow shells.

The nonlinear vibrations and snap-through buckling of shallow spherical shells under transient loads were also investigated. Connor [1.34] analyzed nonlinear transverse axisymmetric vibrations of the shell using Hamilton's principle to modify the problem to Duffing's equations. Grigoliuk [1.35] proposed a buckling criteria for the problem by minimizing the natural frequency and maximizing the strain energy to determine the initial velocity of the shell deformation.

Moreover, Ho [1.36] suggested the finite deformation theory and nonlinear shell equations to analyze the dynamic buckling and stability of deep spherical shells subjected to step pressure loadings. The critical pressure corresponding to the loss of stability of the shell was obtained using Galerkin's method. The occurrence of a jump was indicated in the amplitude of the dynamic response. He used the qualitative analysis to describe the jump phenomena, the geometrical imperfections, and load disturbances related to the buckling of shells.

With the reviews considered, noting that the nature of snap-through buckling is a dynamic phenomenon, there are some interactions established between the stability approach and the dynamic approach. Archer and Famili [1.37] indicated that the lowest critical pressure obtained from the dynamic analysis was in excellent agreement with that obtained from the stability analysis by Huang [1.24] and Parmerter [1.23]. The natural frequencies of free vibration were in agreement with those of Naghdi and Kalnins [1.31-1.33]. While the dynamic analysis put emphasis on the vibrations of the shell and the study of the stiffness of the shell structures under static load, the stability analysis is concerned with the deflections and buckling of the shell. In the past, the two approaches were used to investigate the deformation of the shell and provided equivalent results for further comparison and investigation.

1.3 OBJECTIVE AND OUTLINE

After a review of the background of the large deflections and nonlinear behaviour of spherical thin shells, the thesis will examine the dynamic responses of vibrating spherical shells, under a concentrated load applied at the apex, using Pogorelov's geometrical approach and assumptions. Specifically the objectives for the present investigation are:

1) to formulate a theoretical model, based on the total strain energy obtained previously, for the vibration of spherical shells using a variational principle,

2) to determine all the nonlinear behaviour and relationships resulting from the model,

3) to predict and verify the performance of the model using two different numerical methods,

4) to simplify the model and to predict the behaviour of the model from the linearized equation of motion,

5) to present remarks and recommendations for the accuracy of the results obtained and for future work.

Based on the objectives presented above, the approach in this thesis, devoted to the theory concerning very large deflections, is as follows. The concept of a thin shell and the basic geometrical relationships of a surface are reviewed in Chapter 2. Chapter 3 is devoted to the assumptions and mathematical formulation for the governing equations of motion of the shell. The possible simplification and linearization in the governing equations of motion, which in turn lead to a linear mass-spring model, are analyzed in Chapter 4. Some comparisons of the predictions from the model and the linearized model are examined in Chapter 5. Remarks for the results obtained are summarized in Chapter 6. Finally, some recommendations for further work and overall conclusions are presented in Chapter 7.

CHAPTER 2

DIFFERENTIAL GEOMETRY OF SURFACES

2.1 SCOPE AND CONCEPT

The goal in this chapter is to review the concept of a thin shell and the geometrical relationships of a surface. These results are presented in vector notation. References [1.7, 2.1 - 2.5] are listed here, and no extensive derivations or proofs are attempted here.

A shell is a body bounded by two closely spaced curved surfaces. The thickness of a shell at a given point is the distance between its bounding surfaces which can be measured along the normal to the reference surface at the point. The shell is said to be thin if the maximum ratio of the thickness to the radius of curvature is very small in comparison with unity. In most practical cases, the thickness may be less than one twentieth or sometimes one tenth of the radius of curvature of the reference surface such that [2.3]

$$\max \left(\frac{h}{R} \right) \leq \frac{1}{20} \quad . \tag{2.1a}$$

The most significant feature of a thin shell is its reference surface. It defines the shape and behaviour of the shell. In the following analysis, the middle surface, equidistance from the bounding surfaces, is chosen as the reference surface.

2.2 CURVILINEAR COORDINATES OF A SURFACE

A surface is defined in Cartesian coordinates as a locus of points determined by three equations:

$$x = f_1(\alpha,\beta) \ , \tag{2.1a}$$

$$y = f_2(\alpha,\beta) \ , \tag{2.1b}$$

$$z = f_3(\alpha,\beta) \ , \tag{2.1c}$$

where x,y,z are the coordinates of an orthogonal right handed Cartesian system; f_1,f_2,f_3 are continuous, single-valued functions; and α,β are a set of curvilinear coordinates of a point on the surface. If β is assigned a constant value, a curve α is obtained on the surface as α is varied. By taking different constant values of β, a family of curves α is found on the surface. Similarly, a constant value of α defines the curve β. Giving α different constant values and letting β change, a second family of curves β is obtained. The intersection of two coordinate curves α and β, determines a point on the surface as shown in Figure 2.1. If two families of coordinate curves are mutually perpendicular at all points on the surface, the curvilinear coordinates are said to be *orthogonal*.

2.2.1 FIRST FUNDAMENTAL FORM

The position vector of an arbitrary point on a surface is defined as

$$\vec{r} = \vec{r}\ (\alpha,\beta) = x\ \vec{u} + y\ \vec{v} + z\ \vec{w} \ , \tag{2.2}$$

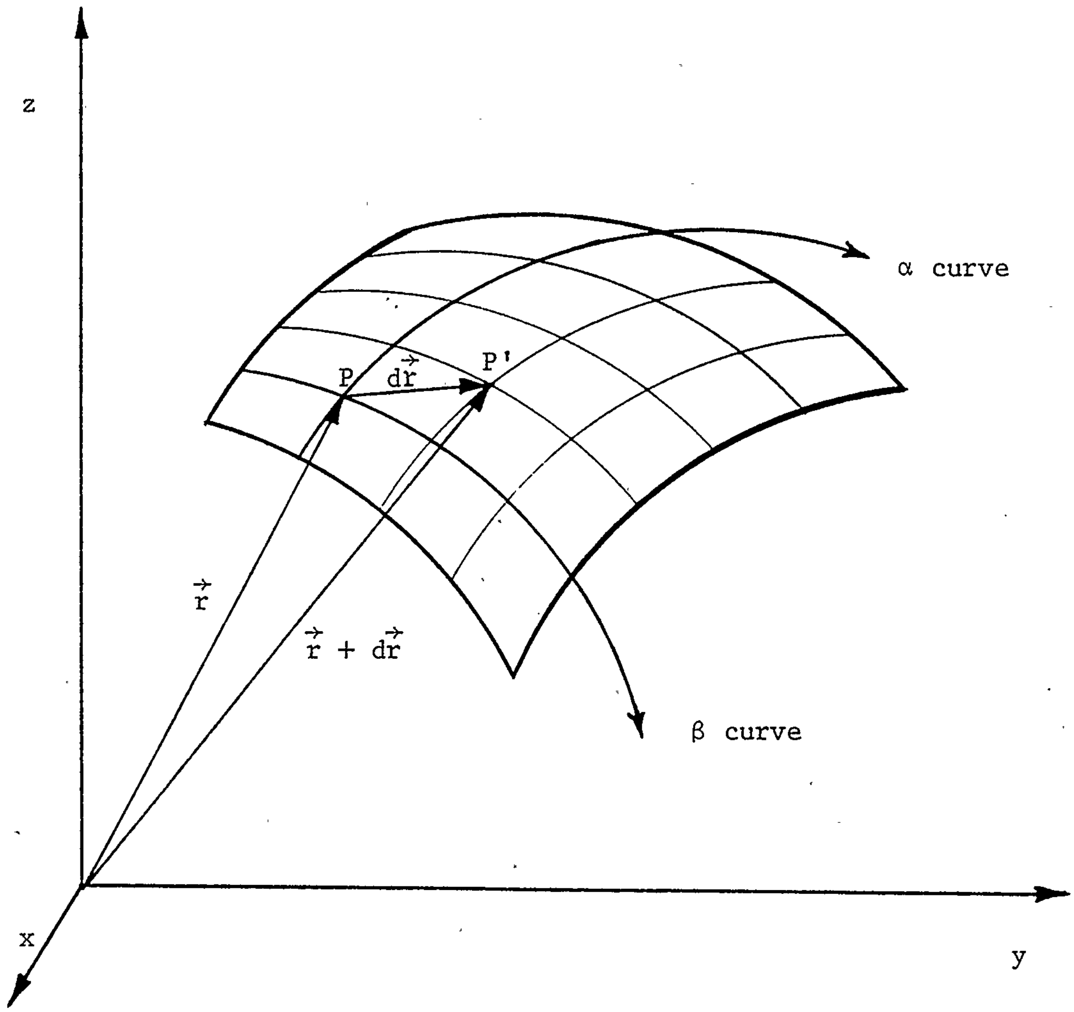

Figure 2.1 Curvilinear Coordinates of a Surface

where $\vec{u}, \vec{v}, \vec{w}$ are unit vectors along the Cartesian coordinates respectively.

The derivatives of $\vec{r}$ with respect to the curvilinear coordinates α and β are vectors tangent to the coordinate curves respectively

$$\frac{\partial r}{\partial \alpha} = \vec{r},_{\alpha} \quad , \tag{2.3a}$$

$$\frac{\partial \vec{r}}{\partial \beta} = \vec{r},_{\beta} \quad . \tag{2.3b}$$

A differential change in the vector $\vec{r}$ is defined as

$$d\vec{r} = \vec{r},_{\alpha}\, d\alpha + \vec{r},_{\beta}\, d\beta \quad . \tag{2.4}$$

The square of the differential change of the arc length is

$$ds^2 = d\vec{r} \cdot d\vec{r} = (\vec{r},_{\alpha} \cdot \vec{r},_{\alpha})\, d\alpha^2 + 2(\vec{r},_{\alpha} \cdot \vec{r},_{\beta})\, d\alpha\, d\beta + (\vec{r},_{\beta} \cdot \vec{r},_{\beta})\, d\beta^2 \quad ,$$

$$ds^2 = E\, d\alpha^2 + 2F\, d\alpha\, d\beta + G\, d\beta^2 \quad , \tag{2.5}$$

where the coefficients are

$$E = \vec{r},_{\alpha} \cdot \vec{r},_{\alpha} = \left(\frac{\partial x}{\partial \alpha} \right)^2 + \left(\frac{\partial y}{\partial \alpha} \right)^2 + \left(\frac{\partial z}{\partial \alpha} \right)^2 , \tag{2.5a}$$

$$F = \vec{r},_{\alpha} \cdot \vec{r},_{\beta} = \frac{\partial x}{\partial \alpha}\frac{\partial x}{\partial \beta} + \frac{\partial y}{\partial \alpha}\frac{\partial y}{\partial \beta} + \frac{\partial z}{\partial \alpha}\frac{\partial z}{\partial \beta} \quad , \tag{2.5b}$$

$$G = \vec{r},_{\beta} \cdot \vec{r},_{\beta} = \left(\frac{\partial x}{\partial \beta} \right)^2 + \left(\frac{\partial y}{\partial \beta} \right)^2 + \left(\frac{\partial z}{\partial \beta} \right)^2 . \tag{2.5c}$$

Eq. (2.5) is known as the first fundamental form of the surface.

From vector algebra,

$$|\vec{r},_{\alpha} \times \vec{r},_{\beta}| = |\vec{r},_{\alpha}| \cdot |\vec{r},_{\beta}| \sin \Theta \ , \tag{2.6}$$

$$\vec{r},_{\alpha} \cdot \vec{r},_{\beta} = |\vec{r},_{\alpha}| \cdot |\vec{r},_{\beta}| \cos \Theta \ . \tag{2.7}$$

The angle Θ between the coordinate curves α and β is given by

$$\cos \Theta = \frac{F}{\sqrt{EG}} \quad . \tag{2.8}$$

In an orthogonal curvilinear coordinate system,

$$ds^2 = A^2 \, d\alpha^2 + B^2 \, d\beta^2 \quad , \tag{2.9a}$$

where

$$A = \sqrt{E} \quad , \tag{2.9b}$$

$$B = \sqrt{G} \quad . \tag{2.9c}$$

The coefficients A and B are called Lamé parameters for the measurement of distances on the surface. Eq. (2.9a) can be written as

$$d\, s_\alpha = A \, d\alpha \quad , \tag{2.10a}$$

$$d\, s_\beta = B \, d\beta \quad , \tag{2.10b}$$

if each of the curvilinear coordinates α and β are varied individually and independently. It is noted that Lamé parameters relate the change in arc length on the surface to the change in the curvilinear coordinate. Examples illustrating a method to determine Lamé parameters from the geometrical relationship of Eq. (2.9a), (2.10a), and (2.10b) are shown in Appendix A.

It is necessary to define the following vectors. The unit vectors tangent to the coordinate curves are given, respectively, by

$$\vec{t}_\alpha = \frac{\vec{r},_\alpha}{\left|\vec{r},_\alpha\right|} = \frac{\vec{r},_\alpha}{A} \quad , \tag{2.11a}$$

$$\vec{t}_\beta = \frac{\vec{r},_\beta}{\left|\vec{r},_\beta\right|} = \frac{\vec{r},_\beta}{B} \quad . \tag{2.11b}$$

The unit normal vector is the cross product of the unit tangent vectors.

$$\vec{n} = \vec{t}_\alpha \times \vec{t}_\beta = \frac{\vec{r},_\alpha \times \vec{r},_\beta}{\left|\vec{r},_\alpha \times \vec{r},_\beta\right|} = \frac{\vec{r},_\alpha \times \vec{r},_\beta}{AB} \quad . \tag{2.12}$$

2.2.2 SECOND FUNDAMENTAL FORM

From the geometry of space curves, the curvature vector $\vec{k}$ is defined as

$$\vec{k} = \kappa\vec{p} = \frac{d^2\vec{r}}{ds^2} \quad , \tag{2.13}$$

where κ is the curvature of the curve at a given point. It is stated that the curvature vector $\vec{k}$ is normal to unit tangent vector $\vec{t}$ to the curve at a given point and is in the direction of the principal normal $\vec{p}$ of the curve at the point.

Generally, the principal normal is not in the same direction as the surface normal $\vec{n}$. The curvature vector $\vec{k}$ may be resolved into two components

$$\vec{k} = \vec{k}_n + \vec{k}_t = \kappa_n\vec{n} + \kappa_t\vec{t} \quad , \tag{2.14}$$

where $\vec{k}_n$ and $\vec{k}_t$ are the normal and tangential components of the curvature vector, respectively. The normal component $\vec{k}_n$ is in the direction normal to the surface. κ_n is known as the normal curvature which is the magnitude of the normal component of the curvature vector. Its reciprocal is called the radius of curvature R which will be further discussed in Eq. (2.17). κ_t is the tangential (geodesic) curvature.

Taking the scalar product of Eq. (2.14) with $\vec{n}$,

$$\kappa_n = \vec{k} \cdot \vec{n} = \frac{1}{R} \quad .$$

From Eq. (2.13),

$$\kappa_n = \frac{d^2\vec{r}}{ds^2} \cdot \vec{n} = \frac{d\vec{r} \cdot d\vec{n}}{d\vec{r} \cdot d\vec{r}} \quad . \tag{2.14a}$$

Further from Eq. (2.4), (2.5) and

$$d\vec{n} = \vec{n},_\alpha \, d\alpha + \vec{n},_\beta \, d\beta \quad , \tag{2.15}$$

Eq. (2.14a) is written as

$$\kappa_n = \frac{\vec{r},_\alpha \cdot \vec{n},_\alpha \, d\alpha^2 + (\vec{r},_\alpha \cdot \vec{n},_\beta + \vec{r},_\beta \cdot \vec{n},_\alpha) \, d\alpha \, d\beta + \vec{r},_\beta \cdot \vec{n},_\beta \, d\beta^2}{d\vec{r} \cdot d\vec{r}} \quad ,$$

$$\kappa_n = \frac{L \, d\alpha^2 + 2M \, d\alpha \, d\beta + N \, d\beta^2}{E \, d\alpha^2 + 2F \, d\alpha \, d\beta + G \, d\beta^2} = \frac{II}{I} \quad , \tag{2.16}$$

where the coefficients E,F, and G are given in Eq. (2.5a) and

$$L = \vec{r},_\alpha \cdot \vec{n},_\alpha \quad , \tag{2.16a}$$

$$2M = \vec{r},_\alpha \cdot \vec{n},_\beta + \vec{r},_\beta \cdot \vec{n},_\alpha \quad , \tag{2.16b}$$

$$N = \vec{r},_\beta \cdot \vec{n},_\beta \quad . \tag{2.16c}$$

The numerator II in Eq. (2.16) is the second fundamental form of a surface which characterizes the curvature of the surface.

Setting the differentials $d\alpha$ and $d\beta$ to zero respectively in Eq. (2.16), the normal curvature along α and β are obtained as, [2.1]

$$(\kappa_n)_1 = \frac{1}{R_1} = \frac{L}{E} \quad , \tag{2.17a}$$

and

$$(\kappa_n)_2 = \frac{1}{R_2} = \frac{N}{G} \quad , \tag{2.17b}$$

which are the principal curvatures of the surface. R_1 and R_2 are the principal radii of curvature such that one corresponds to the maximum radius of curvature and the other to the minimum.

The *lines of curvatures* of a surface are the lines at each point along which the normal curvature is equal to one of the principal curvatures of the surface at the point. When the coordinate curves α and β are the lines of curvature, the curvilinear coordinate system is a *principal orthogonal curvilinear coordinate* such that F = M = 0, and the coordinate curves become the lines of principal curvature.

The Gaussian curvature is defined as, [2.2]

$$G = \frac{1}{R_1 R_2} \quad , \tag{2.18a}$$

and the mean curvature is

$$H = \frac{1}{2} \left(\frac{1}{R_1} + \frac{1}{R_2}\right) \quad . \tag{2.18b}$$

Surface with positive Gaussian curvature is obtained if both centers of R_1 and R_2 lie on the same side of the surface, for examples, the sphere and paraboloid of revolution. If one of the principal radii of curvatures is infinity, the Gaussian curvature is zero. The surface is said to be developable such as a flat plate, a cylinder, or a cone.

2.3 COMPATIBILITY CONDITIONS

To define the geometry of a surface, it is necessary that the coefficients A, B, R_1, and R_2, corresponding to Lamé parameters and the principal radii of curvature, satisfy the compatibility conditions. These coefficients cannot be chosen arbitrarily as functions of curvilinear coordinates. In order for the coefficients to correspond to a surface, three differential equations known as the Gauss-Codazzi relations must be identically satisfied by the coefficients. They are derived from the second mixed derivatives of unit vectors which are assumed to have continuous derivatives up to the second order. The Codazzi relations are given by [2.3]

$$\frac{\partial}{\partial \beta}\left(\frac{A}{R_1}\right) = \frac{1}{R_2}\frac{\partial A}{\partial \beta} \quad , \tag{2.19a}$$

$$\frac{\partial}{\partial \alpha}\left(\frac{B}{R_2}\right) = \frac{1}{R_1}\frac{\partial B}{\partial \alpha} \quad , \tag{2.19b}$$

and the Gauss condition is

$$\frac{\partial}{\partial \alpha}\left(\frac{1}{A}\frac{\partial B}{\partial \alpha}\right) + \frac{\partial}{\partial \beta}\left(\frac{1}{B}\frac{\partial A}{\partial \beta}\right) = \frac{-AB}{R_1 R_2} \quad . \tag{2.19c}$$

If an equation is given by Eq. (2.1), its coefficients can be evaluated from Eq. (2.9b,c) and (2.17a,b); if they satisfy the compatibility conditions Eq. (2.19a,b, and c) identically, then Eq. (2.1) defines a surface.

CHAPTER 3

VARIATIONAL FORMULATION OF THE GOVERNING EQUATIONS FOR VIBRATING SHELLS

3.1 ASSUMPTION

The following analysis, devoted to the theory concerning very large deflections of spherical shells, is based on Pogorelov's geometrical approach [1.1, 1.7]. The deflection pattern of spherical shells due to a concentrated load at the apex has an approximate shape as shown in Figure 3.1. It is a dimple together with a ridge at which the shell is under severe bending. The shell is divided into three regions, namely: I) the central region of the dimple, II) the ridge region including an inner strip and an outer strip, and III) the outer undistorted region. In the central region, the shell undergoes isometric deformation. When the shell is under the action of a concentrated load at the apex, it deflects elastically in isometric deformation. A circular dimple of reverse curvature of the initial surface is formed at the apex and is spread outwardly as the load increases. The mirror reflection of an initial surface, as predicted in experiments on spherical shells under large deflections, is the most simple form of isometric transformation of the surface [1.7, 1.15 and 3.1]. Under the assumption of large deflection in the analysis, the curvature of the deformed surface is equal to the reverse curvature of its initial

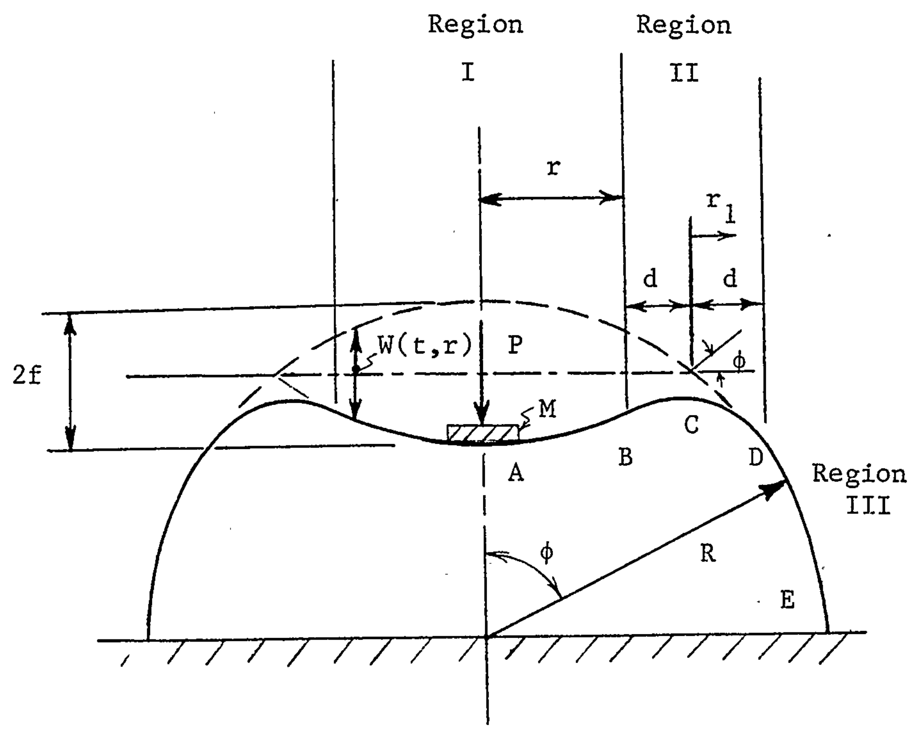

Figure 3.1 Mechanism of Large Deformations of Spherical Shells under the Action of Concentrated Load at the Apex

surface. The deformed surface is said to be isometric to the initial surface, and the deformation of such a surface is said to be isometric deformation. Mathematically, two surfaces are said to be isometric if the coefficients in the first fundamental form Eq. (2.5) of the two surfaces are identical [2.5]. The length of arcs and the angles between the curves on the surface are the same.

The isometrically deformed surface is associated with a change of principle curvature, and only the bending energy is considered. The shell is assumed to be deflected symmetrically with respect to the axis of revolution. The radial displacement along the circumferential circle can be neglected, and the circumferential strain is equal to zero.

At the point of application of the load, the membrane strain may appear in a local area of the applied load. However, this area is very small, and the local deflection is not taken into account. The strain can be neglected in the analysis.

In the ridge region, the shell is under quasi-isometric deformation. The curvature of the deformed surface is no longer equal to the reverse curvature of the initial surface. The energy in this area consists of the bending energy as well as the membrane energy. The region is assumed to be very small so that the deformation of the middle surface is negligible. The strain in the meridian direction is also negligible, and the only strain in the middle surface is the circumferential strain.

The quasi-isometric deformation in the ridge region is imposed by the conditions of continuity between the isometric deformed region and the outer undeformed region. The conditions must satisfy the displacement function and the boundary conditions in the transition region.

In the outer region, the shell undergoes little change of the principal curvature and deflection. There is no energy associated with the bending of the surface, and this region is assumed to be rigid.

Now consider a spherical shell under the action of a concentrated force P applied at the apex as shown in Figure 3.1. There is only one parameter which defines the middle surface of the shell after deformation. It is the vertical deflection of the middle surface $W(t,r)$, which is a function of time t and the radial coordinate from the axis of symmetry r. At any point, the middle surface of the deformed shell can be described by the following equation

$$W \cong 2(f - \frac{r^2}{2R}) , \tag{3.1}$$

where 2f is the total deflection from the apex, and R is the radius of curvature of the shell.

From the geometry of the shell as shown in Figure 3.2, the base radius of the shell is

$$a^2 \cong 2Rf \quad . \tag{3.2}$$

At $r = 0$, the maximum depth of depression becomes

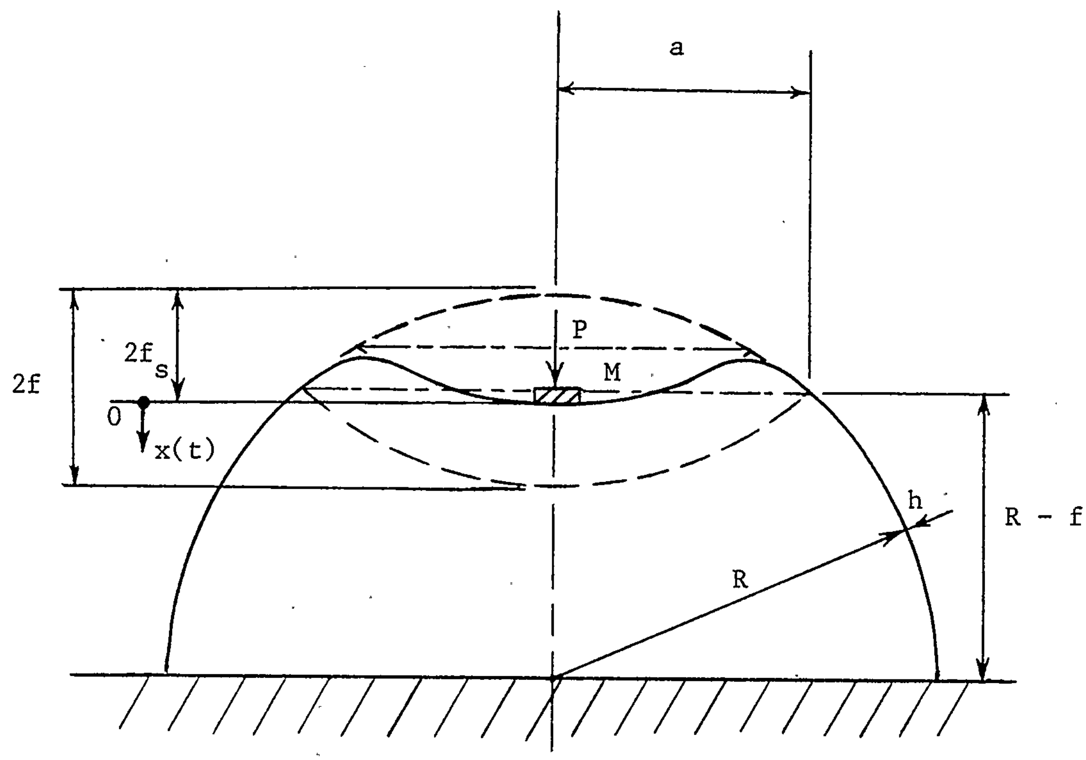

Figure 3.2 Shell Geometry and Coordinate System

$$W_{max} = 2f \quad . \tag{3.3}$$

Considering the x coordinate of the spherical shell, the total deflection at the apex can be written as

$$f = f_s + \frac{x(t)}{2} \quad , \tag{3.4}$$

where f_s is a constant static deflection due to the mass M at the apex, and x(t) is the vertical deflection of the middle surface at the apex. Now, only one unknown parameter x(t), which is a function of time, defines the shape of the shell after deformation.
Therefore, the problem can be reduced to a dynamic problem of one degree-of-freedom. The coordinate is considered positive when the shell is deflected from the static equilibrium position in the inward direction.

Taking the derivatives with respect to time,

$$\dot{f} = \frac{\dot{x}}{2} \quad , \qquad \ddot{f} = \frac{\ddot{x}}{2} \quad . \tag{3.5}$$

Based on the Hamilton's principle, it is necessary to find the total strain energy for each of these three regions. An energy functional must be calculated over the entire system from the total strain energy, the total kinetic energy, as well as the potential energy by the concentrated force. The governing equations of motion are then obtained from the minimization of the energy functional.

3.2 DERIVATIONS FROM HAMILTON'S PRINCIPLE

Hamilton's principle considers the entire motion of the system between the time t_1 and t_2. It is a variational principle which reduces the problem of dynamics to a definite scalar integral. One of the advantages of the formulation is that it does not depend on the coordinate systems used. The condition giving a stationary value of the integral leads to all the equations of motion. For convenience, the derivation for the principle are given in references [3.2 - 3.9].

Mathematically, Hamilton's principle is defined, for a continuous deformable body, in the form of [3.3]

$$\delta I = \delta \int_{t_1}^{t_2} [T - (U - V)] \, dt = 0 \quad . \tag{3.6}$$

It is noted that T is the total kinetic energy of the body and (U - V) is the total potential energy,

$$\pi = U - V \ . \tag{3.7}$$

From Eq. (3.7),

$$\delta I = \delta \int_{t_1}^{t_2} (T - \pi) \, dt = \delta \int_{t_1}^{t_2} L \, dt = 0 \ , \tag{3.8}$$

where L is the Lagrangian

$$L = T - \pi \ . \tag{3.8a}$$

Hamilton's principle states that, of all the paths that the body can take as it goes from a configuration at time t_1 to another configuration at time t_2, only the path that extremizes the time integral of the Lagrangian within the time interval satisfies the equation of motion. The path is thus the actual path. Before the governing equation of motion of the shell is formulated by

Hamilton's principle, the analysis of the total strain energy will be discussed in the following section.

3.2.1 TOTAL STRAIN ENERGY OF THE SHELL

Considering the central region I of the spherical shell as shown in Figure 3.1, the curvature of the isometrically deformed surface is equal to the reverse curvature of the initial surface. The energy associated with the change of curvature takes the following form [1.1, 1.7]

$$U_I = \frac{D}{2} \int\int_{S_I} (\Delta\kappa_1{}^2 + \Delta\kappa_2{}^2 + 2\nu\, \Delta\kappa_1\, \Delta\kappa_2)\, dS_I \quad , \qquad (3.9)$$

where the changes in curvatures of the middle surface are

$$\Delta\kappa_1 = \kappa_1' - \kappa_1 = (-\frac{1}{R}) - \frac{1}{R} = -\frac{2}{R} \quad , \qquad (3.9a)$$

and

$$\Delta\kappa_2 = \Delta\kappa_1 = -\frac{2}{R} \quad . \qquad (3.9b)$$

The curvature of the original surface is κ_1, the reverse curvature of the surface after deformation is κ_1', and the radius of curvature of the shell is R. The bending stiffness is of the form

$$D = \frac{Eh^3}{12(1 - \nu^2)} \quad , \qquad (3.9c)$$

where E is the Young's modulus.

From Eq. (3.9a, 3.9b, and 3.9c), the energy is obtained as

$$U_I = \frac{D}{2} \int\int \frac{8}{R^2} (1 + \nu)\, dS \quad ,$$

$$U_I = \frac{\pi E\ h^3}{3(1 - \nu)} \left(\frac{a}{R} \right)^2 \quad . \tag{3.10}$$

It is noted that the membrane energy in the middle surface is neglected here. Eq. (3.10) is regarded as the total energy in the central region of the dimple.

It is assumed that the region III is rigid. The shell undergoes no changes in the curvatures. There is no energy associated with the bending of the surface. The membrane energy in the middle surface is also absent because of the rigidity of the shell. As a result, the total strain energy in the region III is zero, i.e.,

$$U_{III} = 0 \quad . \tag{3.11}$$

The area of ridge region II is very small and undergoes quasi-isometric deformation. The energy in this area consists of bending energy as well as membrane energy. The bending energy due to the changes in curvatures, and the membrane energy associated with the circumferential strain in the middle surface are obtained by Pogorelov using the variational principle. The total strain energy in the ridge region is summarized in Appendix B. As a result, the total strain energy of the shell associated with the change in geometry takes the following simple form [1.1]

$$U = \frac{2\pi c E\ h^{5/2}\ (W_{max})^{3/2}}{R} \quad , \tag{3.12}$$

where $c \cong 0.19$ which is a constant coefficient, and W_{max} is from Eq. (3.3).

3.2.2 GOVERNING EQUATIONS OF MOTION

The energies that will be needed for the Hamilton's principle are considered first, and the governing equation of motion is derived from the extremization of the energy functional. First, the kinetic energy of the shell in the region I can be written as

$$T_1 = \frac{1}{2} \int\int \gamma h \, \dot{W}^2 \, dS \quad , \tag{3.13}$$

where γ is the mass per unit volume of the shell. The integration over the area of region I is

$$\int\int_{S_I} \gamma h \, dS_I = \gamma h \pi a^2 \quad . \tag{3.13a}$$

From Eq. (3.13a), (3.1), (3.2), and (3.4),

$$T_1 = \pi R \gamma h \, (f_s + \frac{x}{2}) \, \dot{x}^2 \quad . \tag{3.14}$$

The kinetic energy of the body M at the apex is

$$T_2 = \frac{1}{2} M \dot{W}^2 = \frac{1}{2} M \dot{x}^2 \quad . \tag{3.15}$$

From Eq. (3.14) and (3.15), the total kinetic energy of the system takes the form of

$$T = \pi R \gamma h \, (f_s + \frac{x}{2}) \, \dot{x}^2 + \frac{1}{2} M \dot{x}^2 \quad . \tag{3.16}$$

The potential energy of the concentrated force P is calculated as

$$V = (P + Mg) \cdot 2f = 2(P + Mg)(f_s + \frac{x}{2}) \quad . \tag{3.17}$$

With the previous result obtained in Sec. 3.2.1, the total strain energy of the shell in Eq. (3.12) can be rewritten as

$$U = \frac{4\sqrt{2}\pi cE\ h^{5/2}\ (f_s + \frac{x}{2})^{3/2}}{R} \quad . \tag{3.18}$$

From Eq. (3.16), (3.17) and (3.18), the Lagrangian is then

$$L = \pi R\gamma h\ (f_s + \frac{x}{2})\ \dot{x}^2 + \frac{M}{2}\dot{x}^2 - \frac{2\pi E\ h^{5/2}}{R}\ [\ 2(f_s + \frac{x}{2})\ ]^{3/2} + 2\ (P + Mg)(f_s + \frac{x}{2}) \quad . \tag{3.19}$$

Based on Hamilton's principle, the minimization of the time integral of the energy functional Eq. (3.19), is given by

$$\delta \int_{t_1}^{t_2} L\ dt = 0 \quad . \tag{3.8}$$

Carrying out the variation operation using the δ operator and integrating by parts with respect to time, [See Appendix C for detailed derivations.]

$$\delta I = \int_{t_1}^{t_2} [\ -(2\pi R\gamma h\ f_s + M)\ \ddot{x} - \pi R\gamma h\ x\ddot{x} - \frac{\pi R\gamma h}{2}\ \dot{x}^2 - \frac{3\sqrt{2}\ \pi cE\ h^{5/2}}{R}(f_s + \frac{x}{2})^{1/2} + (P + Mg)]\ \delta x\ dt + (2f_s\ \dot{x} + x\dot{x} + M\dot{x})\ \delta x \Big|_{t_1}^{t_2} = 0 \quad . \tag{3.20}$$

It is noticed that the coefficients of the variations δx must be zero as δx is arbitrary. The differential equation of motion for the shell is obtained as

$$2\pi R\gamma h \left[\left(f_s + \frac{x}{2}\right) \ddot{x} + \frac{\dot{x}^2}{4} \right] + M\ddot{x} + \frac{3\sqrt{2}\pi c E\, h^{5/2}}{R} \left(f_s + \frac{x}{2}\right)^{1/2}$$

$$- (P + Mg) = 0 \quad . \tag{3.21}$$

In Eq. (3.21), the first term is associated with the kinetic energy of the shell, the second term is the inertia force by mass M, the third term is associated with the strain energy, and the fourth term represents the external load.

In terms of the deflection f from Eq. (3.4), Eq. (3.21) can be expressed as

$$2\pi R\gamma h \left(2f\ddot{f} + \dot{f}^2\right) + 4M\ddot{f} + \frac{3\sqrt{2}\pi c\ E\ h^{5/2}}{R} \sqrt{f}$$

$$- (P + Mg) = 0 \quad . \tag{3.22}$$

The equation of motion (3.22) is a nonlinear second order ordinary differential equation. It is noticed that the variations at the time t_1 and t_2 are zero, i.e.,

$$\delta x(t_1) = \delta x(t_2) = 0 \quad . \tag{3.23}$$

The line integral in Eq. (3.20) gives the natural boundary conditions.

$$2f_s\ \dot{x} + x\dot{x} + M\dot{x} \Big|_{t_1}^{t_2} = 0 \quad .$$

Introducing the following non-dimensional parameters in Eq. (3.21),

$$y = \frac{x}{R} \quad , \tag{3.24a}$$

$$\dot{y} = \frac{\dot{x}}{R} \quad , \tag{3.24b}$$

$$\ddot{y} = \frac{\ddot{x}}{R} \quad , \tag{3.24c}$$

$$f_o = \frac{f_s}{R} \quad , \tag{3.24d}$$

$$A = \frac{3\sqrt{2}\pi c E \, h^{5/2}}{M_o \, g \, \sqrt{R}}, \quad B = \frac{MR}{M_o \, g}, \quad C = \frac{2\pi\gamma h R^3}{M_o \, g}, \quad D = \frac{P + Mg}{M_o \, g} \quad . \tag{3.24e}$$

A non-dimensional equation of motion can be obtained as

$$(B + C f_o) \ddot{y} + \frac{C}{2} y\ddot{y} + \frac{C}{4} \dot{y}^2 + A \left(f_o + \frac{y}{2}\right)^{\frac{1}{2}} - D = 0 \quad . \tag{3.25}$$

A physical system can be described by a system of simultaneous differential equations of the form [3.10]

$$\begin{aligned} \frac{dy_1}{dt} &= \dot{y}_1 = f_1(y_1, y_2, \ldots y_n) \quad , \\ \frac{dy_2}{dt} &= \dot{y}_2 = f_2(y_1, y_2, \ldots y_n) \quad , \\ \frac{dy_n}{dt} &= \dot{y}_n = f_n(y_1, y_2, \ldots y_n) \quad , \end{aligned} \tag{3.26}$$

where t is the independent variable; y_1, y_2,...y_n are the n dependent variables; and f_1, f_2,...f_n are nonlinear functions of the dependent variables. In the present system, two first order differential equations are obtained as follows:

$$\dot{y}_1 = y_2 \quad , \tag{3.27a}$$

$$\dot{y}_2 = \frac{D - A\left(f_o + \frac{y_1}{2}\right)^{\frac{1}{2}} - C\,\frac{y_2^{\,2}}{4}}{B + C\left(f_o + \frac{y_1}{2}\right)} \quad . \tag{3.27b}$$

It is clear that the set of simultaneous differential equations (3.27a) and (3.27b) is equivalent to the second order differential equation (3.25). The dynamic response characteristic of the system to an input or forcing function will be obtained if the set of differential equations is solved. The system of equations has been set up to be computed by the numerical method discussed in Chapter 5.

3.2.3 SIMPLIFICATION

It is apparent that an attempt to obtain solutions in a closed form for the equation of motion (3.25) is difficult, by far, exceeding the scope of this work. However, the equation (3.25) can be further simplified to

$$\ddot{y} + \frac{C}{2(B + C\,f_o)}\, y\ddot{y} + \frac{C}{4(B + C\,f_o)}\, \dot{y}^2 + \frac{A}{(B + C\,f_o)} \left(f_o + \frac{y}{2}\right)^{\frac{1}{2}} = \frac{D}{B + C\,f_o} \quad . \qquad (3.28)$$

Introducing the following notations,

$$\alpha = \frac{C}{2(B + C\,f_o)} \quad ,$$

$$\beta = \frac{A}{B + C\,f_o} \quad ,$$

$$\gamma = \frac{D}{B + C\,f_o} \quad .$$

Eq. (3.28) becomes

$$\ddot{y}\,(1 + \alpha y) + \frac{\alpha}{2}\,\dot{y}^2 + \beta\left(fo + \frac{y}{2}\right)^{\frac{1}{2}} = \gamma \quad . \tag{3.29}$$

3.3 STABILITY OF EQUILIBRIUM

The stability of equilibrium of a system can be determined by the variation of the total potential energy associated with the system, i.e., $\delta\pi = \delta(U - V)$. The total variation of π can be expressed as a Taylor series expansion in the form of [3.3, 3.11 - 3.12]

$$\begin{aligned}\delta\pi &= \pi(x + \delta x) - \pi(x) \\ &= \frac{\partial\pi}{\partial x}\,\delta x + \frac{1}{2!}\,\frac{\partial^2\pi}{\partial x^2}\,(\delta x)^2 + \frac{1}{3!}\,\frac{\partial^3\pi}{\partial x^3}\,(\delta x)^3 + \dots \quad .\end{aligned} \tag{3.30}$$

To establish the equilibrium configuration of the system, set the first variation equal to zero.

$$\delta^{(1)}\pi = \frac{\partial\pi}{\partial x}\,\delta x = 0 \quad .$$

For the variation δx is arbitrary, $\frac{\partial\pi}{\partial x}$ must vanish, i.e.,

$$\frac{\partial\pi}{\partial x} = 0 \quad . \tag{3.31}$$

The equilibrium configuration of a system is associated with a stationary value of the total potential energy π. This is the principle of *Stationary Total Potential Energy*. In other words, the total potential energy assumes an extremum position for an elastic body in static equilibrium.

The second variation of π gives insight into the stability of equilibrium, i.e.,

$$\delta^{(2)}\pi = \frac{\partial^2\pi}{\partial x^2}(\delta x)^2 \quad . \tag{3.32}$$

If $\frac{\partial^2\pi}{\partial x^2}$ is greater than zero, the system will be in stable equilibrium; if it is equal to zero, the system will be in neutral equilibrium; and if it is less than zero, the system will be unstable. When the second variation of the total potential energy ceases to be positive, the system reaches critical configuration and ceases to have stability.

From Eq. (3.17) and (3.18), the total potential energy of the shell can be obtained as

$$\pi = \frac{4\sqrt{2}\pi cE\ h^{5/2}}{R}(f_s + \frac{x}{2})^{3/2} - 2(P + Mg)\ (f_s + \frac{x}{2}) \quad . \tag{3.33}$$

For the system to be in static equilibrium, Eq. (3.31) must be satisfied,

$$\frac{\partial\pi}{\partial x} = \frac{3\sqrt{2}\pi cE\ h^{5/2}}{R}\ (fs + \frac{x}{2})^{\frac{1}{2}} - (P + Mg) = 0 \quad . \tag{3.34}$$

Thus, the equation of equilibrium is obtained as

$$P_1 = \frac{3\sqrt{2}\pi cE\ h^{5/2}}{R}\ (f_s + \frac{x}{2})^{\frac{1}{2}} \quad . \tag{3.35}$$

where P_1 is the static load. For the applied force P = 0 in static equilibrium,

$$P_1 = Mg \quad .$$

Eq. (3.35) gives a nonlinear relationship between the load and deflection in static equilibrium.

The conditions for the stability of equilibrium are given here. From Eq. (3.34),

$$\frac{\partial^2 \pi}{\partial x^2} = \frac{3\sqrt{2}\pi c E\ h^{5/2}}{4R\ (f_s + \frac{x}{2})^{\frac{1}{2}}} \quad . \tag{3.36}$$

The following results are obtained as

I) If $f_s + \frac{x}{2} > 0$, i.e., $x > -2f_s$,

$\frac{\partial^2 \pi}{\partial x^2} > 0$, the system will be in stable equilibrium.

II) If $f_s + \frac{x}{2} = 0$, i.e., $x = -2f_s$,

$\frac{\partial^2 \pi}{\partial x^2} = 0$, the system will be in neutral equilibrium.

III) If $f_s + \frac{x}{2} < 0$, i.e., $x < -2f_s$, the system will be unstable.

It is shown that the shell loses its stability if it deflects beyond the region $f_s + \frac{x}{2} < 0$. The governing equation of motion Eq. (3.25) is stable only for $f_s + \frac{x}{2} \geq 0$. However, it is possible for the shell to deflect in the normal outward direction from the apex during vibrations. The governing equation of motion for the shell deflected in an outward direction can be derived as follows. Consider the case of $f_s + \frac{x}{2} < 0$ that the shell deflects a small amount Δx from the apex in an outward direction, as shown in Figure 3.3,

$$\Delta x = -(x + 2f_s) \quad . \tag{3.37}$$

The displacement Δx must be very small for the stiffness of the shell tends to restore the mass back to its equilibrium position. The linear approximation of the load and deflection relationship of the shell, loaded by a normal concentrated force in the outward direction, is given by [1.7]

$$P_s = \frac{4E\ h^2}{R[3(1-\nu^2)]^{\frac{1}{2}}} \Delta x \quad . \tag{3.38}$$

The equivalent stiffness of the shell is written as

$$k_{eq} = \frac{4Eh^2}{R[3(1-\nu^2)]^{\frac{1}{2}}} \quad . \tag{3.38a}$$

When the shell deflects in the normal outward direction from the apex, the following governing equation of motion is considered from Hamilton's principle. The kinetic energy of the shell can be obtained in the form of [1.7, 3.13]

$$T = \frac{1}{2} M\ \Delta\dot{x}^2 + \frac{4\pi\gamma h^2 R}{3[12(1-\nu^2)]^{\frac{1}{2}}} \Delta\dot{x}^2 \quad . \tag{3.39}$$

The potential energy of the system due to a displacement Δx is

$$U = \frac{1}{2} k_{eq}\ \ \Delta x^2 \quad . \tag{3.40}$$

The work done by the concentrated force

$$V = (P + Mg)(x + 2f_s) \quad . \tag{3.41}$$

The Lagrangian is written as

$$L = T - (U - V) \quad ,$$

$$L = \frac{1}{2} \left(M + \frac{4\pi\gamma h^2 R}{3[12(1 - \nu^2)]^{\frac{1}{2}}} \right) \dot{x}^2 - \frac{1}{2} k_{eq} (x + 2f_s)^2$$

$$+ (P + Mg)(x + 2f_s) . \qquad (3.42)$$

The minimization of the variation of the energy functional from Eq. (3.42) gives

$$\delta I = \int_{t_1}^{t_2} \left(\{ -M + \frac{8\pi\gamma h^2 R}{3[12(1-\nu^2)]^{\frac{1}{2}}} \} \ddot{x} - k_{eq} (x + 2f_s) \right.$$

$$\left. + (P + Mg) \right) \delta x \, dt + (M + \frac{8\pi\gamma h^2 R}{3[12(1 - \nu^2)]^{\frac{1}{2}}}) \dot{x} \, \delta x \Bigg|_{t_1}^{t_2} . \qquad (3.43)$$

As δx is arbitrary, the coefficient of the variation must vanish, and the equation of motion is then obtained as

$$\left(M + \frac{8\pi\gamma h^2 R}{3[12(1 - \nu^2)]^{\frac{1}{2}}} \right) \ddot{x} + k_{eq} (x + 2f_s) - (P + Mg) = 0 . \qquad (3.44)$$

Also, the equation of equilibrium is written as

$$P_2 = \frac{8E \, h^2}{R[3(1 - \nu^2)]^{\frac{1}{2}}} (f_s + \frac{x}{2}) , \qquad (3.45)$$

where P_2 is the static load for $P = 0$.

Introducing the following non-dimensional parameters in Eq. (3.24) and

$$K = \frac{4 \, E \, h^2}{M_o \, g \, [3(1 - \nu^2)]^{\frac{1}{2}}} ,$$

$$B' = \frac{R}{M_o g}\{M + \frac{8\pi\gamma h^2 R}{3[12(1-\nu^2)]^{\frac{1}{2}}}\} \quad ,$$

Eq. (3.44) becomes

$$B' \dot{y} + K(y + 2f_o) = D \quad . \tag{3.46}$$

The resulting Eq. (3.46) is obtained from the linear approximation of the nonlinear behaviour of the shell provided that the outward deflection from the apex is of the same order as the thickness of the shell.

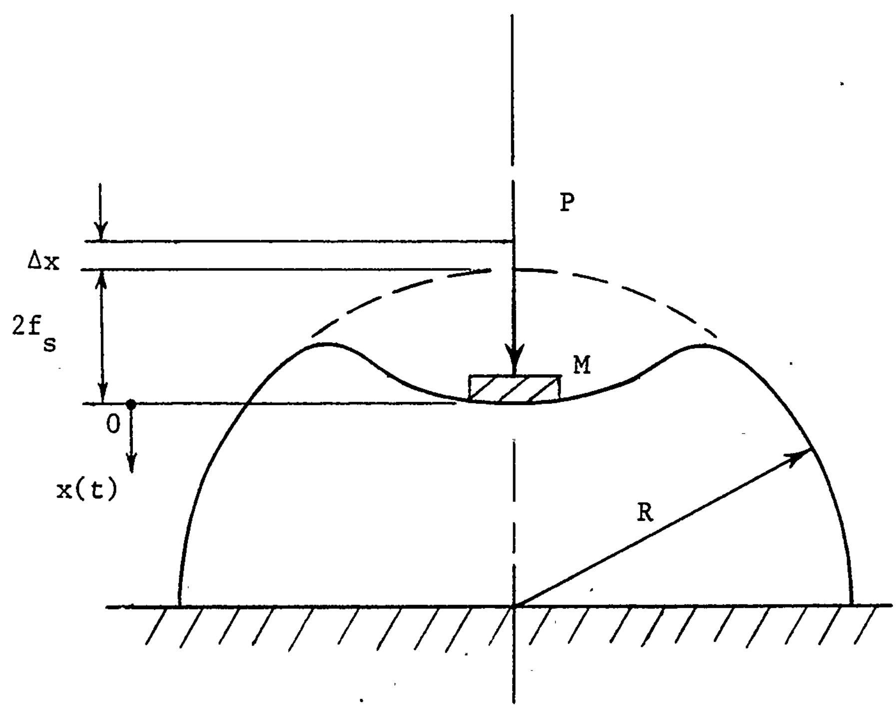

Figure 3.3 Outward Deflection of the Shell Exceeding the Limit $2f_s$

CHAPTER 4

LINEARIZATION OF THE GOVERNING EQUATION

4.1 INTRODUCTION

This chapter presents the concept of linearization of a nonlinear mathematical model [4.1 - 4.6]. This technique is applicable to nonlinear systems. The objective is to linearize the nonlinear mathematical model obtained in Eq. (3.25).

4.2 LINEARIZATION OF A NONLINEAR SYSTEM

Consider a first order nonlinear system whose output y(t) is a function of input p(t),

$$y = f(p) \quad . \tag{4.1}$$

It is assumed that the variable deviates only slightly from the normal operating condition. Eq. (4.1) can be expanded into a Taylor series about the normal condition $\bar{p}$, $\bar{y}$ as follows:

$$y = f(p) = f(\bar{p}) + \frac{df}{dp}(p - \bar{p}) + \frac{1}{2!}\frac{d^2f}{dp^2}(p - \bar{p})^2 + \ldots \quad , \tag{4.2}$$

where the derivatives are evaluated at $p = \bar{p}$. If the variation $(p - \bar{p})$ is small, the higher order terms may be neglected. Then Eq. (4.2) is written as

$$y = \bar{y} + K(p - \bar{p}) \quad , \tag{4.3}$$

where $\bar{y} = f(\bar{p})$ and $K = \left.\frac{df}{dp}\right|_{p=\bar{p}}$.

Eq. (4.3) indicates that $(y - \bar{y})$ is proportional to $(p - \bar{p})$. A linear mathematical model Eq. (4.3) is then obtained from the nonlinear system given by Eq. (4.1). Similarly, the principle can be applied to a second order nonlinear system.

4.3 LINEARIZED EQUATION OF MOTION

The nonlinear differential equation of motion Eq. (3.25) is rewritten here as

$$(B + Cf_o)\ddot{y} + \frac{C}{2}y\ddot{y} + \frac{C}{4}\dot{y}^2 + A(f_o + \frac{y}{2})^{\frac{1}{2}} - D = 0 \quad .$$

The linearization of the equation is possible only if the nonlinear effect due to the higher derivative and square terms, $y\ddot{y}$ and $\dot{y}^2$ respectively, is small enough to be neglected. This will be seen from the comparison of the results between the nonlinear equation of motion and the linearized one.

Using the binomial theorem, the term $(f_o + \frac{y}{2})^{\frac{1}{2}}$ in Eq. (3.25) can be expressed in the following form [3.8]

$$(f_o + \frac{y}{2})^{\frac{1}{2}} = f_o^{\frac{1}{2}}\,[1 + \frac{1}{2}(\frac{y}{2f_o}) - \frac{1}{8}(\frac{y}{2f_o})^2 + \ldots\,]. \quad (4.4)$$

Ignoring the higher order terms in Eq. (4.4),

$$(f_o + \frac{y}{2})^{\frac{1}{2}} = f_o^{\frac{1}{2}}\,(1 + \frac{y}{4f_o}) \quad . \quad (4.5)$$

It is assumed that the terms $y\ddot{y}$ and $\dot{y}^2$ are very small. With the aid of Eq. (4.5), the linearized equation of motion can be obtained as

$$(B + C\ f_o)\ddot{y} + \frac{A}{4\sqrt{f_o}}\, y + (A\sqrt{f_o} - D) = 0 \quad . \tag{4.6}$$

Eq. (3.25) is linearized to a second order linear differential equation. In case of free vibrations in which the prescribed input $A\sqrt{f_o} - D = 0$, the homogeneous differential equation is of the form

$$(B + C\ f_o)\ddot{y} + \frac{A}{4\sqrt{f_o}}\, y = 0 \quad . \tag{4.7}$$

Introducing the following parameters,

$$M' = (B + C\ f_o) \quad ,$$

$$K' = \frac{A}{4\sqrt{f_o}} \quad ,$$

Eq. (4.7) can be written in the form of

$$M'\ddot{y} + K'y = 0 \quad . \tag{4.8}$$

The nonlinear differential equation is linearized to an ordinary differential equation for a simple mass-spring system. The general solution of Eq. (4.8) is known as [3.9, 4.7]

$$y = A_1 \cos \omega_\ell t + A_2 \sin \omega_\ell t \quad , \tag{4.9}$$

where A_1 and A_2 are constants, and ω_ℓ is the linear natural frequency of the system

$$\omega_\ell = \sqrt{\frac{K'}{M'}} \quad . \tag{4.10}$$

CHAPTER 5

NUMERICAL ANALYSIS

5.1 PRELIMINARIES

The governing differential equations of motion obtained by the variational principle presented in Chapter 3 are difficult to solve analytically. However, the availability of high speed digital computers have facilitated the solution to the current initial value problem. The numerical work are carried out on Honeywell Multics and CDC Cyber 175 NOS computer system. IMSL supplied subroutines, Continuous System Simulation Languages (CSSL-IV), and several subroutine subprograms are used for the numerical solution of the governing differential equations. The numerical procedures for analyzing the dynamic response characteristics of the system are described in Section 2. Both the free and forced response are undertaken in the investigation. The numerical results for free vibrations and forced vibrations of the shell are presented and discussed in Section 3. The numerical methods used are the fifth and sixth order Runge-Kutta method [4.4, 5.1 - 5.4], and the fourth order Adam-Moulton predictor-corrector method [5.5].

5.2 NUMERICAL PROCEDURES FOR RESPONSE ANALYSIS

A computer program written in FORTRAN 77 presented in Appendix C is used to solve the nonlinear differential equations of motion of the shell and to analyze the dynamic response of the system, incorporating with the mathematical model formulated in the previous chapter. The system of simultaneous first order differential equations Eq. (3.27a) and (3.27b) are evaluated for the vertical deflection at the apex and its velocity, at discrete points from time $t = 0$ to $t = 120$ seconds, i.e., the interval $0 \leqq t \leqq 120$ seconds with an increment of one second. The criteria for thin elastic shells in Eq. (2.1a) is satisfied, and the corresponding strain in the middle surface does not exceed the yield strain,

$$\varepsilon_y = \frac{\sigma_y}{E} \quad ,$$

where σ_y is the yield strength of the material. The ratio of E/σ_y can be varied between the limits 2500 to 250 [1.7, 5.6]. In other words, the limits of the corresponding strain in the middle surface can be varied between 0.0004 to 0.004. The geometrical parameters of the shells are listed in Table 5.1.

The dynamic response characteristics are classified into the *transient response* and the *steady state* response due to the nature of the input. Consider the model of a mass-spring-damper system as shown in Figure 5.1. The resultant motion depends on the initial conditions and the excitation. If the excitation is a sinusoidal input, once the system is set into motion, it will start to vibrate at its natural frequency and then will be affected by the frequency of the excitation. If the system has damping, the motion not sustained by the sinusoidal input will eventually decay. This

TABLE 5.1

Geometrical Parameters of Spherical Shells

Case	R in	h in	$\frac{R}{h}$	f_s in	$\frac{f_s}{h}$	$f_o = \frac{f_s}{R}$	Deflection Limit $y_{min} = -2f_o$
I. A.	200.	0.1	2000.	2.0	20.	0.0100	-0.020
B.				1.0	10.	0.0050	-0.010
C.				0.5	5.	0.0025	-0.005
D.				0.1	1.	0.0005	-0.001
II. A.	100.	0.1	1000.	2.0	20.	0.020	-0.040
B.				1.0	10.	0.010	-0.020
C.				0.5	5.	0.005	-0.010
D.				0.1	1.	0.001	-0.002
III. A.	50.	0.1	500.	2.0	20.	0.040	-0.080
B.				1.0	10.	0.020	-0.040
C.				0.5	5.	0.010	-0.020
D.				0.1	1.	0.002	-0.004
IV. A.	30.	0.1	300.	2.0	20.	0.0667	-0.133
B.				1.0	10.	0.0333	-0.067
C.				0.5	5.	0.0167	-0.033
D.				0.1	1.	0.0033	-0.0066

Materials Constants: Steel

Young's modulus $E = 30 \times 10^6$ psi

Unit Mass $\gamma = 0.282$ lbm/in^3

Coefficient $c = 0.19$

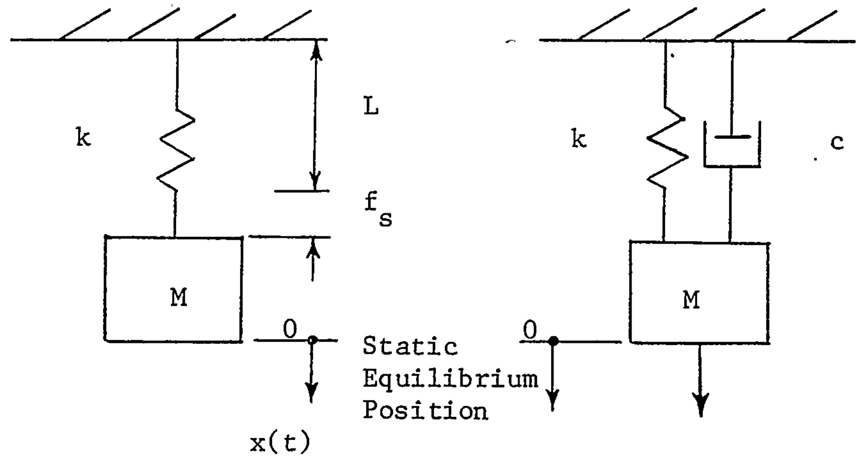

(a)
Undamped Free
Vibration

(b)
Forced
Vibration

Figure 5.1 Models of Simple Oscillatory System

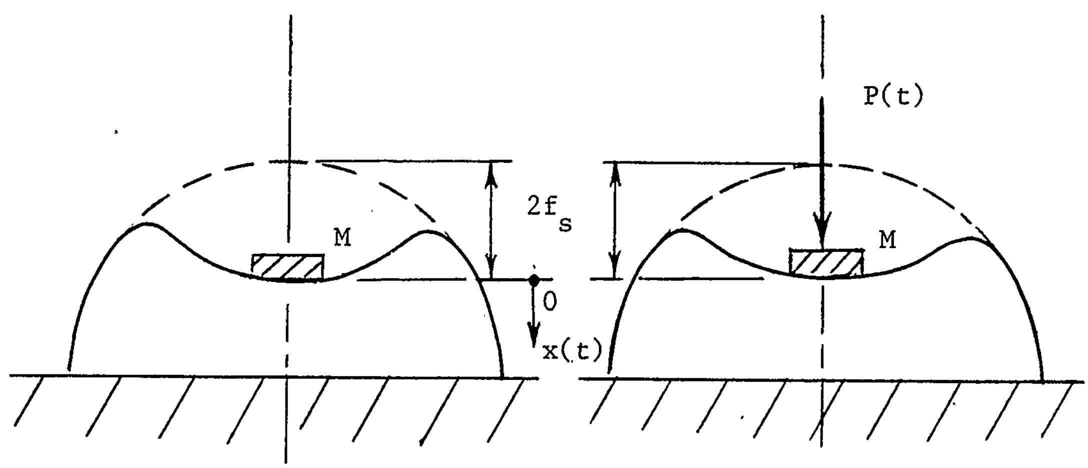

(a)
Free Vibration

(b)
Forced Vibration

Figure 5.2 Vibrations of Spherical Shells is the transient or free response which is the oscillation under free vibrations at the natural frequency of the system. The motion sustained by the sinusoidal input is the steady state response.

In other words, the motion depends on how the energy is input to the system. The initial condition, or the disturbances at time equal to zero, is an energy input. If a spring is initially elongated or compressed, the input will be potential energy. If a mass is given an initial velocity, the input will be kinetic energy. In general, the free response characterizes the behaviour of a system under an impulse or unit step input, which depends only on the initial conditions. The steady state response or frequency response is the system response caused by a periodic input.

5.2.1 FREE RESPONSE

In the investigation of the dynamic response of a spherical shell depicted in Figure 5.2a, the response due to the initial conditions, the so called free response in which all input variables vanish, is studied. Assume that the mass M is initially at rest in its static equilibrium position prior to a static deflection f_s is introduced. The coordinate of the vertical deflection x is then set at the equilibrium position. The static force P_m at the apex of the shell is evaluated from the relationship of load and deflection in Eq. (3.35). The mass M is displaced from equilibrium by an initial deflection x_o and is then released with zero initial velocity. In the computer program, the geometrical parameters, material constants, as well as the initial conditions for deflection x_o and velocity $\dot{x}_o$ are introduced. For convenience in comparing the free response of shells in various cases, it is a common practice to use a standard initial condition that the system is initially at rest. The vertical deflection at the apex and its velocity as a function of time are evaluated for the total time interval of 120 seconds. The dynamic response characteristics are studied through the deflection response curve and phase plane diagram, which indicates the stability of the oscillatory system. The discussion of the results will be given in the next sections.

5.2.2 FORCED RESPONSE

The forced response of the system to a sinusoidal input is observed. Consider the spherical shell shown in Figure 5.2b. The application of a sinusoidal force at the apex of the shell is studied. The forcing function is of the form

$$P(t) = P_m + \alpha P_m \sin \omega_e t \quad ,$$

where P_m is the static force, ω_e is the forcing frequency, and α is the dynamic load factor of the sinusoidal input function which is a constant. The amplitude of the sinusoidal input function is held constant, while its frequency is varied slowly; and the amplitude of the system response is then observed. For further investigation, the forcing frequency is fixed, and the amplitude factor of the sinusoidal input function is varied. In the computer program, the amplitude of the sinusoidal force is input by the dynamic load factor α. Similarly, the geometrical parameters and material constants are also introduced. It is noted that zero initial conditions are input and that the vertical deflection $y(t)$ at the apex and its velocity $\dot{y}(t)$ are evaluated for the total time interval of 256 seconds.

5.2.3 FREQUENCY ANALYSIS

The technique of fast Fourier transform simplifies the analysis of the complex waveform of the deflection response. IMSL supplied subroutine is used to transform the 256 data points of deflection response in time domain into a sum of sinusoids of different frequencies. The transform analysis distinguishes the different frequency sinusoids and their respective amplitudes, which combines to give the original deflection waveform in time domain. A general review for the Fourier transform is given here. Detailed derivation or theoretical development is beyond the scope of the work. For convenience, references [5.2, 5.7 - 5.10] are listed here.

The Fourier transform is a frequency domain representation of a function. The Fourier transform frequency domain contains exactly the same information as the original function. The Fourier transform of a waveform is to decompose the waveform into a sum of sinusoidals of different frequencies. Mathematically, the Fourier transform S(f) is defined by the complex quantity,

$$S(f) = \int_{-\infty}^{\infty} s(t)\ e^{-j2\pi ft} dt \quad , \tag{5.1}$$

where s(t) is the waveform to be decomposed into a sum of sinusoids, S(f) is the Fourier transform of s(t).

Restricting the limits to a finite time interval of x(t) in the range, $0 \leqq x(t) \leqq T$, the finite range of Fourier transform is defined as

$$S(f,T) = \int_{0}^{T} s(t)\ e^{-j2\pi ft} dt \quad . \tag{5.2}$$

Numerical integration of Eq. (5.2) gives the discrete Fourier transform (DDT)

$$S(f) = \sum_{i=0}^{N=1} s(t_i)\ e^{-j2\pi fk\ t_i}\ (t_{i+1} - t_i) \quad , \tag{5.3}$$

where k = 0, 1, ..., N-1.

If there are N data points of function $s(t_i)$ and the amplitude of N different sinusoids to be determined, the total work computing the full sequence S(f) will require N^2 multiplications. In 1965, Cooley and Tukey [5.11] presented a computational algorithm known as the fast Fourier transform. The FFT reduces the work of computing discrete Fourier transfrom Eq. (5.3) to a number of operations of order $N\log_2 N$. For example, if the number of data points N is 256 as required in the computer calculation, the square of N will be 65536. However, $N\log_2 N = 2048$, which is only about 1/32th. of the number of operations. There is an increase in accuracy and reduction in round-off error since fewer operations are performed by the computer.

5.3 NUMERICAL RESULTS

The numerical approximations of the vertical deflection y and velocity $\dot{y}$ of the apex point were evaluated for the analysis of free and forced vibrations of the shell, by the use of the theoretical model and application of numerical techniques discussed in the previous sections. The maximum and minimum nondimensional values y, for free vibrations of spherical shells loaded by static forces, are summarized in Tables 5.2 - 5.4. The relationship between the applied static load and linear natural frequency for R/h = 2000. and 1000. is presented in Table 5.5. The corresponding values of analytically measured frequency from the numerical results and linear frequency are compared in Table 5.6. Results for the case of forced vibrations of the shell, under the action of a concentrated force of sinusoidal input, are presented in Tables 5.7 - 5.10.

The results of analysis for the relationship between an applied static load and the resulting deflection are obtained from the equation of equilibrium (3.35) and (3.45). Typical nondimensional load and deflection curves are compared for all cases as listed in Table 5.1. The results are depicted in Figures 5.3 to 5.9.

TABLE 5.2

Comparison of Deflection Response of Free Vibration (Case I)

R = 200. in   h = 0.1 in   R/h = 2000.

Case	f_s (in)	$\frac{f_s}{h}$	$-2f_o$ ($\cdot 10^{-2}$)	x_o (in)	$\frac{x_o}{h}$	$y = \left\lvert \frac{x}{R} \right\rvert \cdot 10^{-2}$ Maximum Deflection, Runge-Kutta Method, Inward	Runge-Kutta Method, Outward	Number of Equations Evaluation	$y = \left\lvert \frac{x}{R} \right\rvert \cdot 10^{-2}$ Maximum Deflection, Adam-Moulton Method, Inward	Adam-Moulton Method, Outward	Computed Time (sec)
I A.	2.0	20.	-2.0	0.01	0.10	0.005	0.005	968.	0.005	0.005	87.
				0.10	1.00	0.055	0.050	968.	0.050	0.050	76.
				1.00	10.00	0.530	0.048	1701.	0.500	0.048	159.
				2.00	20.00	1.000	0.800	1818.	1.000	0.093	110.
				3.98	39.80	--	--	--	1.990	1.664	24.
				4.80*	48.00	--	--	--	2.400	1.968	67.
Linear	2.0	20.	-2.0	3.98*	39.80	--	--	--	1.998	1.998	32.
B.	1.0	10.	-1.0	0.01	0.10	0.020†	0.018†	1965.	0.005	0.005	163.
				0.10	1.00	0.054†	0.048†	1920.	0.050	0.050	191.
				1.00	10.00	0.050†	0.040†	2706.	0.530	0.048	44.
				1.96	19.60	--	--	--	0.980	0.815	48.
				2.00	20.00	1.000†	0.080†	4477.	1.000	0.830	84.
				2.25*	22.50	--	--	--	1.170	0.978	45.
Linear	1.0	10.	-1.0	1.96*	19.60	--	--	--	0.980	0.980	97.
D.	0.1	1.0	-0.1	0.01	0.10	0.010†	0.006†	9478.	0.005	0.005	187.
				0.10	1.00	†	†	14400.	0.050	0.046	176.
				0.199	1.99	--	--	--	0.098	0.083	137.
				0.20	2.00	†	†	10869.	0.100	0.085	159.
				0.25*	2.50	--	--	--	0.125	0.099	67.
Linear	0.1	1.0	-0.1	0.199*	1.99	--	--	--	0.100	0.100	146.

* Critical Initial Condition   -- Not Evaluated   † Divergent Solution

TABLE 5.3

Comparison of Deflection Response of Free Vibration (Case II)

R = 100. in   h = 0.1 in   R/h = 1000.

Case	f_s (in)	$\frac{f_s}{h}$	$-2f_o$ (10^{-2})	Initial Condition x_o (in)	Initial Condition $\frac{x_o}{h}$	$y = \left\|\frac{x}{R}\right\| \cdot 10^{-2}$ Maximum Deflection Runge-Kutta Method Inward	Runge-Kutta Method Outward	Number of Equations Evaluation	$y = \left\|\frac{x}{R}\right\| \cdot 10^{-2}$ Maximum Deflection Adam-Moulton Method Inward	Adam-Moulton Method Outward
II A.	2.0	20.	-4.0	0.01	0.1	0.010	0.010	2158.	0.010	0.010
				1.00	10.0	1.000	1.000	3377.	1.020	0.978
				2.00	20.0	2.000	1.800	4097.	2.066	1.885
				3.47	34.7	--	--	--	3.470	2.977
				5.00*	50.0	--	--	--	5.000	3.970
Linear	2.0	20.	-4.0	3.47*	34.7	--	--	--	3.999	3.999
B.	1.0	10.	-2.0	0.01	0.1	0.020†	0.030†	3136.	0.010	0.010
				0.10	1.0	†	†	3643.	0.104	0.103
				1.00	10.0	†	†	6570.	1.050	0.950
				1.99	19.9	--	--	--	1.942	1.650
				2.00	20.0	†	†	9079.	2.000	1.670
				2.40*	24.0	--	--	--	2.500	2.020
Linear	1.0	10.	-2.0	1.99*	19.9	--	--	--	1.997	1.997
D.	0.1	1.0	-0.2	0.01	0.1	0.018†	0.018†	15527.	0.010	0.010
				0.10	1.0	†	†	22864.	0.100	0.092
				0.20	2.0	†	†	Terminated	0.200	0.169
				0.22	2.2	--	--	--	0.220	0.182
				0.25*	2.5	--	--	--	0.250	0.200
Linear	0.1	1.0	-0.2	0.22*	2.2	--	--	--	0.220	0.206

* Critical Initial Condition   -- Not Evaluated   † Divergent Solution

TABLE 5.4

Comparison of Deflection Response of Free Vibration Under Large Deflections (Case II)

R = 100. in   h = 0.1 in   R/h = 1000.

Case	f_s (in)	$\frac{f_s}{h}$	$-2f_o \cdot 10^{-2}$	Initial Condition x_o (in)	Initial Condition $\frac{x_o}{h}$	Maximum Deflection $y = \left\lvert \frac{x}{R} \right\rvert \cdot 10^{-2}$ Runge-Kutta Inward	Runge-Kutta Outward	Number of Equation Evaluation	Adam-Moulton Inward	Adam-Moulton Outward
II E.	15.0	150.	-30.	0.01	0.1	0.01	0.01	968.	0.01	0.01
				0.10	1.0	0.10	0.10	968.	0.10	0.10
				2.00	20.0	2.00	2.00	968	2.00	1.97
				10.00	100.0	10.00	9.50	1016.	10.00	9.47
				15.00	150.0	15.00	13.81	1302.	15.00	13.82
				20.00	200.0	20.00	17.76	1340.	20.00	17.93
				29.90	299.0	--	--	--	29.97	25.30
				40.00*	400.0	--	--	--	40.00	30.70
Linear	15.0	150.	-30.	29.90*	299.0	--	--	--	29.99	29.99
F.	10.0	100.	-20.	10.0	100.0	10.00	9.20	1464.	10.00	9.22
				19.9	199.0	--	--	--	19.99	16.78
				25.0*	250.0	--	--	--	25.00	20.00
Linear	10.0	100.	-20.	19.9*	199.0	--	--	--	19.90	19.90
G.	20.0	200.	-40.	20.0	200.0	20.0	18.30	1117.	20.00	18.43
				39.9	399.0	--	--	--	39.93	33.74
				50.0*	500.0	--	--	--	50.00	39.95
Linear	20.0	200.	-40.	39.9*	399.0	--	--	--	39.97	39.92

* Critical initial condition -- Not evaluated

TABLE 5.5

Summary of Frequency Response of Free Vibration

CASE I   R = 200. in   h = 0.1 in   R/h = 2000.

Case	f_s in	$\frac{f_s}{h}$	$-2f_o \cdot 10^{-2}$	Measured Frequency rad/sec Runge-Kutta	Measured Frequency rad/sec Adam-Moulton	Linear Frequency ω_ℓ(rad/sec)
I. A.	2.0	20.	-2.0	1.621	1.747	1.678
B.	1.0	10.	-1.0	2.859	2.890	2.790
D.	0.1	1.	-0.1	†	15.700	14.480

CASE II   R = 100. in   h = 0.1 in   R/h = 1000.

Case	f_s in	$\frac{f_s}{h}$	$-2f_o \cdot 10^{-2}$	Measured Frequency rad/sec Runge-Kutta	Measured Frequency rad/sec Adam-Moulton	Linear Frequency ω_ℓ(rad/sec)
II. A.	2.0	20.	-4.0	3.707	3.142	3.098
B.	1.0	10.	-2.0	†	5.234	5.008
D.	0.1	1.0	-0.2	†	3.846	3.587
E.	15.0	150.	-30.	0.679	0.685	0.731
F.	10.0	100.	-20.	0.993	1.013	0.982
G.	20.0	200.	-40.	0.628	0.628	0.593

† Divergent solution

TABLE 5.6

Relationship between Applied Static Load and Linear Natural Frequency

R	h	$\frac{R}{h}$	f_o	$\frac{f_s}{h}$	ω_ℓ^2	P_m
in	in				$(rad/sec)^2$	lbf
200.	0.1	2000.	0.1	1.0	209.770	379.81
			0.5	5.0	17.640	849.28
			1.0	10.0	7.780	1201.07
			2.0	20.0	2.820	1698.56
			15.0	150.0	0.142	4651.70
			20.0	200.0	0.093	5371.33
100.	0.1	1000.	0.01	0.1	7507.5	240.21
			0.1	1.0	508.1	759.62
			0.5	5.0	64.0	1698.56
			1.0	10.0	25.1	2402.13
			2.0	20.0	9.0	3397.1

TABLE 5.7

Dynamic Response of Forced Vibration

at Constant Dynamic Load Factor $\alpha = 0.1$

R	h	$\frac{R}{h}$	f_s	$\frac{f_s}{h}$	$f_o = \frac{f_s}{R}$	$-2f_o \cdot 10^{-2}$	ω_ℓ
in	in		in				rad/sec
100.	0.1	1000.	2.0	10.	0.02	-4.00	3.098

Forcing Frequency ω_e	Dynamic Load Factor α	Maximum Deflection $y = \left\lvert\frac{x}{R}\right\rvert \cdot 10^{-2}$ Inward	Outward	Forcing Frequency ω_e	Dynamic Load Factor α	Maximum Deflection $y = \left\lvert\frac{x}{R}\right\rvert \cdot 10^{-2}$ Inward	Outward
0.1	0.1	0.866	0.790	5.0	"	1.634	1.228
0.5	"	1.010	0.926	5.5	"	1.365	0.930
1.0	"	1.335	1.152	5.8	"	1.779	1.08
2.0	"	2.176	2.422	5.9	"	3.300	2.434
2.5	"	3.327	3.561	6.0	"	4.910	3.926
2.6	"	3.971	3.844	6.1	"	10.750	5.854
2.7	"	4.754	4.270	6.2	"	31.830	9.362
2.8	"	13.699	6.343	6.21	"	39.172	8.890
3.0	"	37.540	9.786	6.3	"	11.527	6.076
3.05	"	70.289	13.516	6.5	"	1.698	1.897
3.2	"	47.788	10.86	7.0	"	0.647	0.785
3.4	"	6.911	4.684	8.0	"	0.532	0.563
3.5	"	6.138	4.272	9.3	"	0.822	0.793
3.6	"	4.969	3.701	10.0	"	0.379	0.382
4.0	"	3.021	2.361				

TABLE 5.8

Dynamic Response for Forced Vibration

at Constant Dynamic Load Factor $\alpha = 0.3$

R in	h in	$\frac{R}{h}$	f_s in	$\frac{f_s}{h}$	$f_o = \frac{f_s}{R}$	$-2f_o \cdot 10^{-2}$	ω_ℓ rad/sec
100.	0.1	1000.	2.0	20.	0.02	-4.00	3.098

Forcing Frequency ω_e rad/sec	Dynamic Load Factor α	Maximum Deflection $y=\left\|\frac{x}{R}\right\| \cdot 10^{-2}$ Inward	Outward	Forcing Frequency ω_e rad/sec	Dynamic Load Factor α	Maximum Deflection $y=\left\|\frac{x}{R}\right\| \cdot 10^{-2}$ Inward	Outward
0.1	0.3	2.842	2.151	3.2	0.3	50.993	12.686
0.5	"	3.479	2.586	3.5	"	22.030	8.026
1.0	"	4.888	3.857	3.6	"	14.482	6.043
1.01	"	36.919	9.590	4.0	"	8.057	4.211
1.2	"	4.879	4.422	5.0	"	5.290	2.537
1.4	"	15.427	6.400	5.5	"	6.806	4.336
1.5	"	42.799	12.118	5.8	"	30.082	8.953
1.7	"	36.400	10.037	5.9	"	41.173	11.481
1.8	"	30.630	7.371	6.1	"	70.190	12.250
2.0	"	50.490	12.287	6.3	"	48.683	10.758
2.5	"	14.90	6.489	6.5	"	18.720	6.145
2.6	"	126.07	33.80	7.0	"	3.172	3.031
2.7	"	42.887	9.673	8.0	"	1.443	1.646
2.8	"	40.270	9.348	9.0	"	1.645	1.284
2.9	"	36.669	11.439	9.2	"	24.068	6.602
3.0	"	127.59	13.960	10.0	"	1.044	1.062

TABLE 5.9

Dynamic Response of Forced Vibration

at Constant Dynamic Load Factor $\alpha = 0.5$

R in	h in	$\frac{R}{h}$	f_s in	$\frac{f_s}{h}$	$f_o = \frac{f_s}{R}$	$-2f_o \cdot 10^{-2}$	ω_ℓ rad/sec
100.	0.1	1000.	2.0	20.	0.02	-4.00	3.098

Forcing Frequency ω_e rad/sec	Dynamic Load Factor α	Maximum Deflection $y=\left\|\frac{x}{R}\right\|\cdot 10^{-2}$ Inward	Outward	Forcing Frequency ω_e rad/sec	Dynamic Load Factor α	Maximum Deflection $y=\left\|\frac{x}{R}\right\|\cdot 10^{-2}$ Inward	Outward
0.1	0.5	5.201	3.345	3.6	"	21.707	7.261
0.3	"	5.679	3.508	4.0	"	39.312	8.611
0.5	"	6.061	3.639	5.0	"	29.110	8.392
0.6	"	6.561	3.920	5.5	"	13.410	6.234
0.7	"	16.723	7.758	5.9	"	37.625	10.406
0.8	"	7.623	6.118	6.0	"	72.049	12.044
0.9	"	20.560	7.123	6.1	"	66.681	14.716
1.0	"	495.481	33.885	6.2	"	33.923	8.303
1.5	"	69.595	12.489	6.26	"	730.760	31.856
2.0	"	121.190	25.478	6.3	"	41.960	11.002
2.2	"	47.020	11.409	6.5	"	32.033	10.340
2.3	"	122.836	14.299	7.0	"	12.336	6.106
2.4	"	91.059	13.093	8.0	"	3.014	2.748
2.8	"	59.645	12.094	8.5	"	2.821	2.424
3.0	"	65.690	12.490	8.9	"	69.102	12.085
3.05	"	107.637	14.698	9.1	"	43.598	10.666
3.09	"	1286.560	47.366	9.2	"	36.407	8.775
3.1	"	39.308	11.533	9.28	"	99.479	14.006
3.2	"	39.276	9.174	9.5	"	17.027	6.406
3.4	"	19.078	7.579	10.0	"	1.707	1.771

TABLE 5.10

Dynamic Response of Forced Vibration

at Constant Forcing Frequency $\omega_e = 0.1$ rad/sec

R	h	$\frac{R}{h}$	f_s	$\frac{f_s}{h}$	$f_o = \frac{f_s}{R}$	$-2f_o$	ω_ℓ
in	in		in			$\cdot 10^{-2}$	rad/sec
100.	0.1	1000.	2.0	20.	0.02	-4.0	3.098

ω_e rad/sec	α	Maximum Deflection $y=\left\lvert \frac{x}{R} \right\rvert \cdot 10^{-2}$ Runge-Kutta Method Inward	Outward	Number of Equations Evaluations	Computed Time (sec)	Maximum Deflection $y=\left\lvert \frac{x}{R} \right\rvert \cdot 10^{-2}$ Adam-Moulton Method Inward	Outward	Computed Time (sec)
0.1	0.1	1.000	0.900	4039.	16.1	0.866	0.790	50.0
"	0.2	1.800	1.600	4092.	15.6	1.816	1.504	48.0
"	0.4	3.900	2.700	5382.	17.6	3.973	2.756	39.0
"	0.5	--	--	--	--	5.198	3.344	58.0
"	0.6	--	--	--	--	6.554	3.683	36.0
"	0.7	--	--	--	--	7.754	3.742	40.0
"	0.72	--	--	--	--	8.043	3.778	52.0
"	0.74	--	--	--	--	8.332	3.902	41.0
"	1.00	†	†	14608.	36.4	12.275	5.204	45.0
"	1.50	†	†	21360.	45.3	21.500	4.730	48.0

-- Not Evaluated † Divergent Solution

Measured Frequency for All Cases is 0.098 rad/sec.

5.4 DISCUSSION OF RESULTS

The preceeding formulation has been tested on various geometrical parameters of spherical shells. The emphasis has been on several numerical examples for which the solutions are compared with results from two different numerical methods to assess the accuracy of the simplified theoretical model. The analysis of the numerical results, presented in Tables 5.2 - 5.10, indicates that the applicability of the simplified theoretical model to the current vibration problem is acceptable. However, the simplified relation for the energy in the ridge region, Eq. (3.12) may introduce certain errors into the expressions of the energy functional, which has been based on the simplified assumptions of isometric deformation of the shell.

5.4.1 LOAD AND DEFLECTION ANALYSIS

Typical results of the nondimensional applied load and the corresponding static deflection are compared for various geometrical parameters listed in Table 5.1. In Figures 5.3 - 5.4, the ratio of radius of curvature to thickness R/h is held constant, and the static deflection ratio f_s/h is increased from one to twenty. The point of zero deflection, shown as the origin of the coordinate of the shell in Figure 3.2, is the position of static equilibrium about which the shell vibrates. The inward deflection from equilibrium is considered positive in the curves. The limit of outward deflection from equilibrium is defined as

$$x_{min} = -2f_s \quad ,$$
$$y_{min} = -2f_o \quad . \tag{5.54}$$

It is twice the value of static deflection, i.e., $2f_s$. The results of analysis show a *nonlinear softening behaviour* associated with the stiffness and geometry of the shell when the shell is inwardly deflected from the apex towards the radius of curvature, corresponding to the range of $x \geqq -2f_s$. This behaviour is observed as the deflection increases rapidly with a slow increase of loading. The slope of the curve goes to zero under large deflection as shown in Figure 5.5. From the equation of static equilibrium (3.35),

$$\frac{\partial P}{\partial x} = \frac{3\sqrt{2}\ \pi c E\ h^{5/2}}{4R\sqrt{f_s + \frac{x}{2}}} \quad . \tag{5.5}$$

If the total deflection $f_s + \frac{x}{2}$ goes to infinity, the slope will be zero, $\frac{\partial P}{\partial x} = 0$. The softening behaviour has been confirmed in recent analysis of nonlinear vibration of cylindrical shells [5.12 - 5.14] and large deflection of spherical shells [1.13 and 1.18]. Similar equation of static equilibrium (3.35) has been obtained previously by Pogorelov's theory [1.1, p.40], and the results have been compared with Penning's experiments [1.7, p.466].

If the shell is outwardly deflected from the apex in the range of $x < -2f_s$, the results show that the stiffness of the shell increases. It may be noted from the steep slope of the curve for $x < -2f_s$ in Figure 5.5. The hardening behaviour is predicted as the shell is outwardly deflected from the equilibrium position. From Eq. (5.5), as $f_s + \frac{x}{2} = 0$, $\frac{\partial P}{\partial x} \to \infty$. The slope of the curve is much steeper than the slope of the linear approximation equation shown by a dotted line in Figure 5.5 used in the range. In other words, the steeper the slope of the curve, the harder the stiffness of the shell will be when the shell outwardly deflects from equilibrium. The deviation of slope of the linear approximation from that of the theoretical model becomes significant when the thickness of the shell is increased as the R/h ratio decreases from 2000. to 300. A comparison of the results for different R/h ratio with constant static deflections are presented in Figures 5.6 - 5.9. The linear approximated equation of static equlibrium (3.45) of the actual nonlinear behaviour of the outward deflection is only sufficiently accurate for deflections of the same order as the thickness.

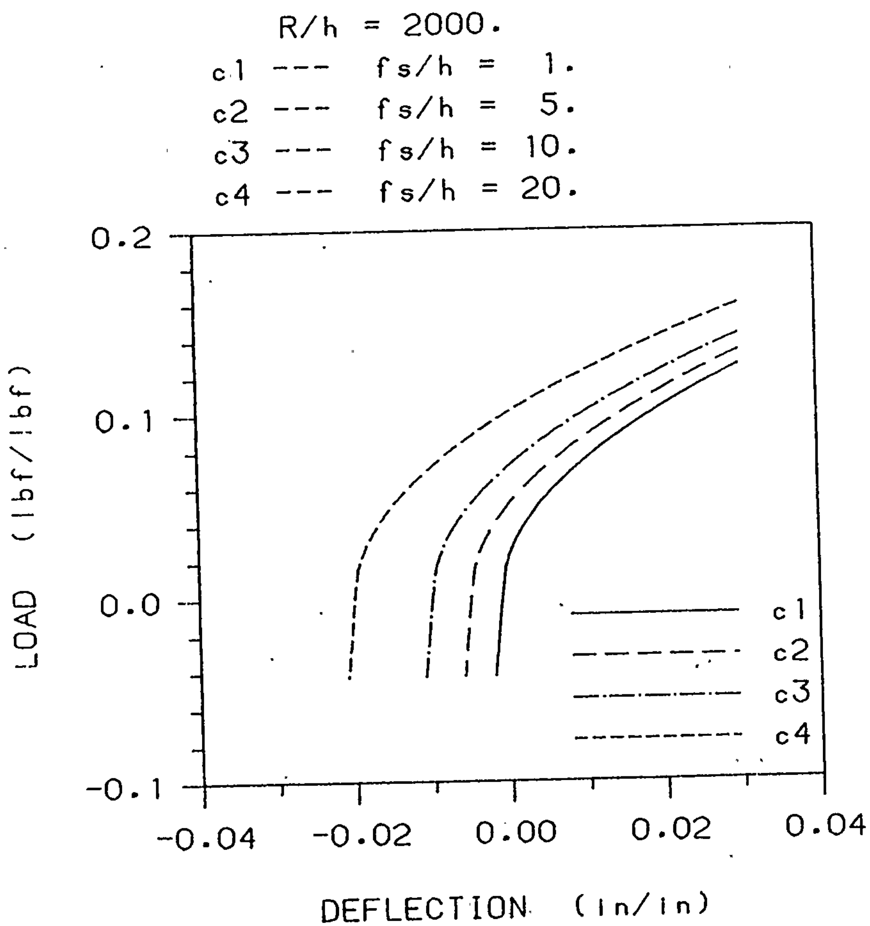

Figure 5.3 Comparison of Load-Deflection Curves for Different Static Deflection Ratios at Constant R/h = 2000.

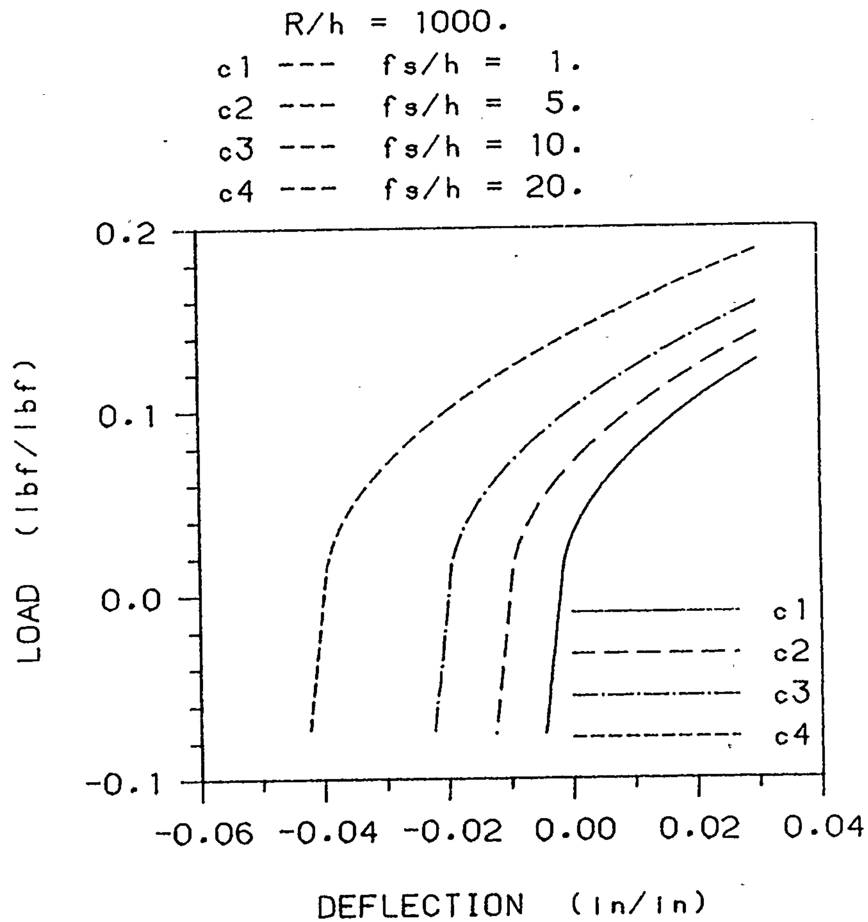

Figure 5.4 Comparison of Load-Deflection Curves for Different Static Deflection Ratios at Constant R/h = 1000.

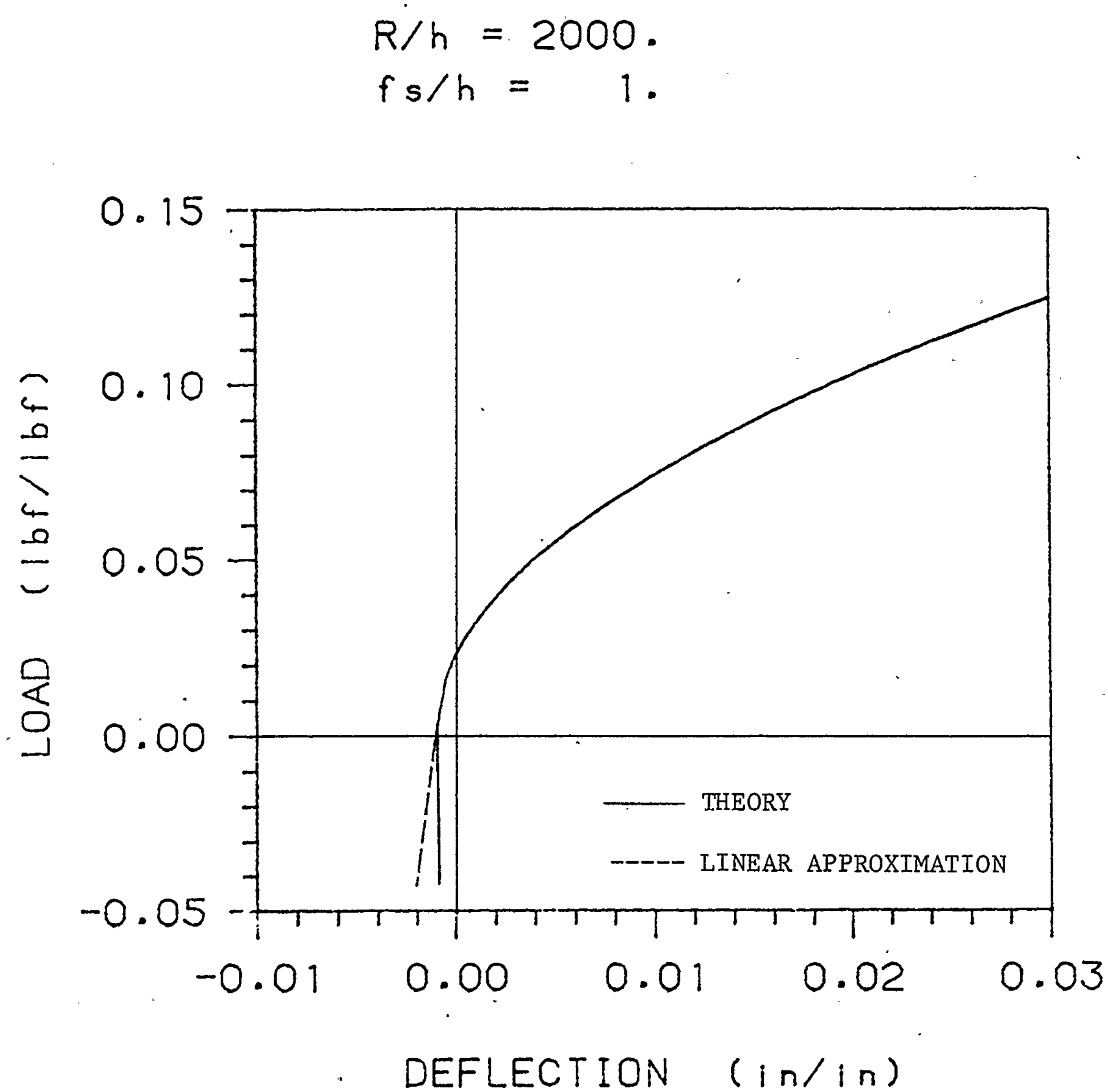

Figure 5.5 Load-Deflection Curve at Constant R/h = 2000. and f_s/h = 1. for Comparing the Theoretical Model and Linear Approximation

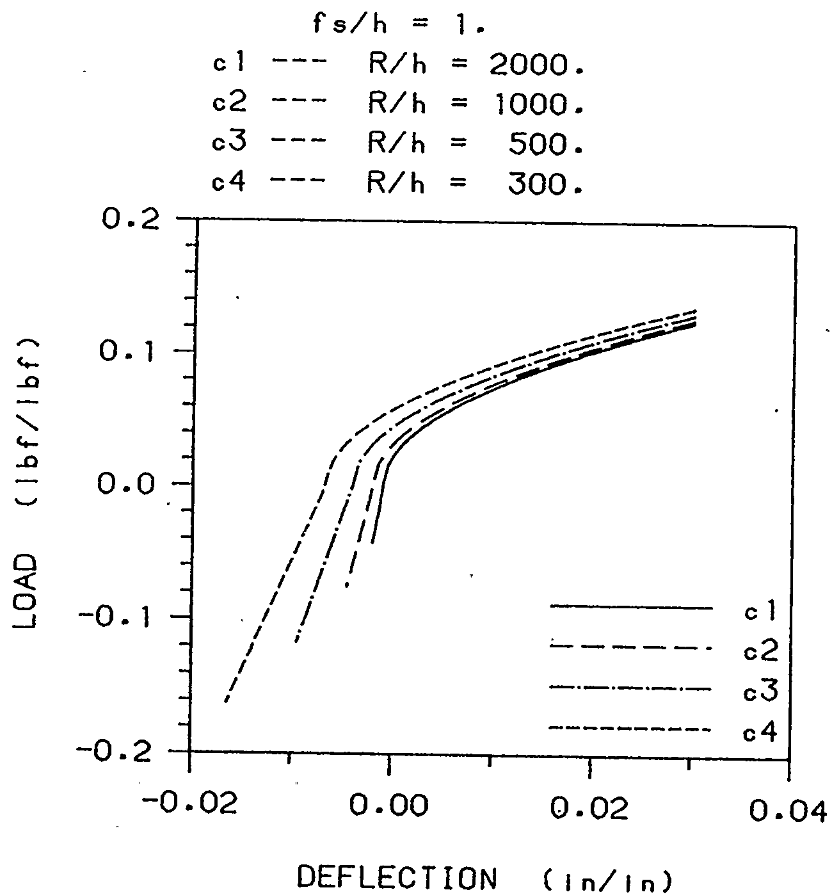

Figure 5.6 Comparison of Load-Deflection Curves for Different R/h Ratios at Constant $f_s/h = 1$.

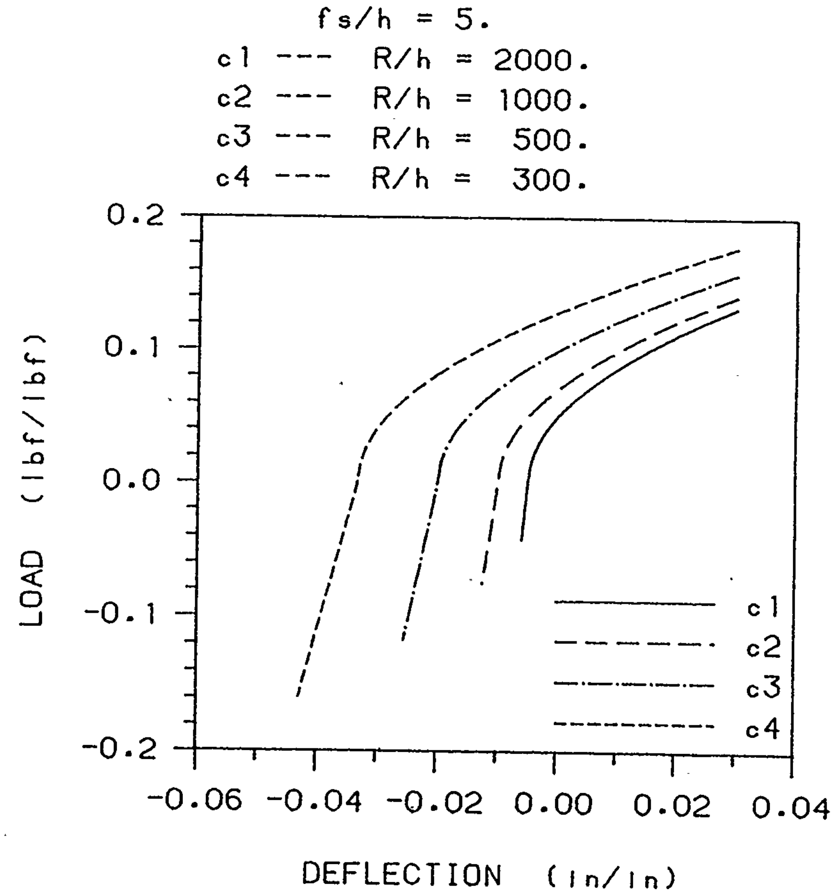

Figure 5.7 Comparison of Load-Deflection Curves for Different R/h Ratiós at Constant $f_s/h = 5$.

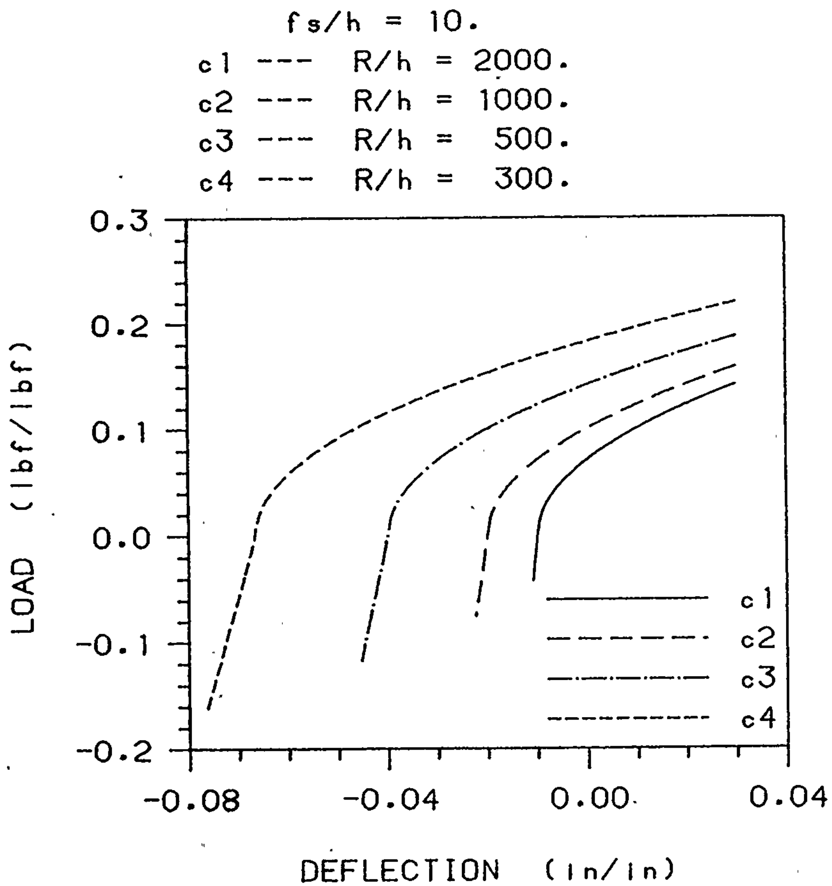

Figure 5.8 Comparison of Load-Deflection Curves for Different R/h Ratios at Constant $f_s/h = 10$.

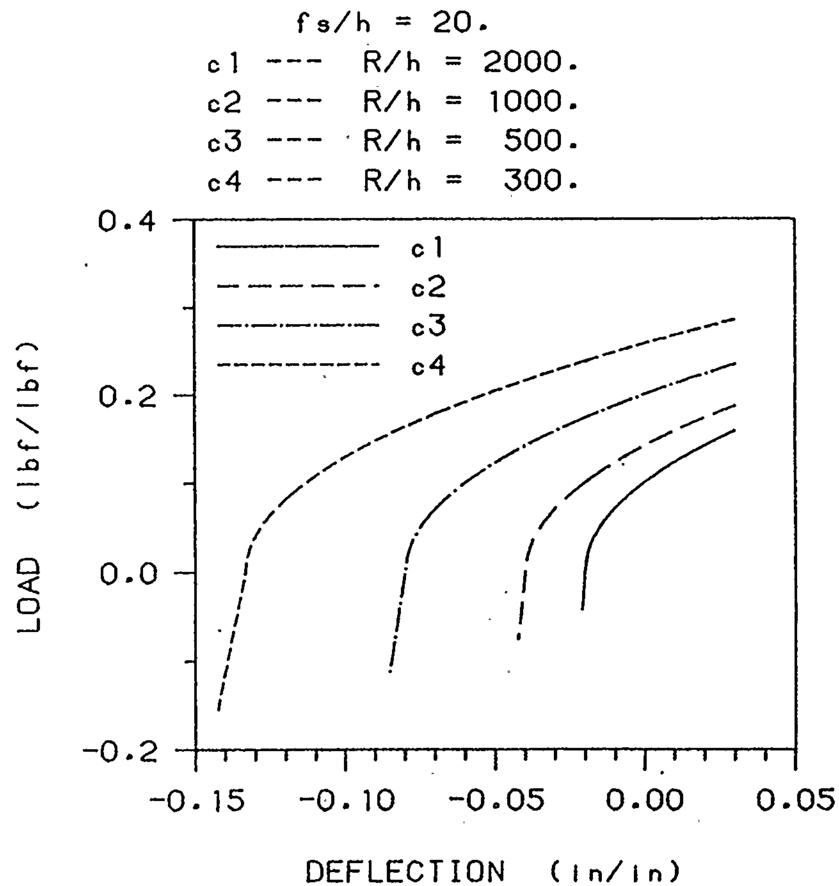

Figure 5.9 Comparison of Load-Deflection Curves for Different R/h Ratios at Constant $f_s/h = 20$.

5.4.2 FREE VIBRATION

Typical results of vertical apex deflection response, corresponding to the ratio of R/h = 2000 in Case I A, I B, and I D of Table 5.2, are shown in Figures 5.10 - 5.11, 5.12 - 5.14, and 5.15, respectively. For R/h = 1000 in Case II, typical results are presented in Figure 5.16. These results were obtained from the Runge-Kutta method, and the instability of the solution in Figure 5.10 - 5.11 was due to the insufficiently small step size as adjusted by the supplied subroutine. With decreasing static deflection f_s/h, in Tables 5.1 and 5.2, the solutions become divergent and unstable after the first ten seconds as shown in Figures 5.12 - 5.16. The results obtained from the linearization of the equation of motion as shown in Figure 5.14 are unsatisfactory because of the instability of the solutions. Therefore, Adam-Moulton predictor-corrector method in the CSSL-IV simulation language is used to compare the results, which are discussed further. However, the increase in static deflection f_s/h improves the convergence and stability of the solutions for all cases presented in Table 5.4. The number of equation evaluations in the subroutine is significantly decreasing. The results for free vibrating shells under large deflections are presented in Figures 5.17 - 5.22, corresponding to the ratio of R/h = 1000 in Case II E of Table 5.4. Typical results for static deflection ratio f_s/h of 100 in Case II F, and of 200 in Case II G are also shown in Figures 5.23 and 5.24 respectively.

The relationship between the nondimensional deflection $y = \frac{x}{R}$ and time t is shown in the curves. As time increases, the amplitude of free vibrations does not decay. The results show that the system has no damping effect. The irregularity of the amplitude of deflection is observed at the peaks of the response. This may relate to the truncation errors in the numerical approximation. The point of zero deflection is the static equilibrium position, and the outward deflection from equilibrium is considered negative in the curves. When the shell is outwardly deflected from equilibrium exceeding the limit of outward deflection Eq. (5.4), such that, $x < -2f_s$, the equation of motion (3.44) is used for the approximation in this range.

The results of analysis obtained by the Adam-Moulton method in the CSSL-IV simulation language are summarized in Tables 5.2-5.4. The maximum amplitudes of inward and outward deflection are compared for all cases. The critical input initial deflection, denoted by x_o^*, has been obtained in each case. Exceeding the critical initial conditions of deflection, the shell will deflect in an outward direction over the limit of outward deflection, i.e. $y < -2f_o$, and the divergence of the results will be obtained. Typical results obtained by the Adam-Moulton method are depicted in Figures 5.25 - 5.31, 5.32, and 5.33, corresponding to R/h = 2000 in Case I A, I B, and I D of Table 5.2, respectively. A comparison of the results presented in Figures 5.25 - 5.26 with the results from

Runge-Kutta Method, corresponding to Figures 5.10 - 5.11, indicates the improvement of the stability in the solutions. However, the step size used in the Adam-Moulton method is 0.1 which is ten times less than that in Runge-Kutta for this particular case. Typical results from linearization are shown in Figures 5.28. It is noticed from the results that the damping in the present nonlinear model has no effect on the system and that the shell vibrates almost at the same frequency as the natural frequency in the linear case.

The phase plane diagram describing the response of the system to initial conditions is depicted in Figure 5.27. The motion is periodic in time, and the trajectory is an ellipse centred at the origin. The system is in neutral equilibrium.

Numerical values of vertical deflection resulting from the Adam-Moulton predictor corrector method are, in general, higher than the values obtained from the adaptive Runge-Kutta method. However, the step size used in the Runge-Kutta method is 10 to 2.5 times larger than that used in Adam-Moulton method to obtain results of desired accuracy, and the accumulated truncation error in the Runge-Kutta method is also increasing. Moreover, there are too many steps required to cover a fixed time interval in the Runge-Kutta method, and the accumulated round-off error is larger than that in Adam-Moulton method. From Tables 5.2 - 5.4, it is noticed that the number of equation evaluations in the Runge-Kutta method was very large for shells with the lowest f_s/h ratio. The convergence was slow, and a progressive increase of computational time was observed with increasing x_o/h ratio. The computation was terminated for x_o/h ratio higher than 2.0 in Case II D of Table 5.3. The results for the lowest f_s/h ratio are not recorded in Tables 5.2 - 5.3 due to the divergence of the solutions. With increasing R/h and f_s/h ratios, the number of equation evaluations is significantly decreasing. In general, the results show that a small initial step size is required to obtain the same accuracy in the Adam-Moulton method. However, the step size is chosen and adjusted by the adaptive Runge-Kutta method, and a larger step size is usually taken. The results of calculations between the two numerical methods differ a little in detail, but the overall agreement has been confirmed.

In a nonlinear system, the free response depends only on the system equations and initial conditions. The frequency of vibration is no longer a particular constant. However, the linear natural frequency is used to predict the frequency of vibration of the nonlinear system, and the frequency measured from the numerical results has been compared, where possible, with the linear frequency as shown in Table 5.5. The largest difference is only 8.4% for the case of the lowest f_s/h ratio. Such a small difference shows that the system is vibrating almost at the same frequency as the linear system.

The variation of frequency of vibration with the applied force is shown in Figures 5.34, corresponding to Table 5.6. As the applied static force increases, the frequency of free vibrations of the shell decreases until it vanishes. The system is in divergent and is no longer vibrating. Similar results of the dynamic analysis of stability of a bar were obtained by Vol'mir [5.15]. For a conservative system free vibrations of a simply supported bar under the action of axial compressive forces at the ends are considered. The relation between the frequency of vibration and the compressive force is shown in Figure 5.35. As the force P increases, the natural frequency of vibration ω decreases until P reaches the critical load. At $P = P_{cr}$, the natural frequency approaches to zero, and the beginning of the instability of the bar is characterized by the vanishing frequency of free vibration. Therefore, the natural frequency of vibration depends inversely on the compressive force.

FREE-VIBRATION RESPONSE USING RUNGE-KUTTA METHOD

FIGURES 5.10 - 5.24

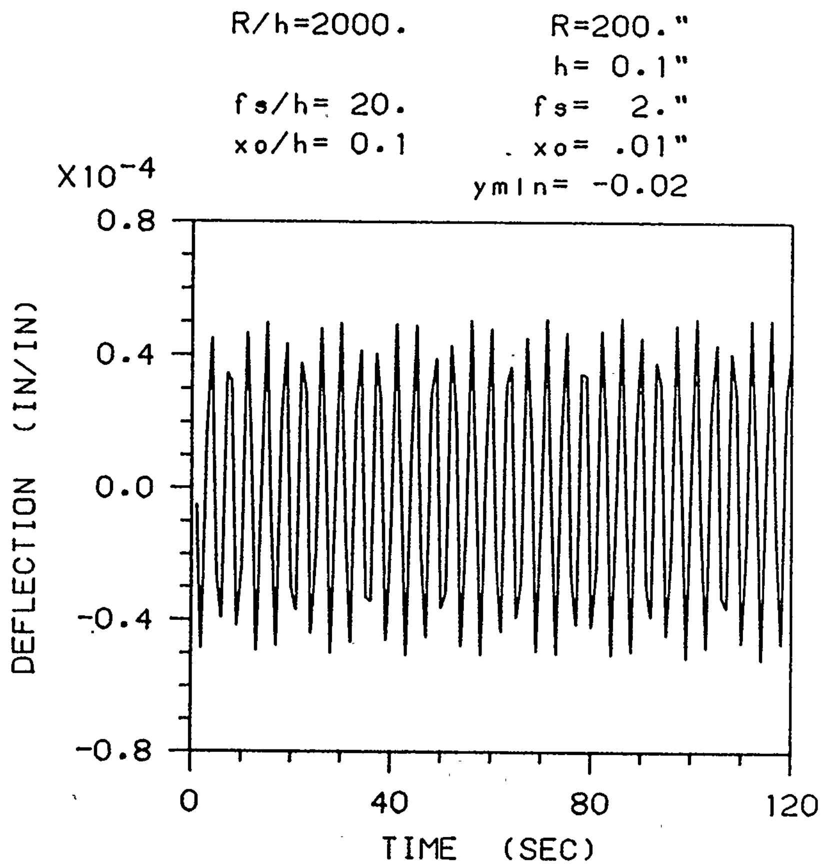

Figure 5.10 Deflection Y(in/in) vs. Time T(sec). Typical Free-Vibration Response of Spherical Shells Using Runge-Kutta Method.
Case I A: R/h = 2000. f_s/h = 20. x_o/h = 0.1

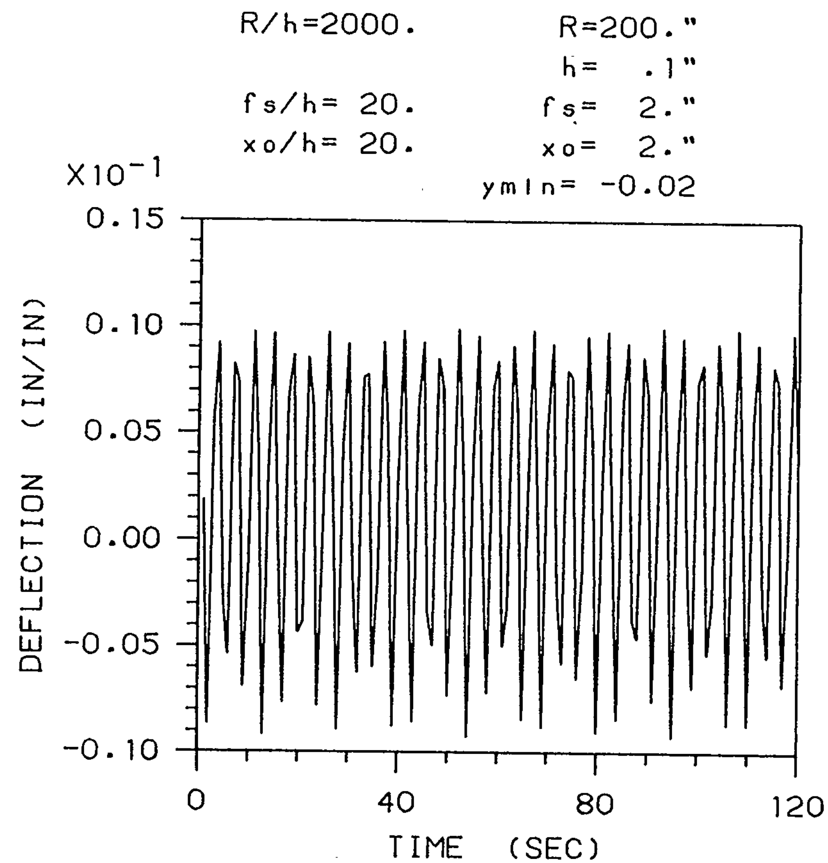

Figure 5.11 Deflection Y(in/in) vs. Time T(sec). Free-Vibration Response of Spherical Shells Using Runge-Kutta Method.
Case I A: R/h = 2000. f_s/h = 20. x_o/h = 20.

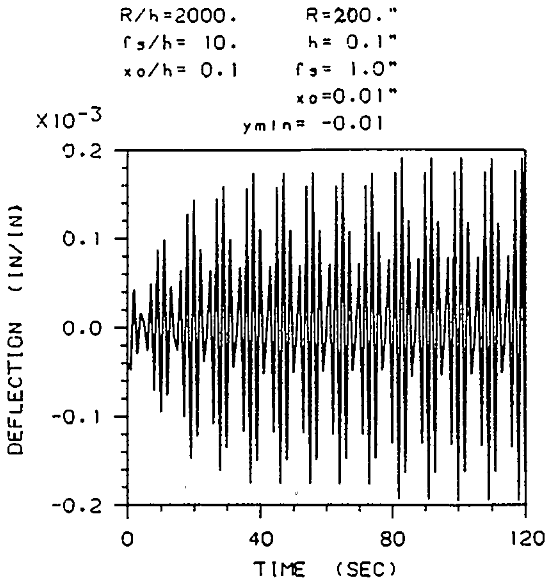

Figure 5.12 Free-Vibration Response. Case I B: R/h = 2000. $f_s/h = 10.$ $x_o/h = 0.1$

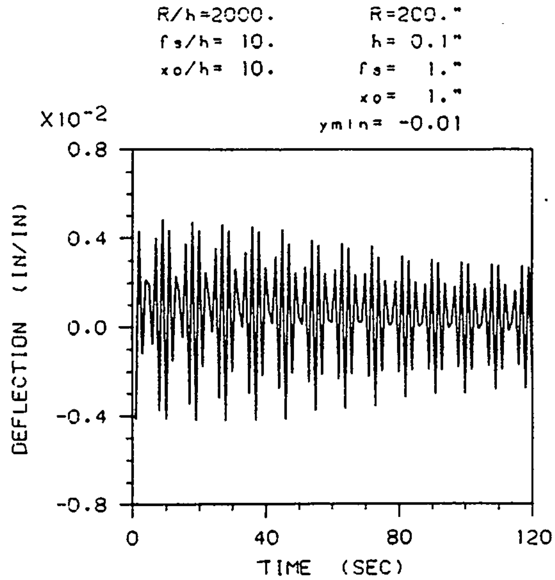

Figure 5.13 Free-Vibration Response. Case I B: R/h = 2000. $f_s/h = 10.$ $x_o/h = 10.$

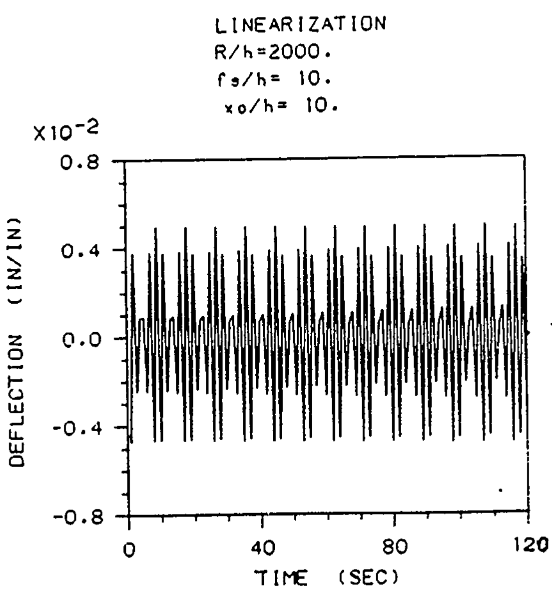

Figure 5.14 Free-Vibration Response of Spherical Shells from Linearizations. Case I B: R/h = 2000. $f_s/h = 10.$ $x_o/h = 10.$

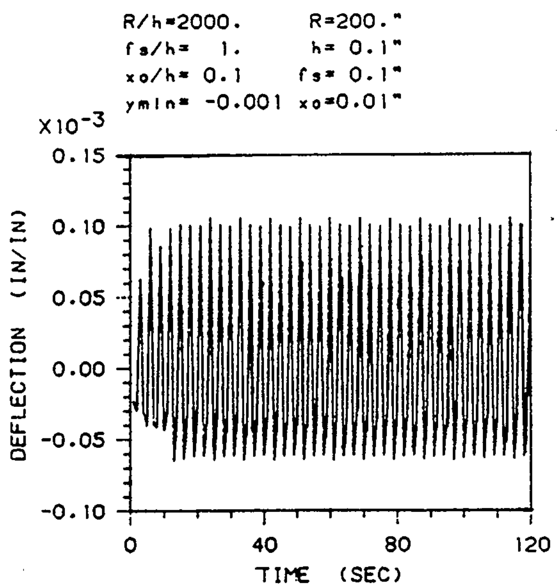

Figure 5.15 Free-Vibration Response. Case I D: R/h = 2000. $f_s/h = 1.$ $x_o/h = 0.1$

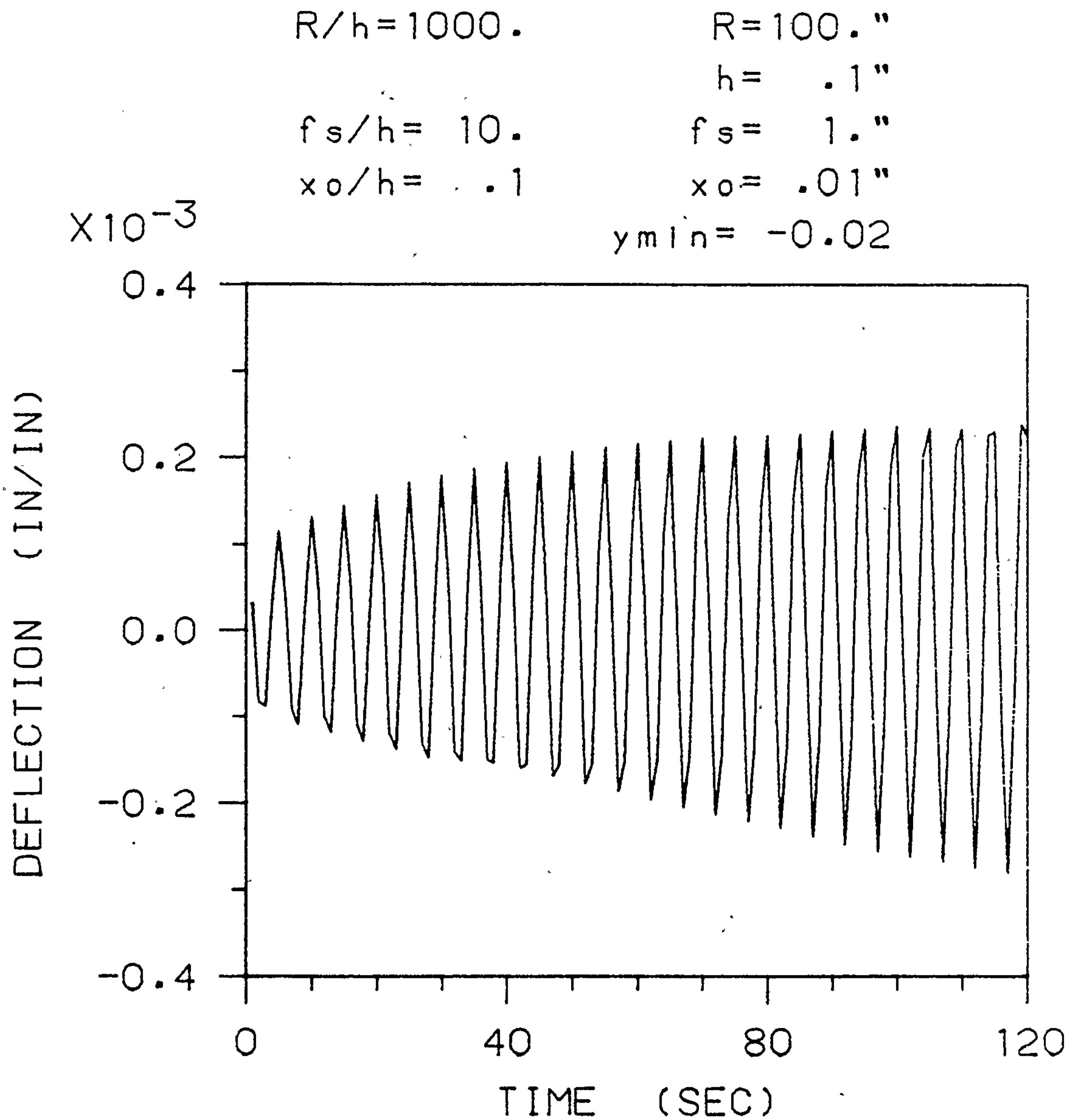

Figure 5.16 Deflection Y(in/in) vs. Time T(sec). Free-Vibration Response of Spherical Shells Using Runge-Kutta Method. Case II B: R/h = 1000. f_s/h = 10. x_o/h = 0.1

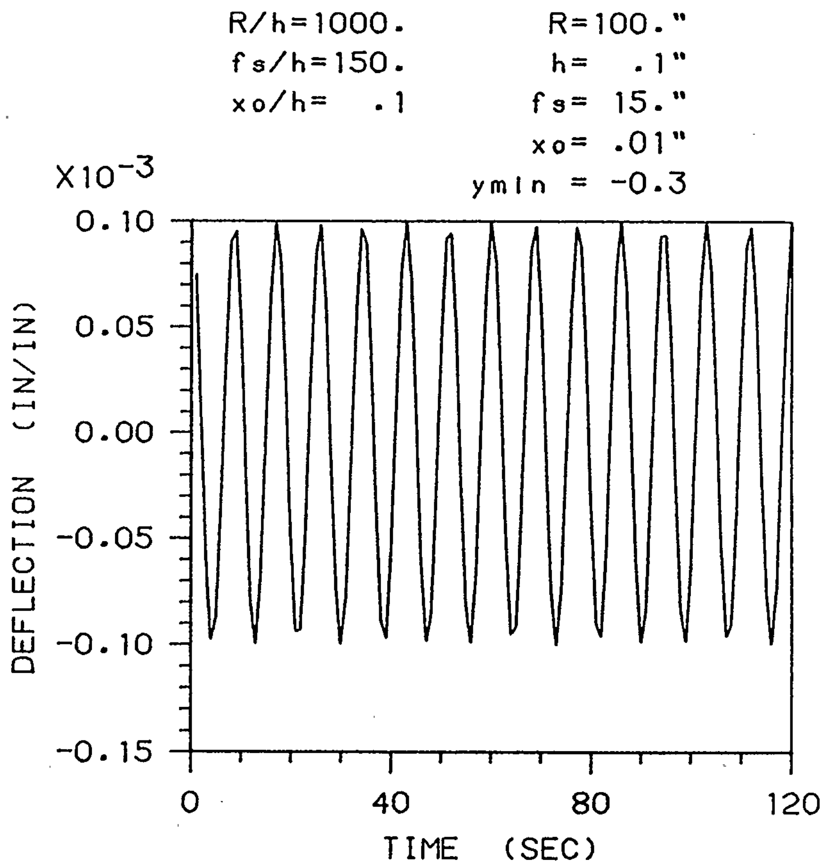

Figure 5.17 Deflection Y(in/in) vs. Time T(sec). Free-Vibration Response Curve of Spherical Shells under Large Deformations Using Runge-Kutta Method. Case II E: R/h = 1000. f_s/h = 150. x_o/h = 0.1

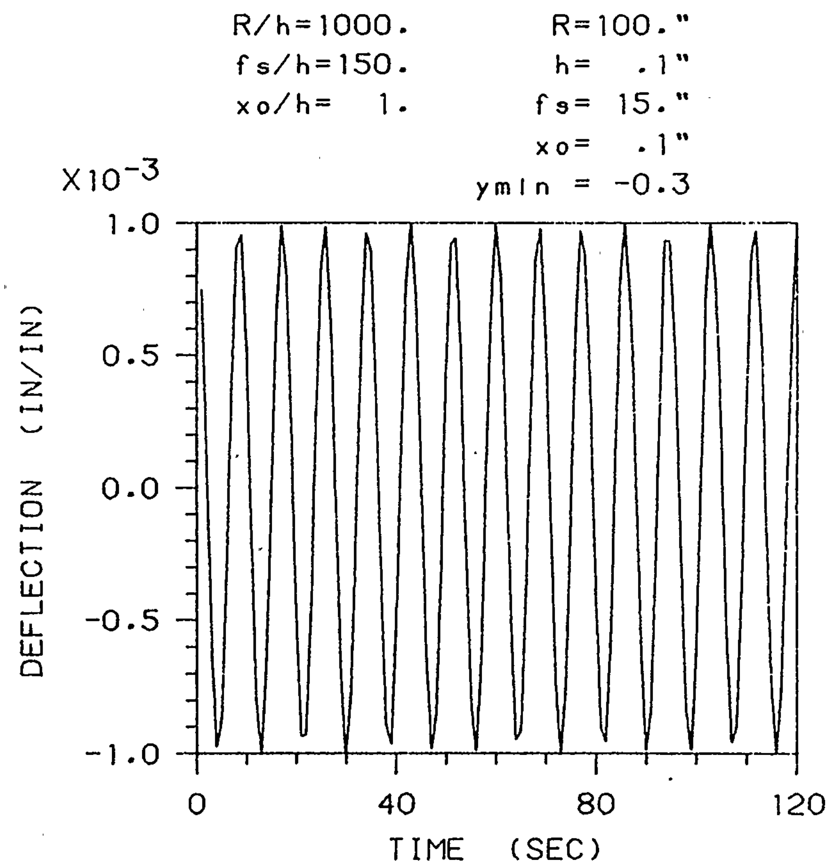

Figure 5.18 Deflection Y(in/in) vs. Time T(sec). Free-Vibration Response Curve of Spherical Shells under Large Deformations Using Runge-Kutta Method. Case II E: R/h = 1000. f /h = 150. x_o/h = 1.

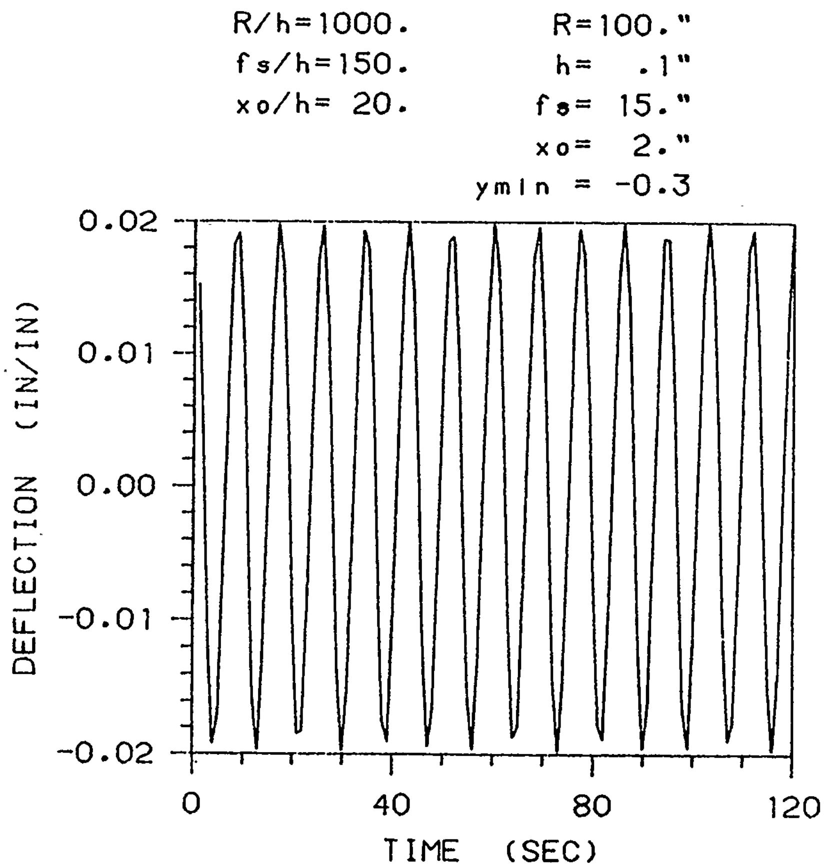

Figure 5.19 Free-Vibration Response Curve of Spherical Shells under Large Deformations Using Runge-Kutta Method. Case II E: R/h = 1000. $f_s/h = 150.$ $x_o/h = 20.$

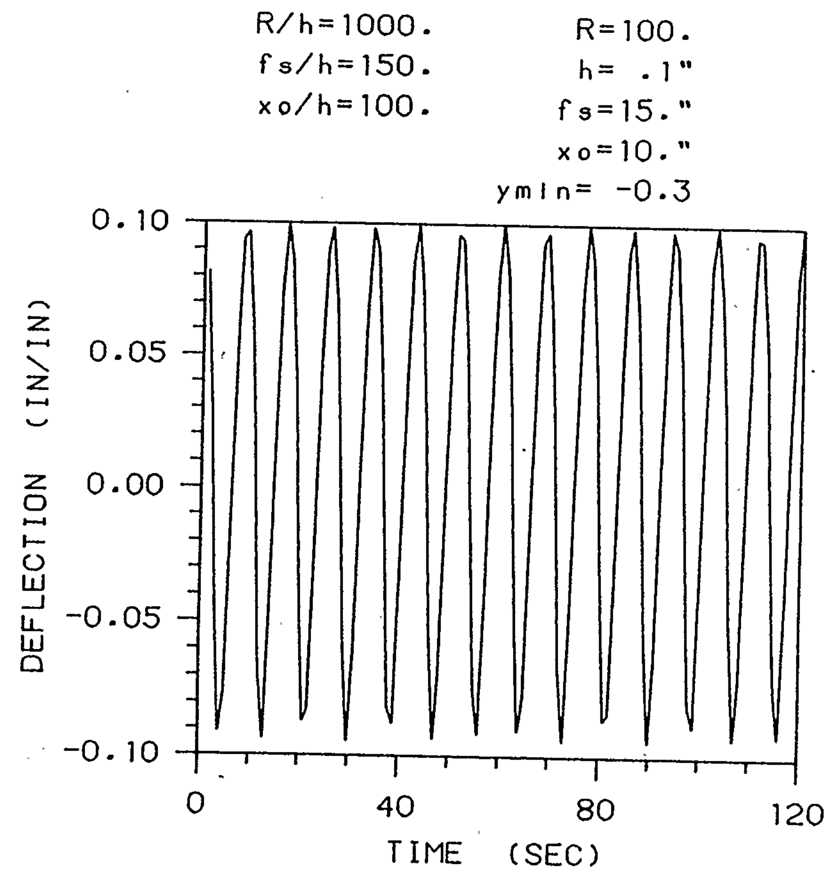

Figure 5.20 Free-Vibration Response Curve of Spherical Shells under Large Deformations Using Runge-Kutta Method. Case II E: R/h = 1000. $f_s/h = 150.$ $x_o/h = 100.$

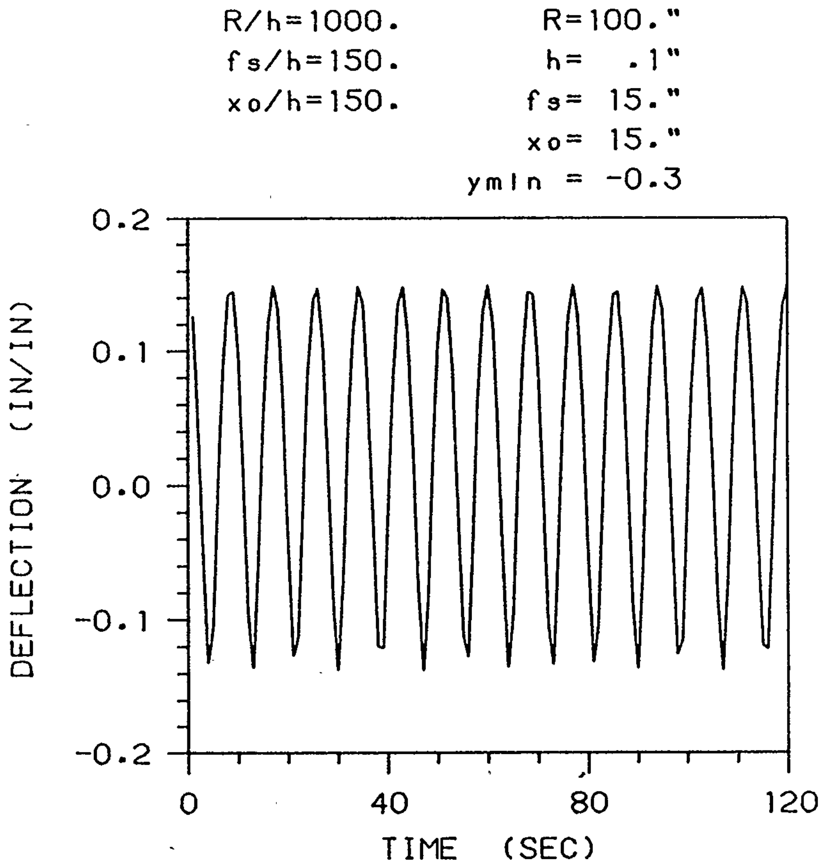

Figure 5.21 Free-Vibration Response Curve of Spherical Shells under Large Deformations Using Runge-Kutta Method.
Case II E: $R/h = 1000.$ $f_s/h = 150.$ $x_o/h = 150.$

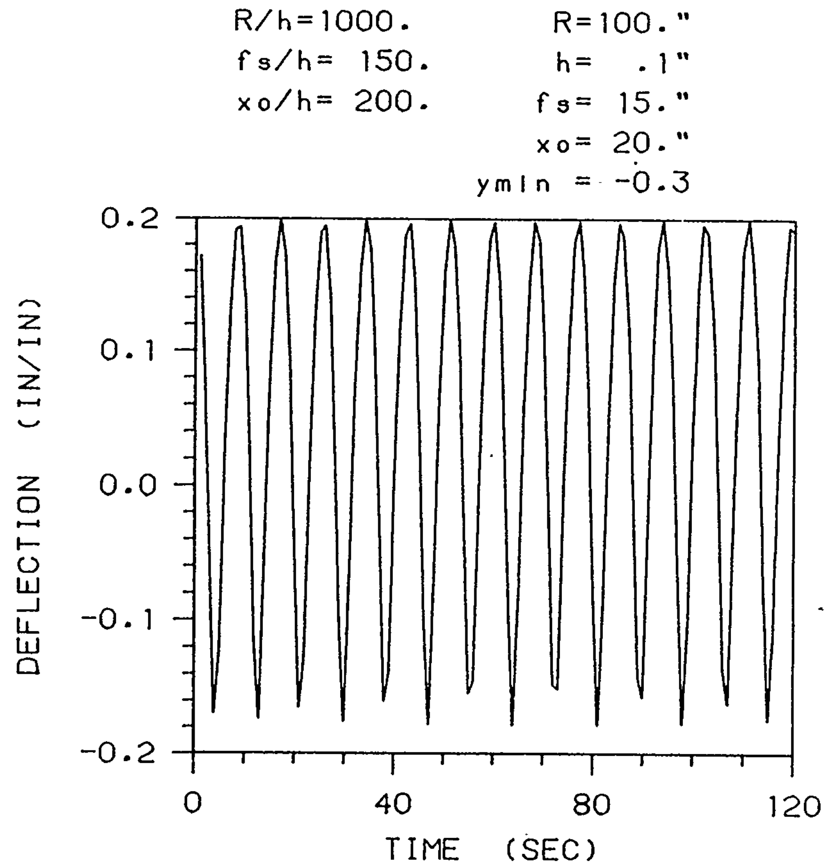

Figure 5.22 Free-Vibration Response Curve of Spherical Shells under Large Deformations Using Runge-Kutta Method.
Case II E: $R/h = 1000.$ $f_s/h = 150.$ $x_o/h = 200.$

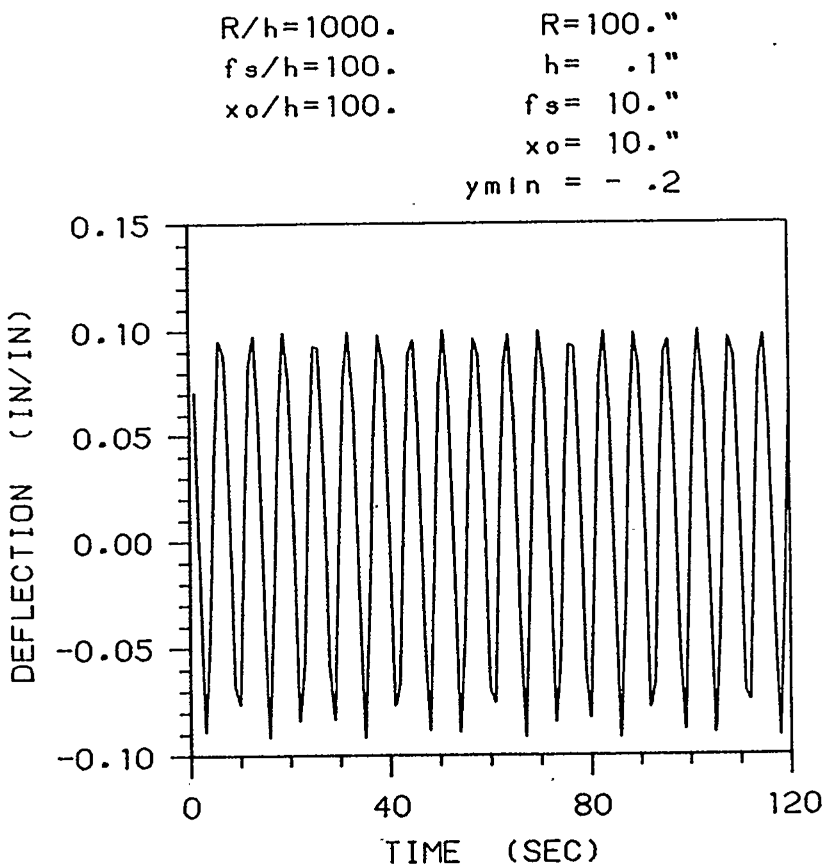

Figure 5.23 Free-Vibration Response Curve of Spherical Shells under Large Deformations Using Runge-Kutta Method. Case II F: $R/h = 1000.$ $f_s/h = 100.$ $x_o/h = 100.$

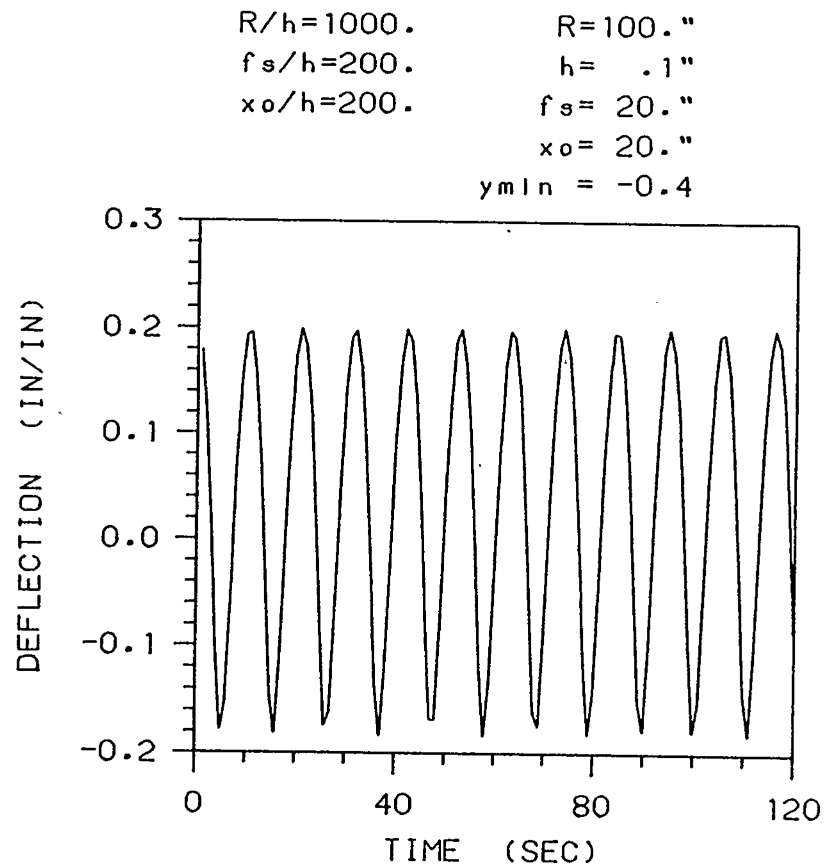

Figure 5.24 Free-Vibration Response Curve of Spherical Shells under Large Deformations Using Runge-Kutta Method. Case II G: $R/h = 1000.$ $f_s/h = 200.$ $x_o/h = 200.$

FREE-VIBRATION RESPONSE USING ADAM-MOULTON METHOD

FIGURES 5.25 - 5.33

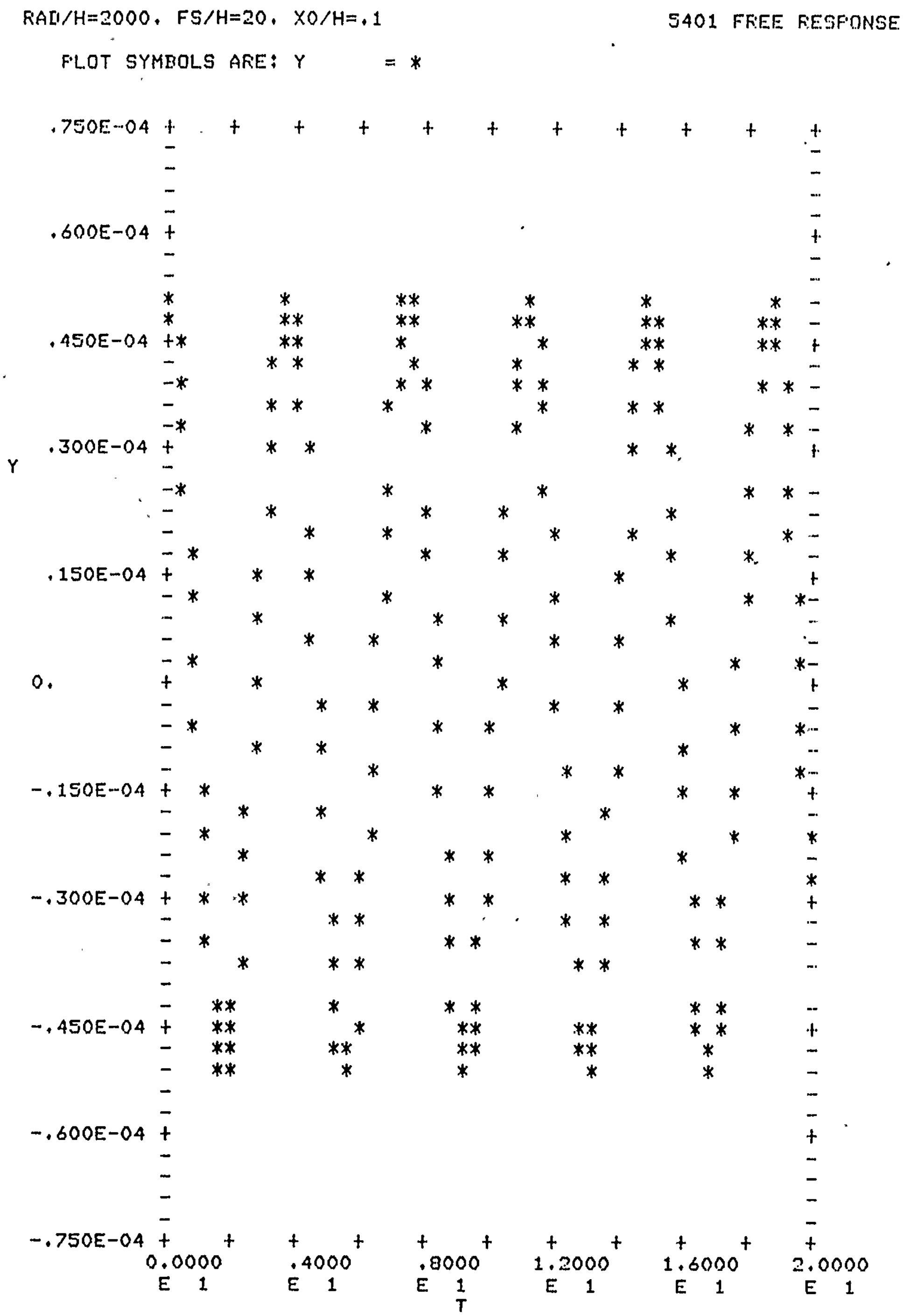

Figure 5.25 Deflection Y(in/in) vs. Time T(sec). Typical Free-Vibration Response of Spherical Shells Using Adam-Moulton Method. Case I A: R/h = 2000. $f_s/h = 20.$ $x_o/h = 0.1$

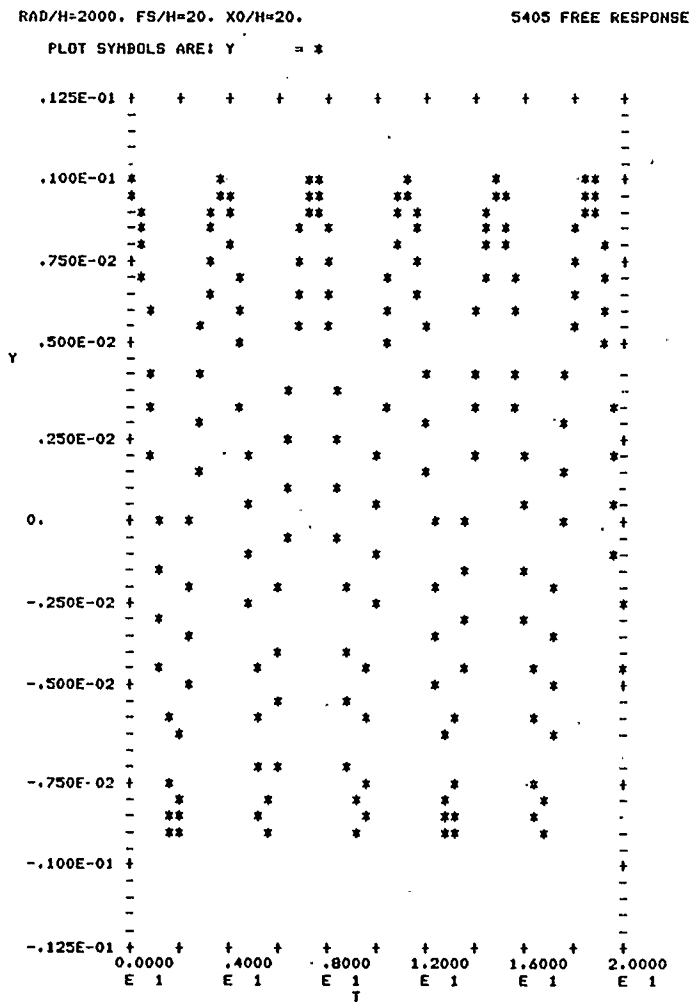

Figure 5.26 Deflection Y(in/in) vs. Time T(sec). Free-Vibration Response of Spherical Shells Using Adam-Moulton Method. Case I A: R/h = 2000. $f_s/h = 20$. $x_o/h = 20$.

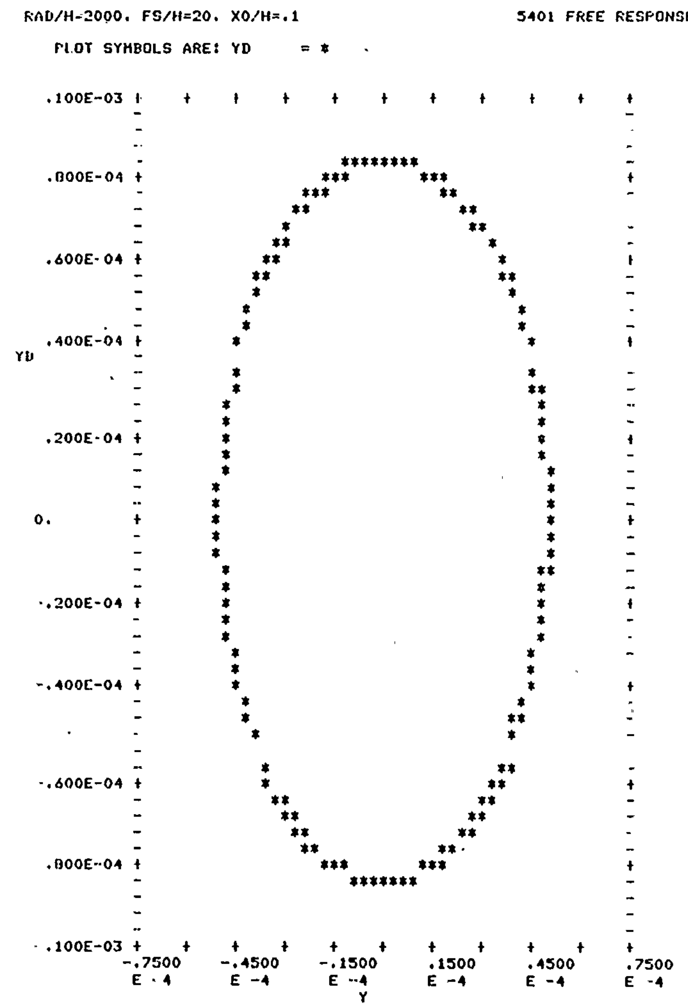

Figure 5.27 Velocity (1/sec) vs. Deflection Y(in/in). Typical Phase-Plane Diagram. Case I A: R/h = 2000. $f_s/h = 20$. $x_o/h = 0.1$

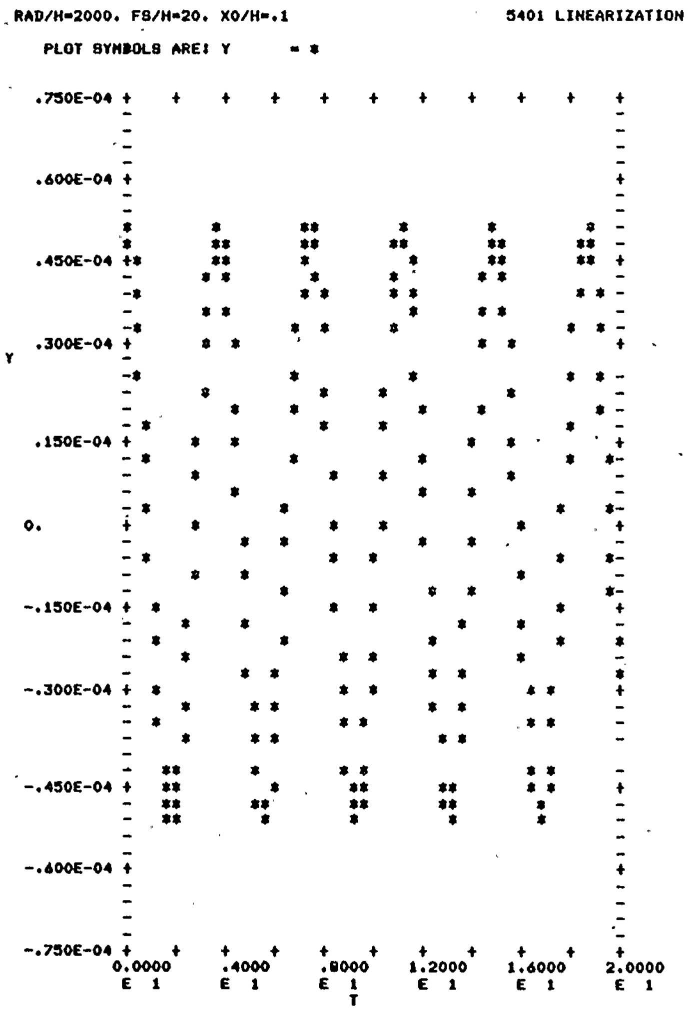

Figure 5.28 Deflection Y(in/in) vs. Time T(sec). Free-Vibration Response of Spherical Shells from Linearization. Case I A: R/h = 2000. $f_s/h = 20$. $x_o/h = 0.1$

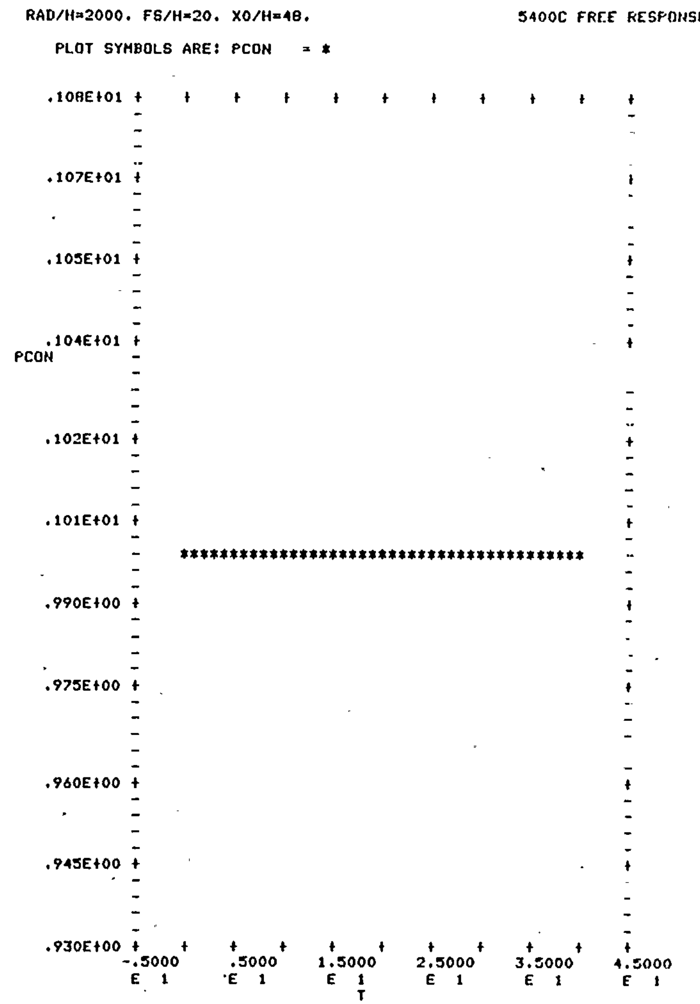

Figure 5.29 Dimensionless Static Load PCON(lbf/lbf) vs. Time T(sec). Typical Static Load-Time Curve in Free-Vibration Showing a Constant Step Input.

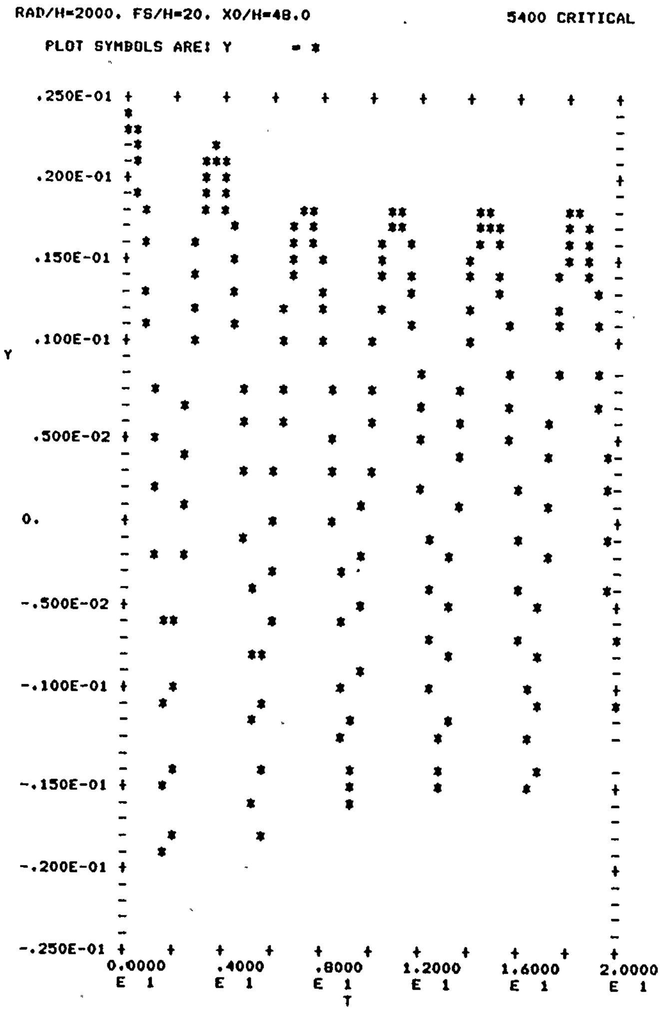

Figure 5.30 Deflection Y(in/in) vs. Time T(sec). Free-Vibration Response of Spherical Shells Using Adam-Moulton Method at Critical Initial Conditions. Case I A: $x_o/h = 48$.

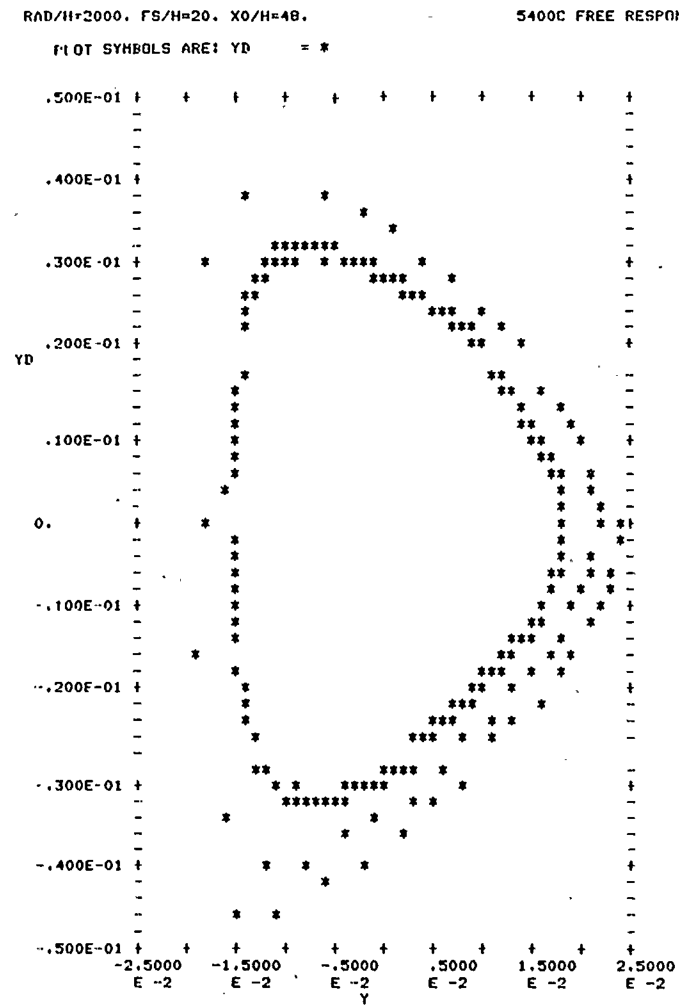

Figure 5.31 Velocity (1/sec) vs. Deflection Y(in/in). Phase-Plane Diagram at Critical Initial Conditions. Case I A: $x_o/h = 48$.

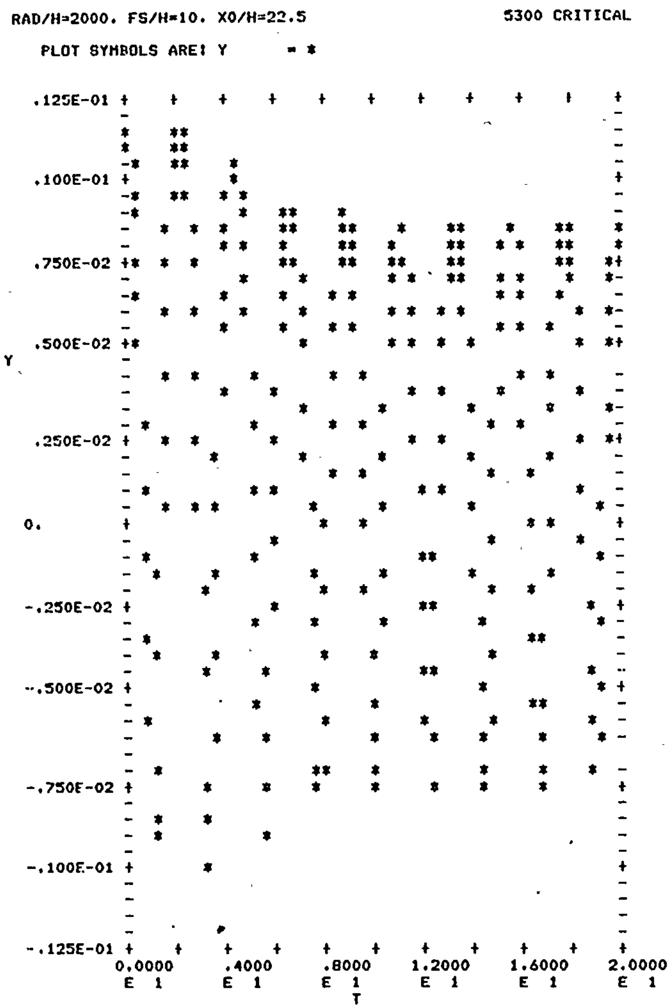

Figure 5.32 Deflection Y(in/in) vs. Time T(sec). Free-Vibration Response of Spherical Shells Using Adam-Moulton Method at Critical Initial Conditions. Case I B: $x_o/h = 22.5$

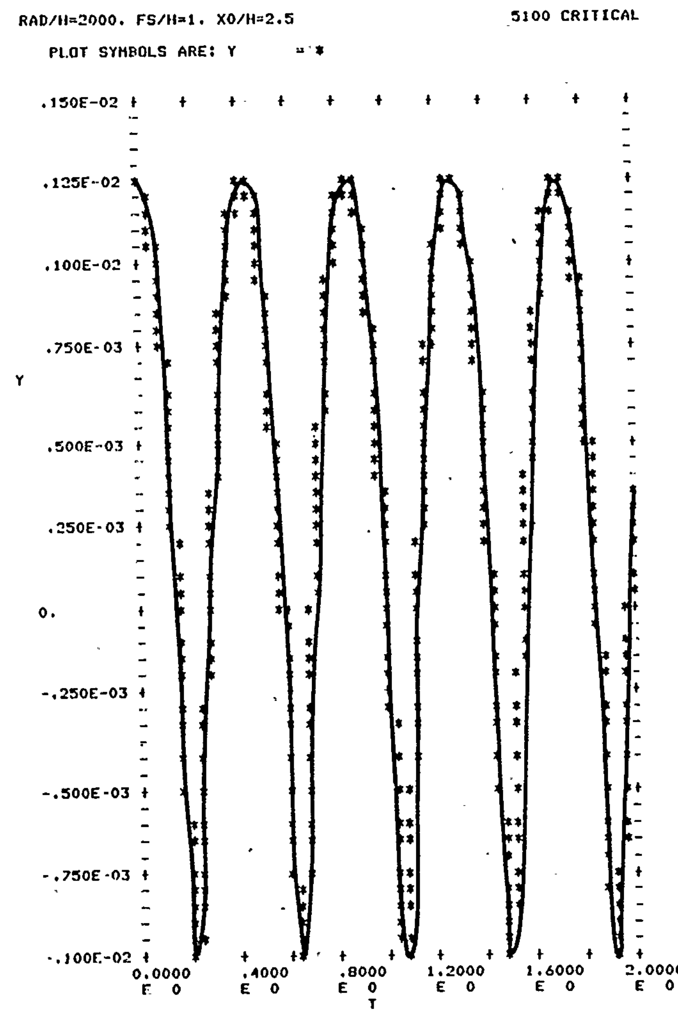

Figure 5.33 Deflection Y(in/in) vs. Time T(sec). Free-Vibration Response of Spherical Shells Using Adam-Moulton Method at Critical Initial Conditions. Case I C: $x_o/h = 2.5$

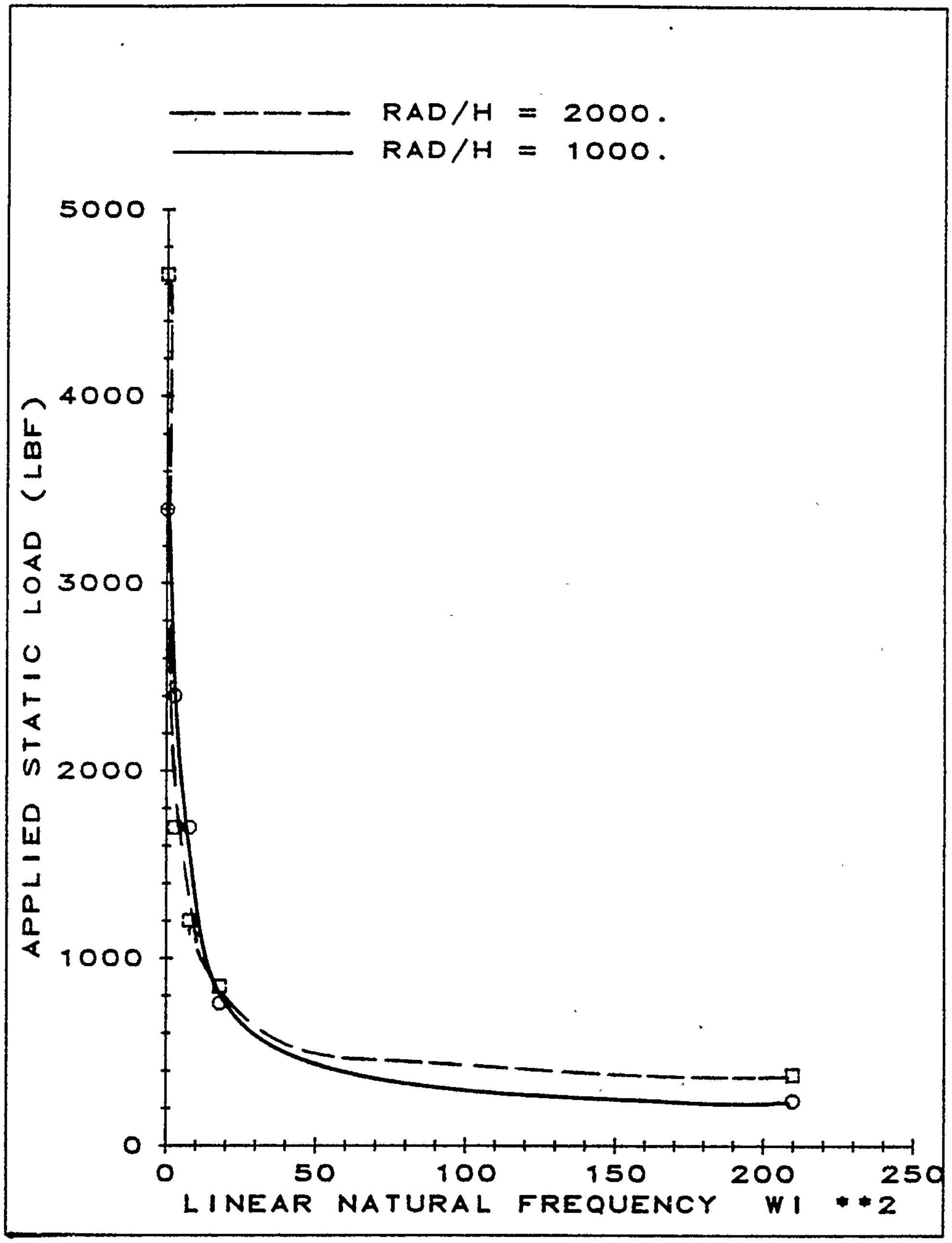

Figure 5.34 Relationship between Applied Static Load and Linear Natural Frequency of Vibration of Spherical Shells.

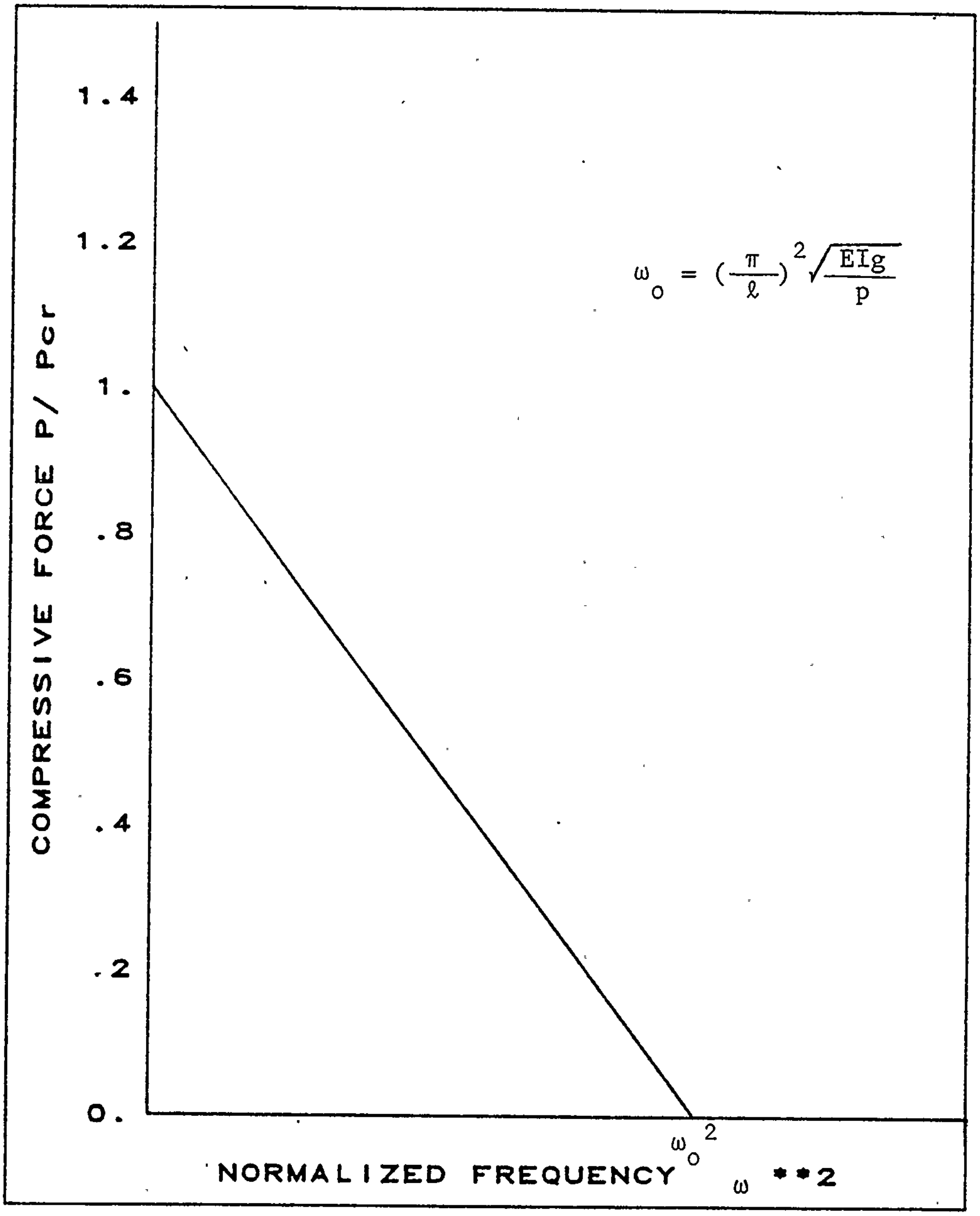

Figure 5.35 Relationship between Compressive Force and Natural Frequency of Vibration of a Bar [5.15]. ω_o is the First Fundamental Frequency of Vibration of the Bar.

5.4.3 FORCED VIBRATION

The results of dynamic response analysis presented in Tables 5.7-5.9 are obtained by holding the amplitude factor of dynamic load α constant, slowly sweeping over the range of input forcing frequency, and measuring the maximum amplitude of inward and outward deflection of the response. In Table 5.7, the amplitude factor α is held constant at 0.1, and the input forcing frequency ω_e is increased slowly from 0.1 to 10 rad/sec. (The results for ω_e higher than 10 rad/sec are not shown here.) Steady periodic responses are observed from the deflection-time curve at frequencies below or far below the linear natural frequency ω_ℓ. The behaviour of the shell is similar to the results obtained from the analysis of free vibration. Typical results of dynamic response to a sinusoidal input at ω_e = 0.1 rad/sec are presented in Figure 5.36 - 5.37. The technique of FFT is shown in Figure 5.37. The transform analysis decomposes the output response in time domain into sinusoids of different frequencies and their respective amplitudes. The input forcing frequency is identified at 0.1 rad/sec. The harmonics of the frequency of vibration of the system are indicated by different frequencies from 2.5 to 3.1 rad/sec. The magnitude of these harmonic components is very small, so that the system is vibrated at the input forcing frequency. Similar results of analysis, obtained for the response at ω_e = 0.1 rad/sec and α = 0.1 using the Adam-Moulton method, are shown in Figure 5.38 for the first 100 seconds. The applied static force as a function of time are depicted in Figures 5.39 - 5.40.

As the forcing frequency approaches the linear natural frequency, the harmonics of the forcing frequency are generated at the same time. The dynamic response is obtained as a combination of harmonic components. Typical results at forcing frequency 2.6, 3.098, 3.6, and 5.0 rad/sec are shown in Figures 5.41 - 5.44, respectively. Each component has its own amplitude and frequency and is combined with the other components. The existence of beats is observed in Figures 5.41 - 5.43, and the waveform indicates that there are at least two components of nearly equal frequency combined in the response, namely: the forcing frequency and the frequency of harmonic components. However, the waveform shown in Figure 5.44 indicates that it has components of widely different frequencies. The forced-vibration response at the resonance frequency is shown in Figure 5.42.

If the amplitude factor of the dynamic load is increased slowly from 0.2 to 1.5 as shown in Figures 5.45 - 5.47, the amplitude of the inward and outward deflection response will also increase. A slow divergence and instability of the solution is observed. The results of the transform analysis are depicted in Figures 5.48 - 5.52, corresponding to the input amplitude factor 0.2, 0.4, 1.0, 1.5, and 5., respectively. When the applied load is increased further, the frequency of vibration of the shell vanishes.

It is noticed that an amplitude at zero frequency is increased rapidly with increasing amplitude factor from 0.2 to 5. This results in divergent of the system as discussed in the analysis of load and frequency curve in Figure 5.34. The shell will simply stop vibrating and collapse for the applied load at $\alpha = 5$.

The relationship between the output amplitude of inward and outward deflection and the normalized frequency ω_e/ω_ℓ are depicted in Figures 5.53 - 5.55, corresponding to the constant input $\alpha = 0.1$ in Table 5.7. As the forcing frequency is increased to the value of linear natural frequency of vibration ω_ℓ, the effect of the dynamic force becomes significant, and a sudden jump in the deflection amplitude is observed. In Figure 5.53, the occurrence of a dynamic jump is indicated at $\omega_e/\omega_\ell = 1.$ by a sudden increase in amplitude. The response of the shell experiences a sharp change in magnitude of deflection. This is a resonant condition. A second and a third dynamic jumps are observed at $\omega_e/\omega_\ell = 2.$ and 3., corresponding to the second and third harmonics respectively. When the shell structure experiences a sudden increase in amplitude of deflection, the system loses its stability. It has been obtained from the analysis of the results and confirmed experimentally [1.35, 5.16] that such a jump leads to the instability of the system.

A system with a mass on a nonlinear spring as shown in Figure 5.1(b) is described by Duffing's equation [4.1]

$$M\ddot{x} + c\dot{x} + k(x + \alpha x^3) = P \cos \omega t \tag{5.6}$$

where $k(x + \alpha x^3)$ is the nonlinear spring force, with α being positive for a hard spring and negative for a soft spring. A typical idealized amplitude response curve for a nonlinear softening system as a function of forcing frequency for the constant amplitude of forcing function is presented in Figure 5.56. Physically, the nonlinear response bends toward lower frequencies. As the forcing frequency is decreased toward the resonance, the amplitude decreases; therefore, the stiffness of the spring also decreases. This lowers the natural frequency of the system and pushes the resonance frequency to a lower value. In Figure 5.56, the amplitude response is increasing along the curve 1-2-3 with decreasing frequency. At point 3, a small decrease in frequency will cause a jump to point 4. With further decrease in frequency, the response is decreased along the curve 4-5. Similar jump phenomenon occurs with increasing frequency. The response is increased along the curve 5-4-2, with the jump occurring at point 2'. The response along the curve 2'-3 is unstable.

The result of analysis for the actual response curve as a function of normalized frequency are shown in Figures 5.53 - 5.55, 5.57 - 5.58, and 5.59 - 5.60, corresponding to the constant input amplitude factor α = 0.1, 0.3, and 0.5 in Tables 5.7 - 5.9, respectively. In Figure 5.57 - 5.58, the response curve for α = 0.3 shows a steep slope and several jumps in amplitude occurred before the apparent resonant frequency and a gentle slope after, as it is expected for a nonlinear softening system described by Duffing's equation. In the investigation of the nonlinear axisymmetric vibrations of spherical caps with various edge conditions [5.17], the behaviour of a nonlinear softening system is obtained, and the resonance is shifted to the left. The results further examine the effect of curvatures on the nonlinear behaviour of spherical shells. As the curvature is changed from a flat circular disk to a shallow spherical shell, the nonlinear behaviour gradually reverses from hardening into softening.

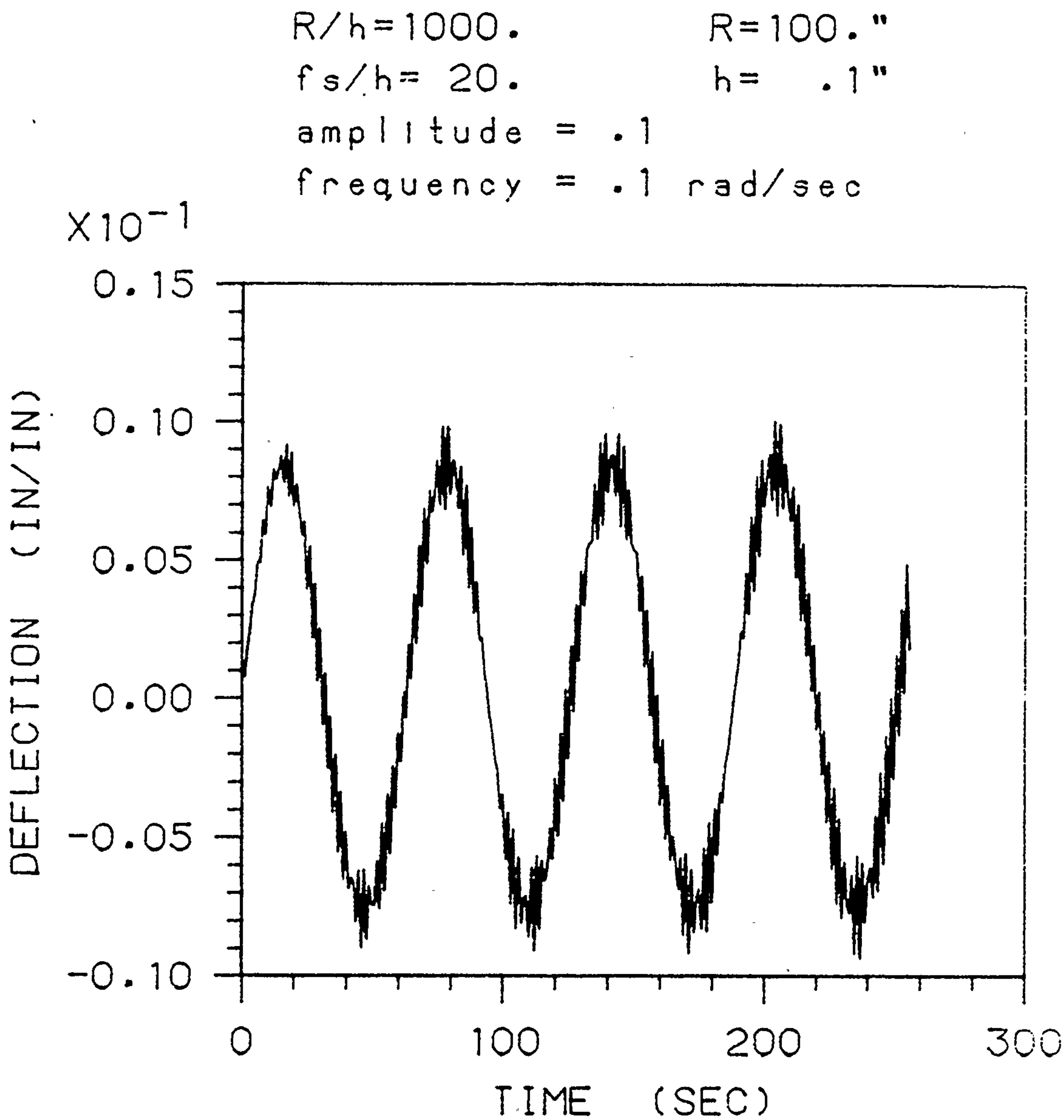

Figure 5.36 Forced-Vibration Response of Spherical Shells Using Runge-Kutta Method. $\alpha = 0.1$, $\omega_e = 0.1$ rad/sec

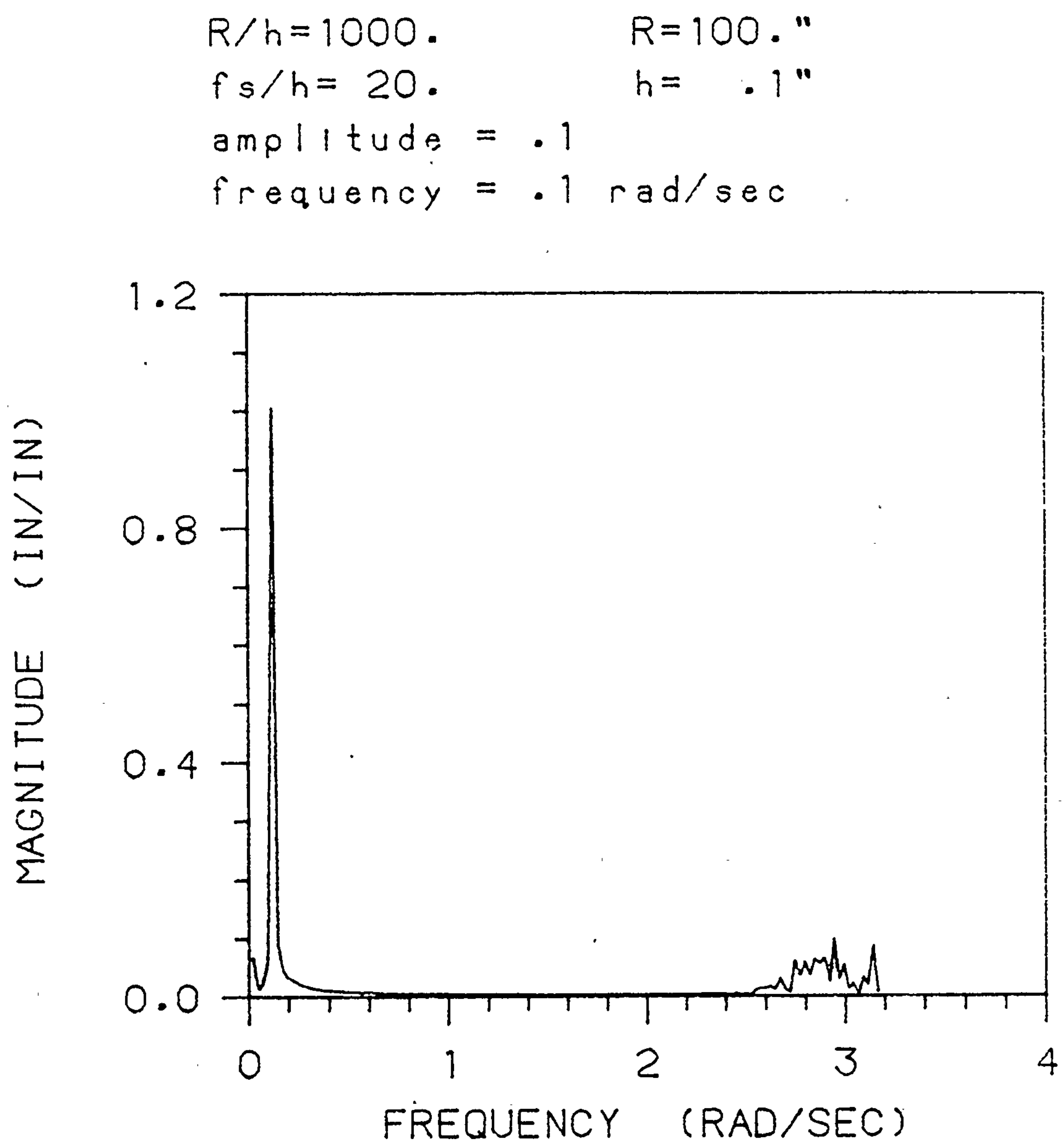

Figure 5.37 Typical Frequency Response Curve of Forced Vibration Using Fast Fourier Transform Showing Sinusoids of Forcing Frequency at $\omega_e = 0.1$ rad/sec.

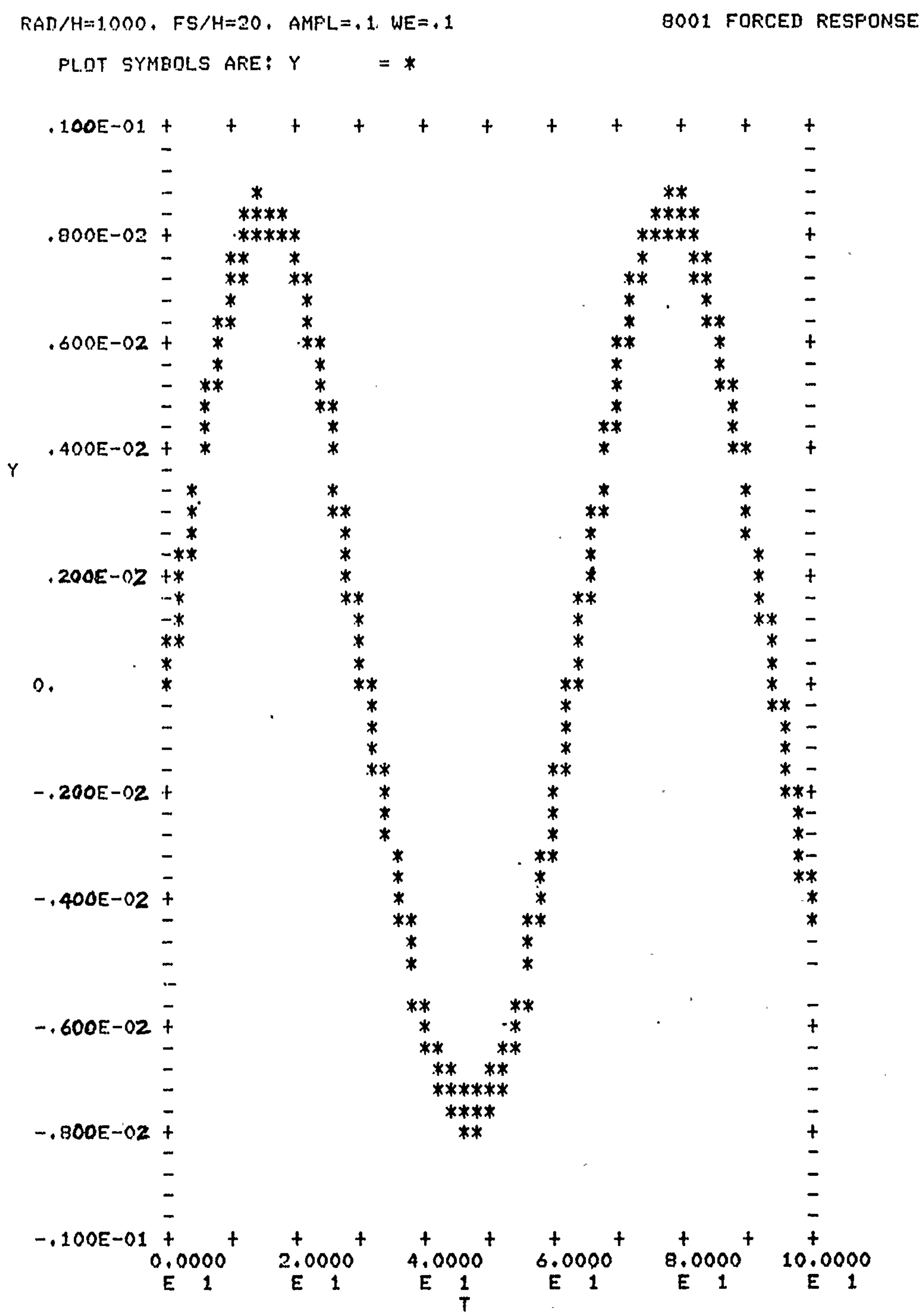

Figure 5.38 Forced-Vibration Response of Spherical Shells Using Adam-Moulton Method.
$\alpha = 0.1$, $\omega_e = 0.1$ rad/sec

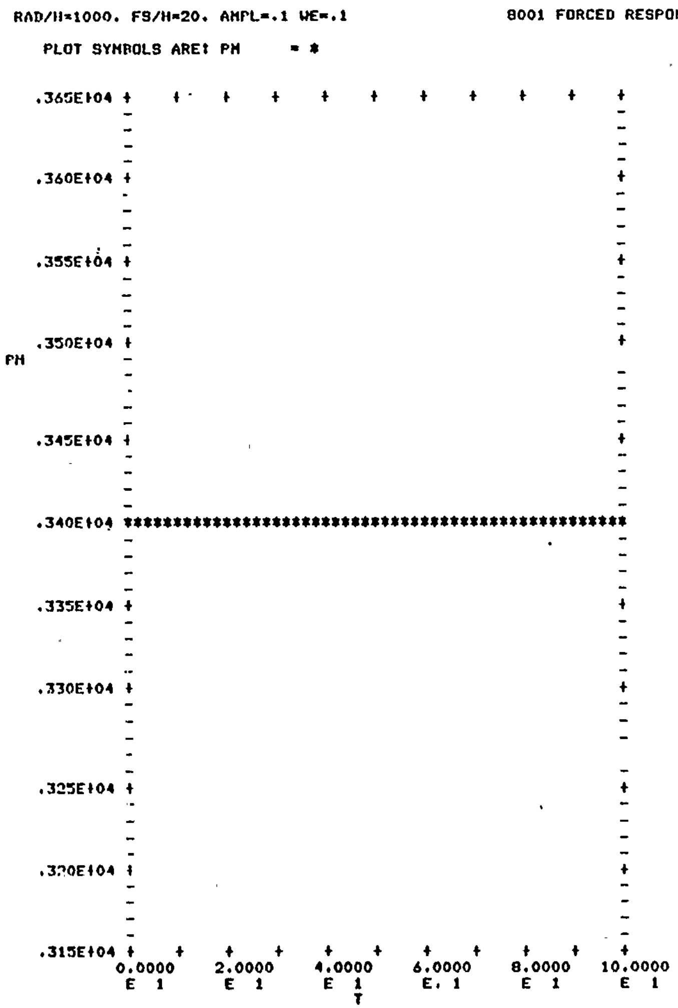

Figure 5.39 Applied Static Force (lbf) vs. Time T(sec).
Typical Static Force-Time Curve in Forced Vibration.

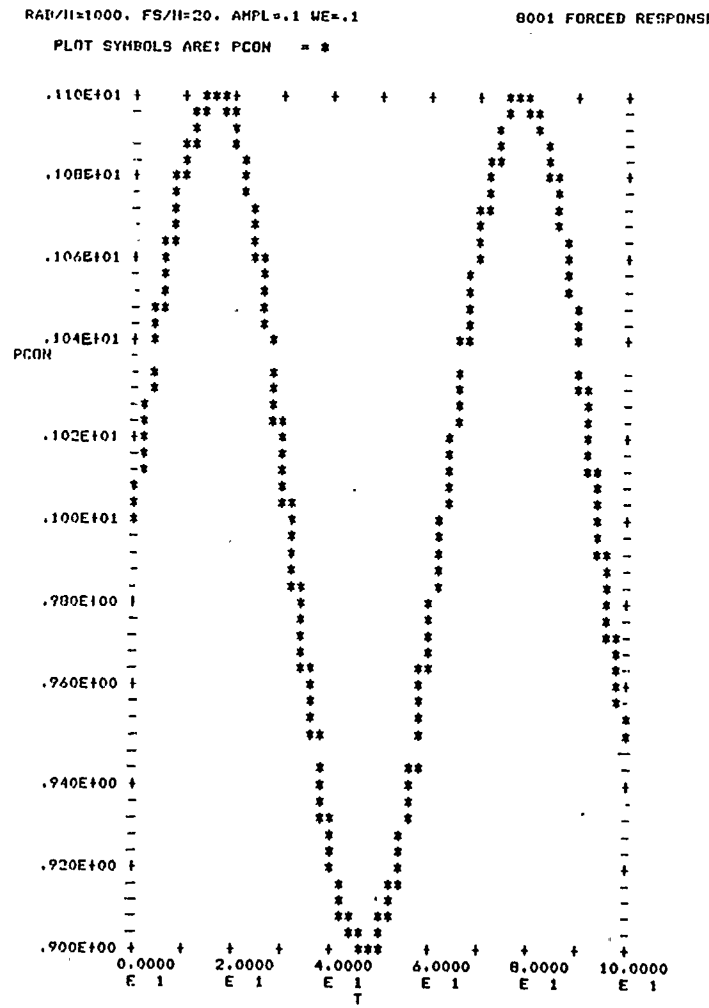

Figure 5.40 Dimensionless Total Force (lbf/lbf) vs. Time T(sec).
Typical Total Force-Time Curve Showing a Sinusoidal Input in Forced Vibration.

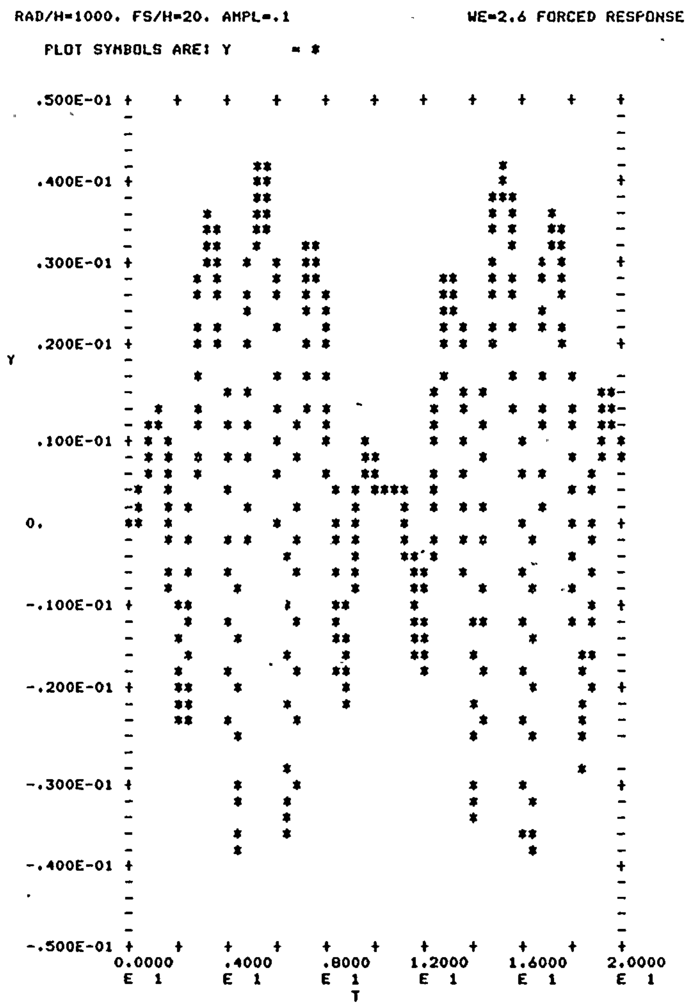

Figure 5.41 Forced-Vibration Response of Spherical Shells Using Adam-Moulton Method. $\alpha = 0.1$, $\omega_e = 2.6$ rad/sec

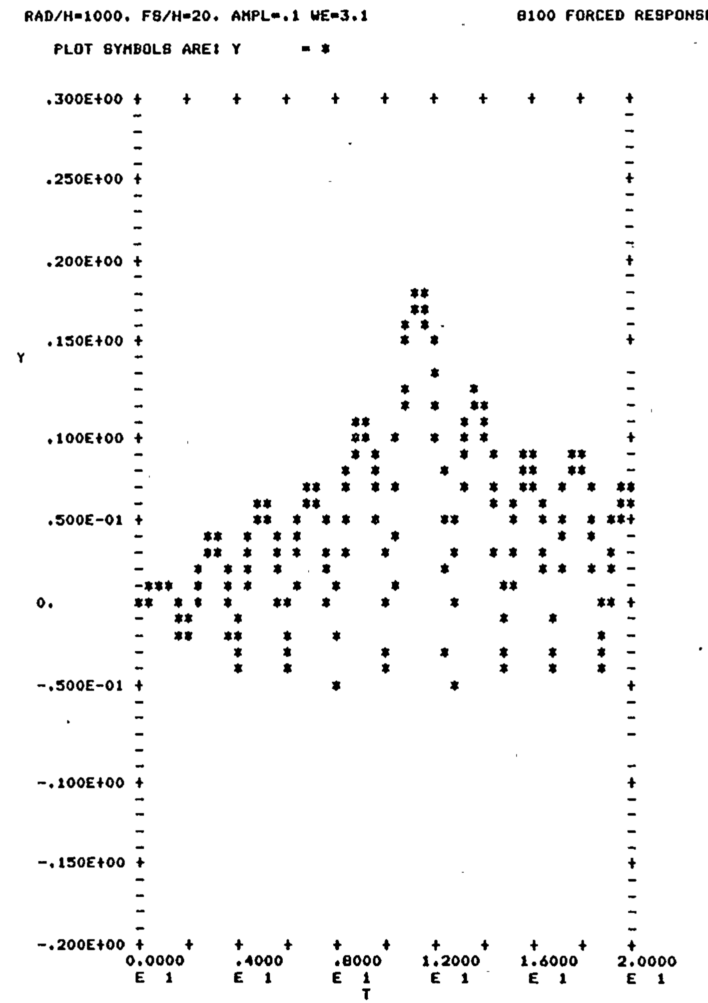

Figure 5.42 Forced-Vibration Response of Spherical Shells at Linear Natural Frequency $\omega_e = 3.1$ rad/sec Using Adam-Moulton Method. $\alpha = 0.1$

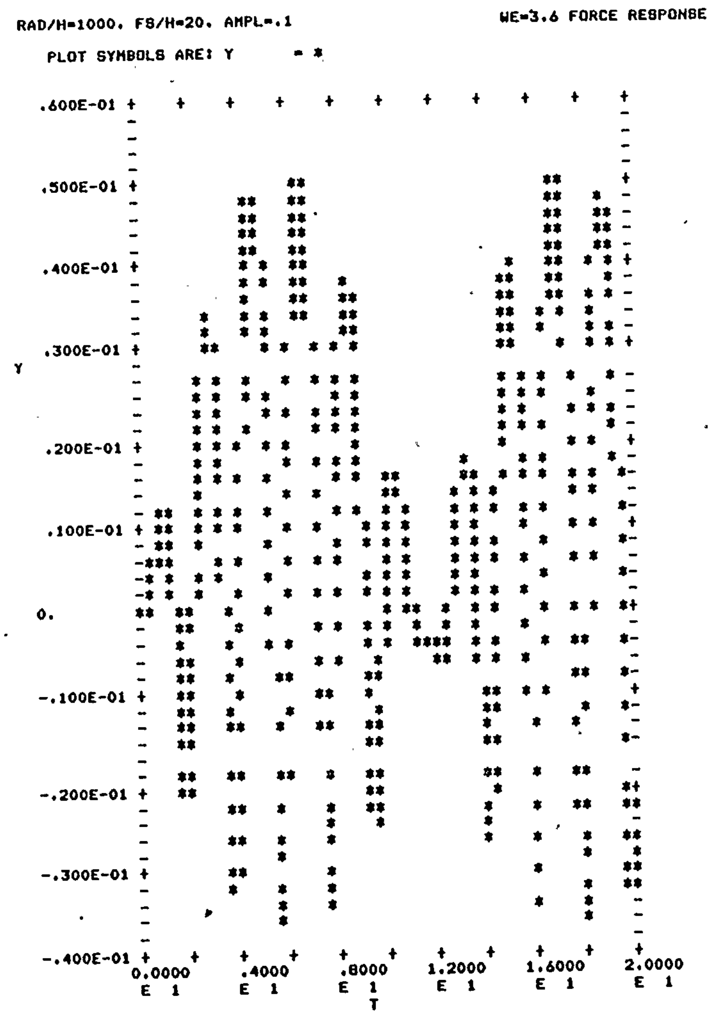

Figure 5.43 Forced-Vibration Response of Spherical Shells Using Adam-Moulton Method. $\alpha = 0.1$, $\omega_e = 3.6$ rad/sec

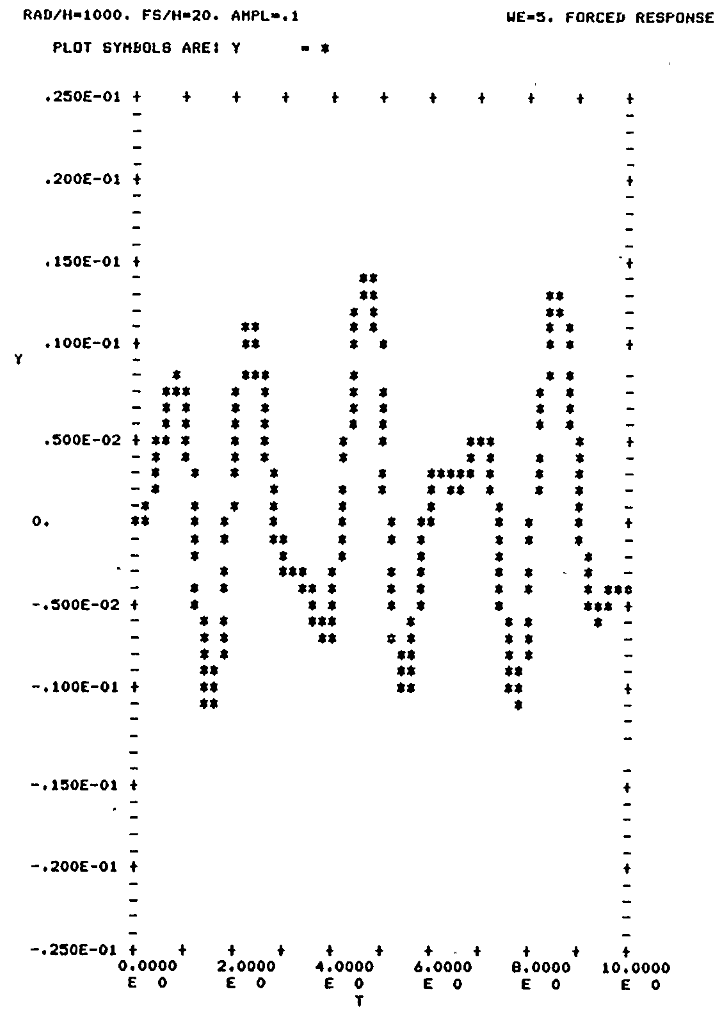

Figure 5.44 Forced-Vibration Response of Spherical Shells Using Adam-Moulton Method. $\alpha = 0.1$, $\omega_e = 5.0$ rad/sec

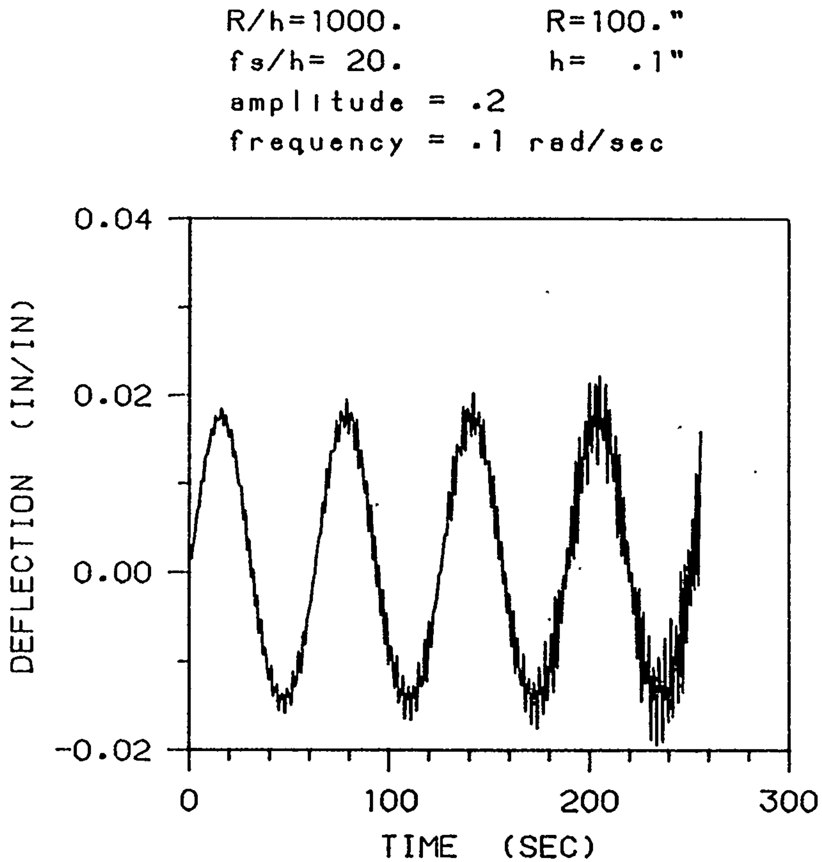

Figure 5.45 Forced-Vibration Response of Spherical Shells Using Runge-Kutta Method. $\alpha = 0.2$, $\omega_e = 0.1$ rad/sec

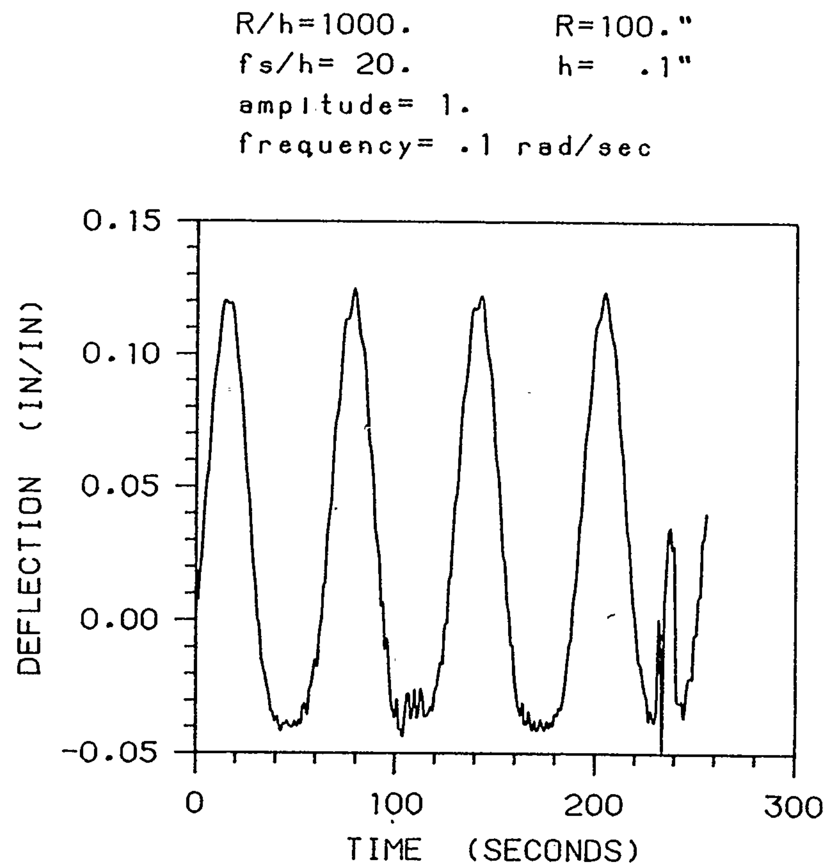

Figure 5.46 Forced-Vibration Response of Spherical Using Runge-Kutta Method. $\alpha = 1.0$, $\omega_e = 0.1$ rad/sec

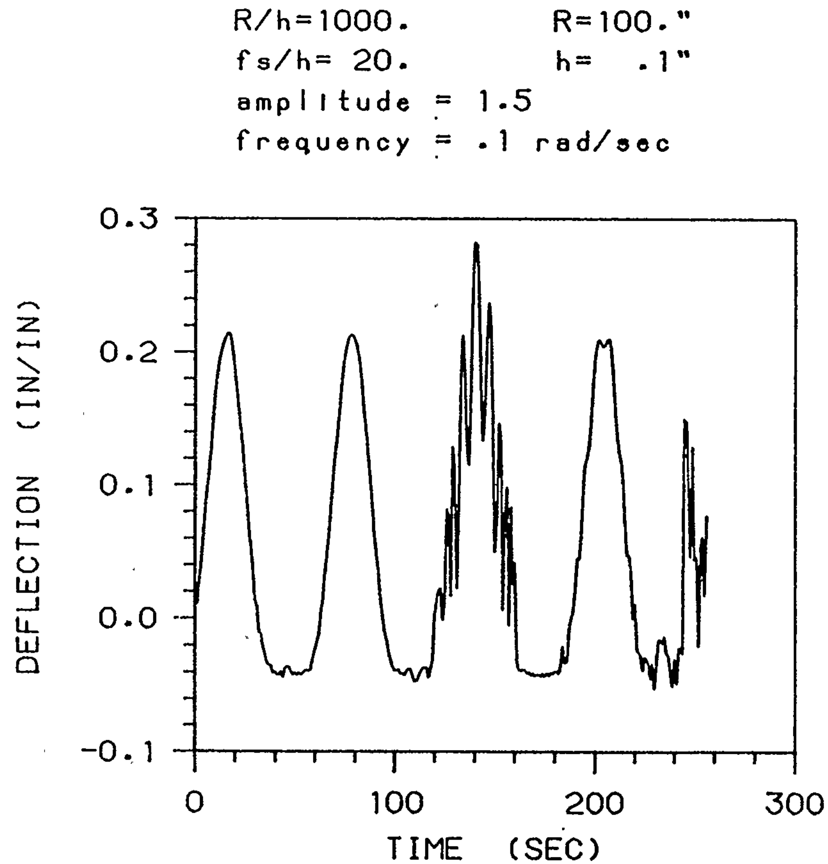

Figure 5.47 Forced-Vibration Response of Spherical Shells Using Runge-Kutta Method. $\alpha = 1.5$, $\omega_e = 0.1$ rad/sec

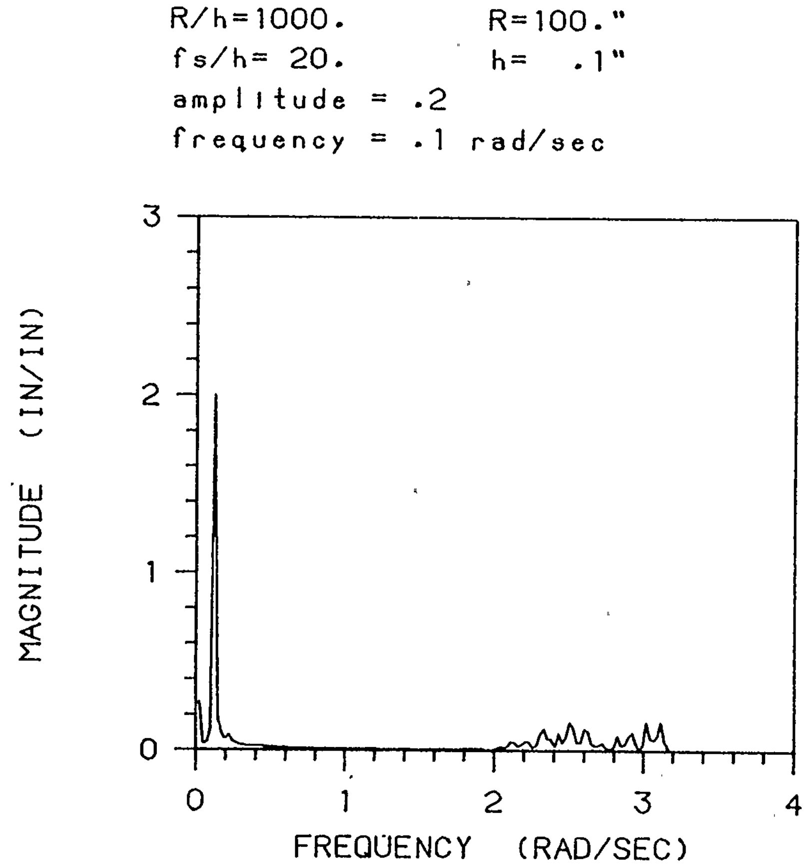

Figure 5.48 Forced-Vibration Frequency Response Using Fast Fourier Transform. $\alpha = 0.2$, $\omega_e = 0.1$ rad/sec

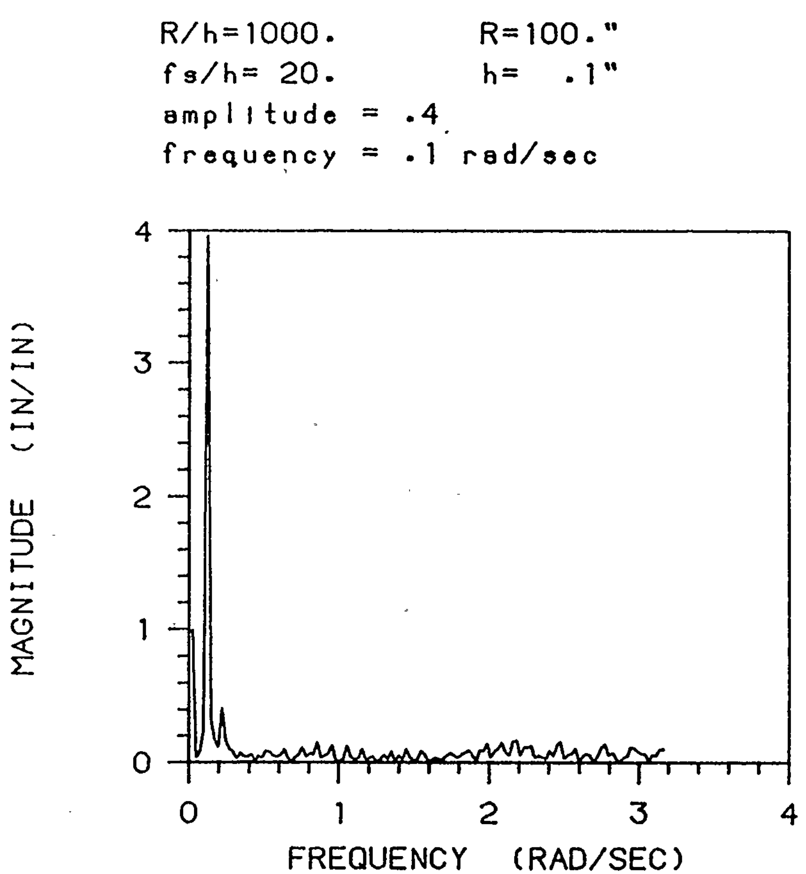

Figure 5.49 Forced-Vibration Frequency Response Using Fast Fourier Transform. $\alpha = 0.4$, $\omega_e = 0.1$ rad/sec

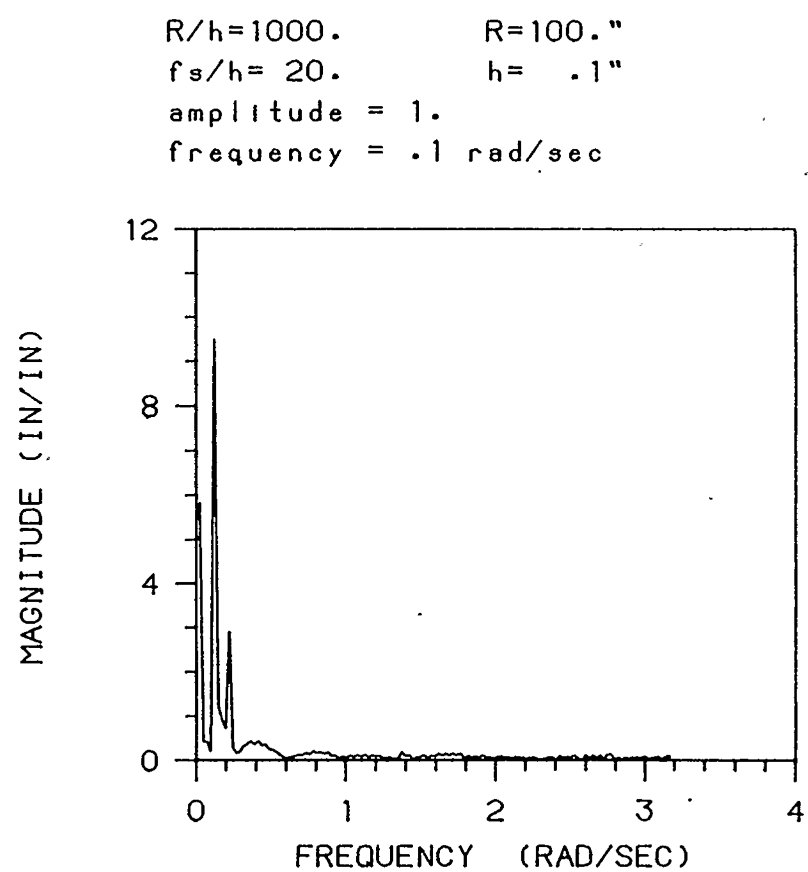

Figure 5.50 Forced-Vibration Frequency Response Using Fast Fourier Transform. $\alpha = 1.0$, $\omega_e = 0.1$ rad/sec

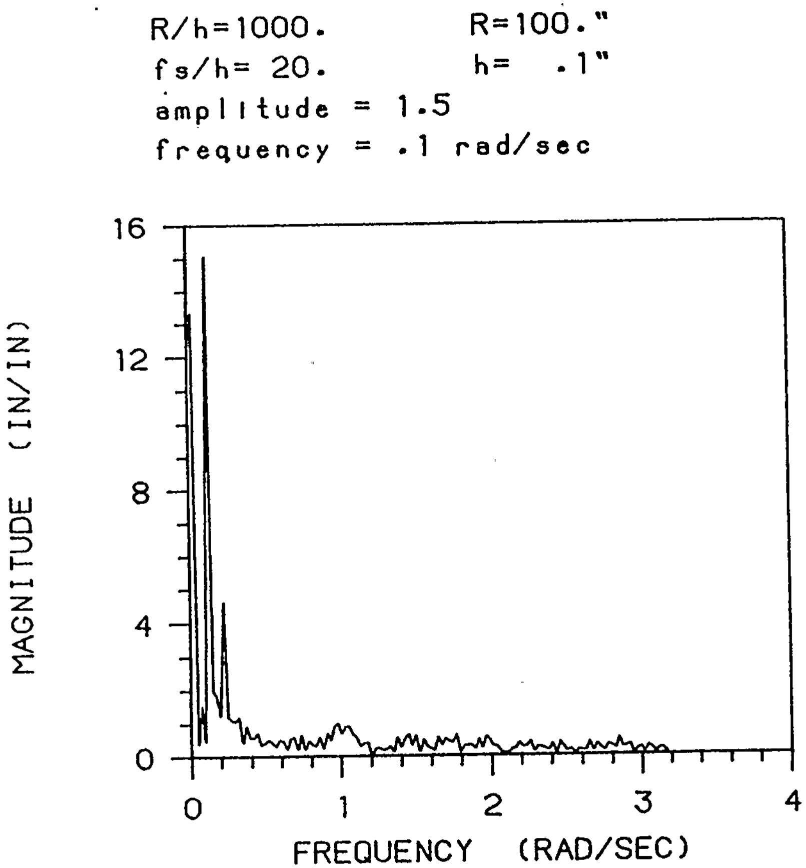

Figure 5.51 Forced-Vibration Frequency Response Using Fast Fourier Transform. $\alpha = 1.5$, $\omega_e = 0.1$ rad/sec

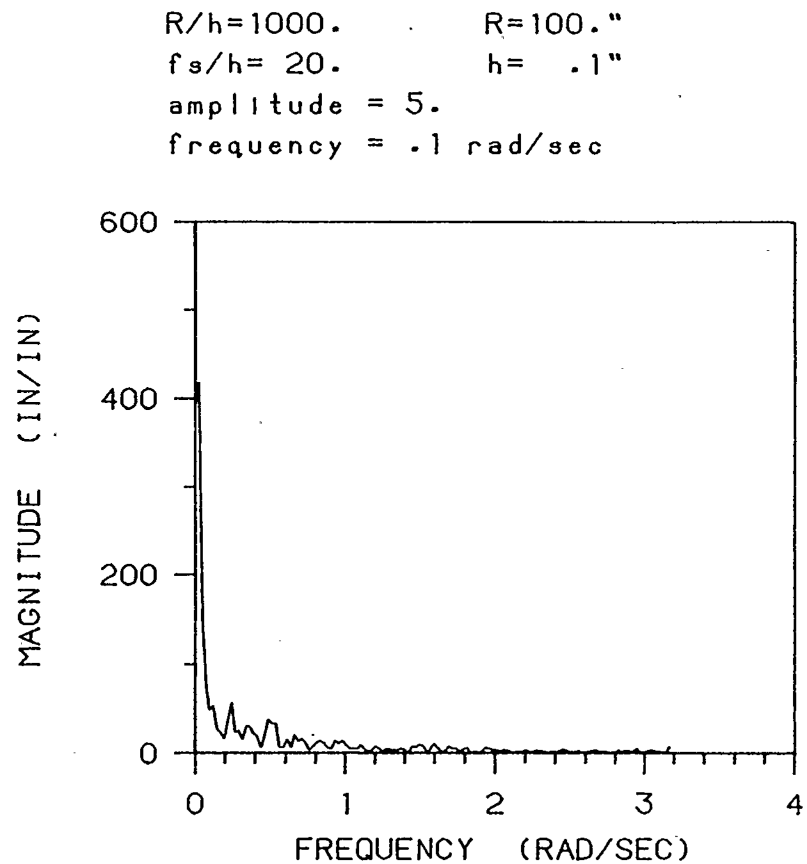

Figure 5.52 Forced-Vibration Frequency Response Using Fast Fourier Transform. $\alpha = 5.0$, $\omega_e = 0.1$ rad/sec

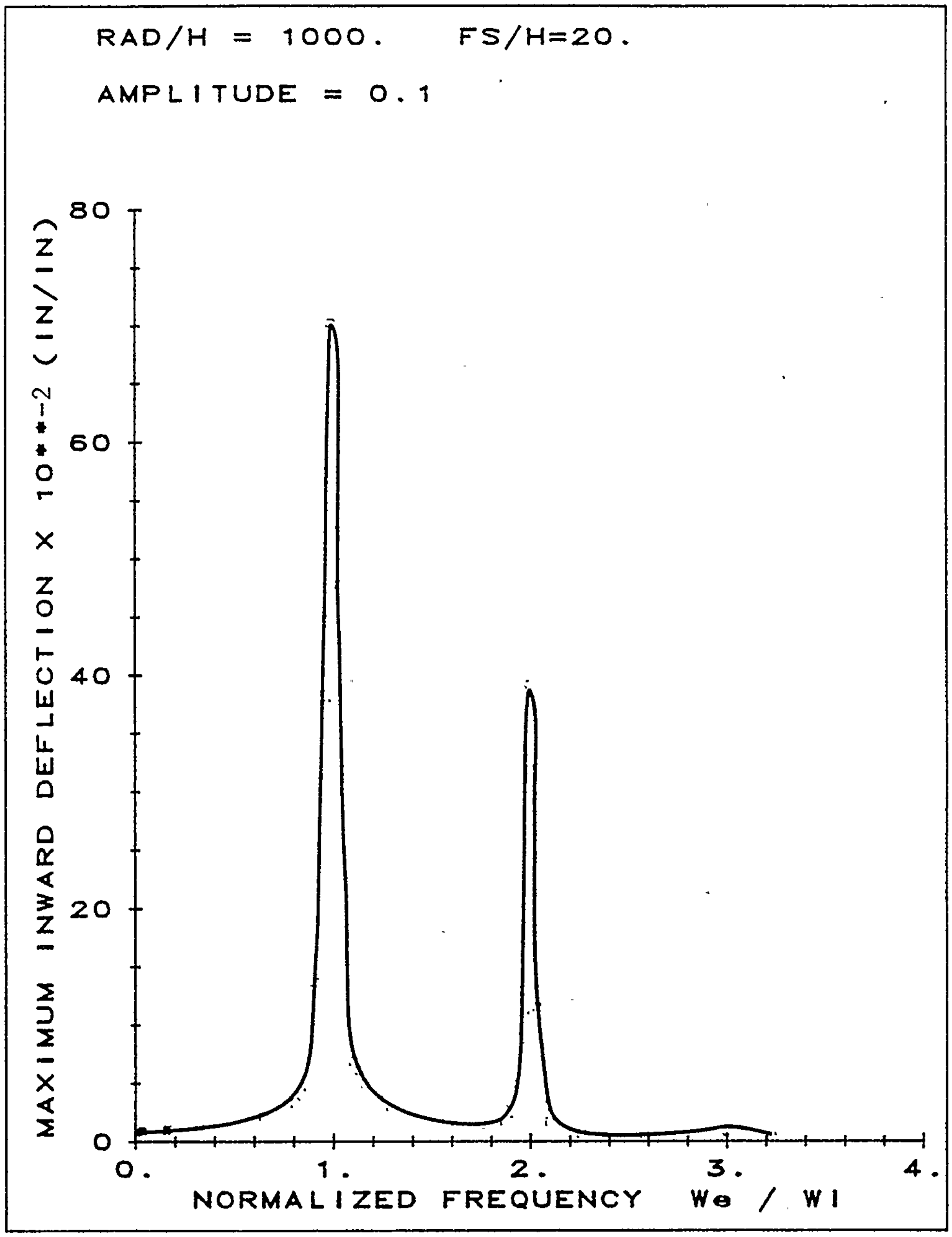

Figure 5.53 Typical Response Curve Showing the Amplitude of Maximum Inward Deflection of Spherical Shells with Excitation of Constant Amplitude α = 0.1 at Varying Frequency.

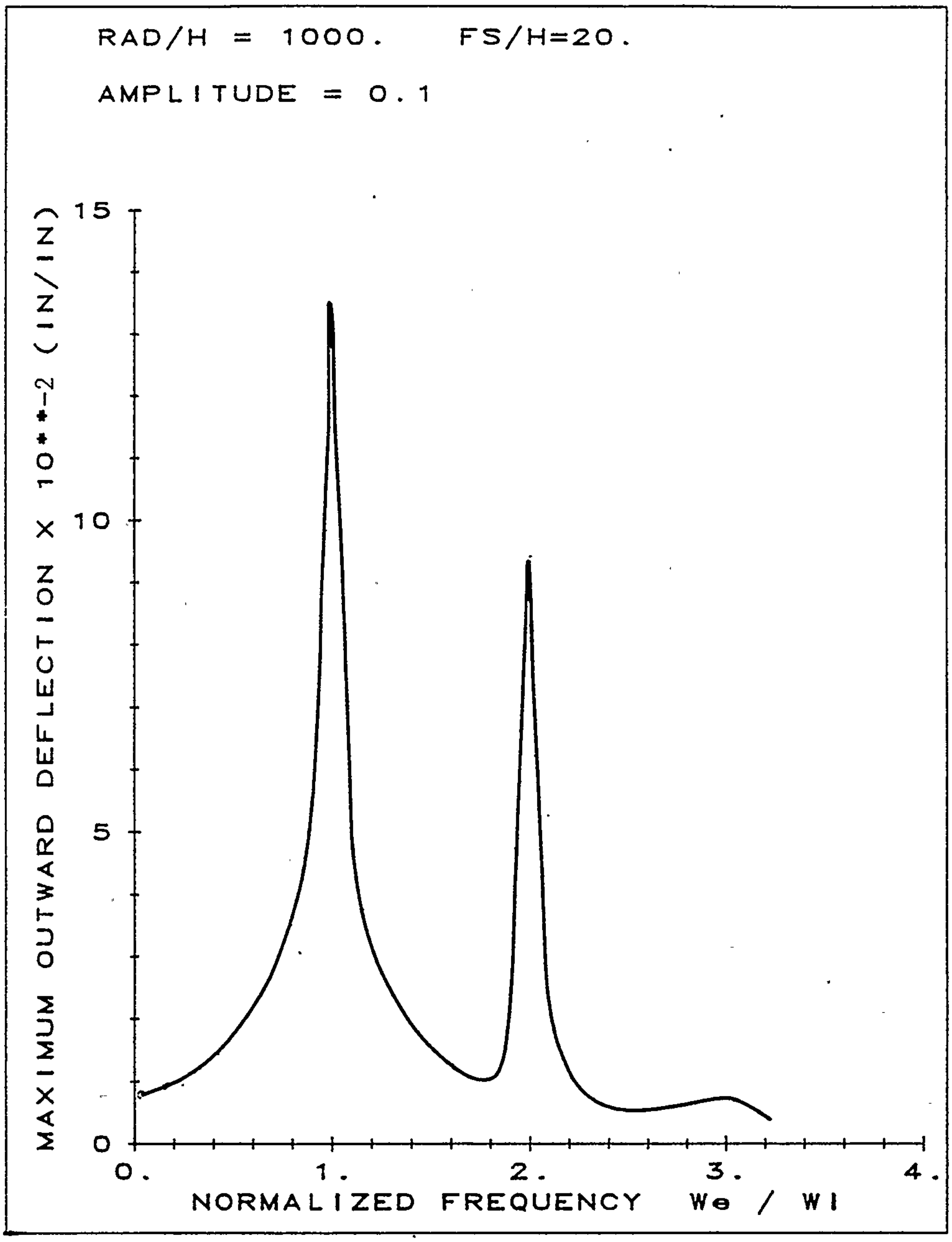

Figure 5.54 Typical Response Curve Showing the Amplitude of Maximum Outward Deflection of Spherical Shells with Excitation of Constant Amplitude $\alpha = 0.1$ at Varying Frequency.

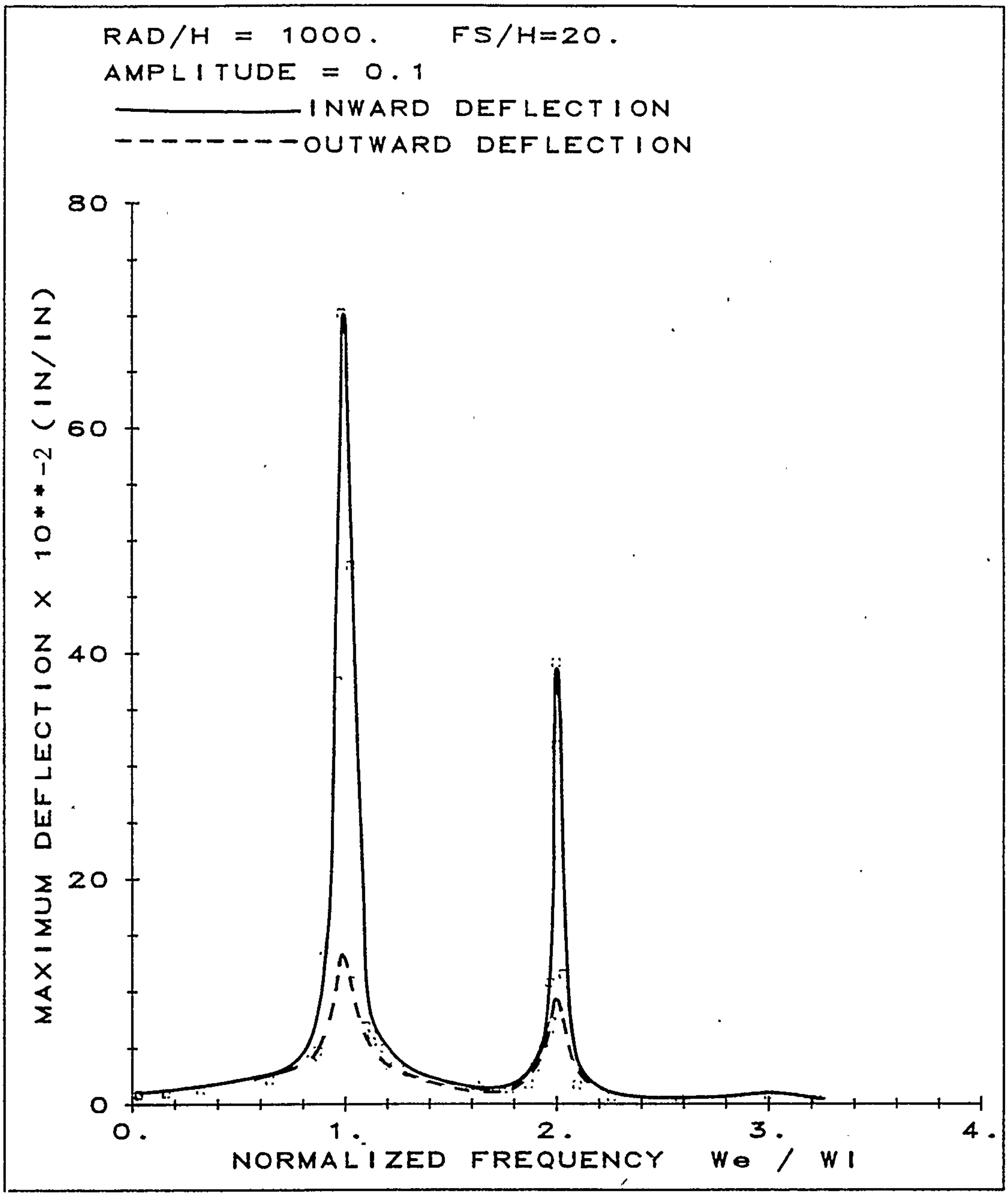

Figure 5.55 Typical Response Curve Showing the Amplitude of Maximum Inward and Outward Deflection of Spherical Shells with Excitation of Constant Amplitude α = 0.1 at Varying Frequency.

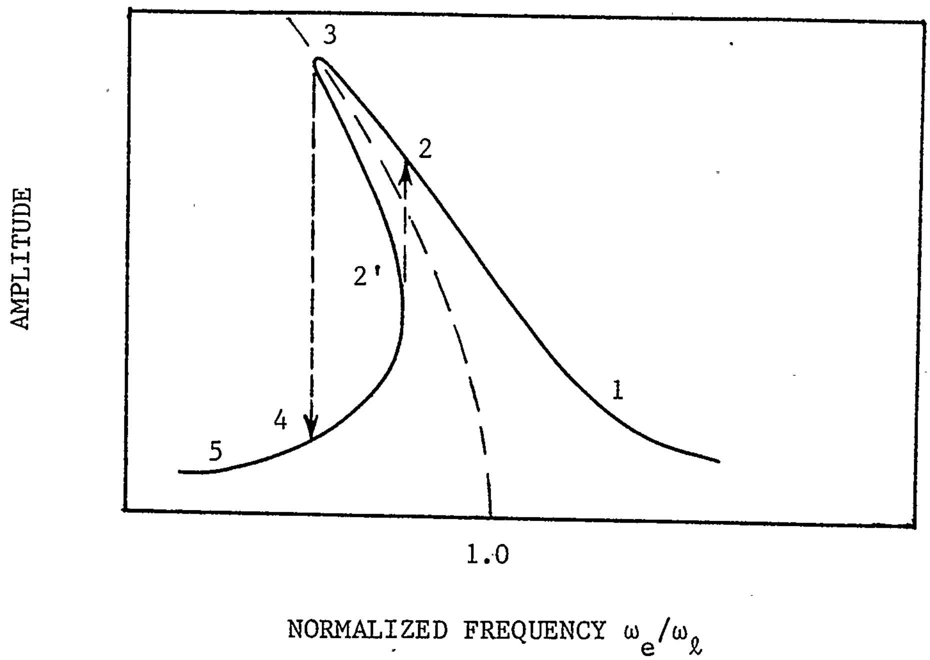

Figure 5.56 Idealized Amplitude Response of a Softening System Subjected to Sinusoidal Forced Vibration.

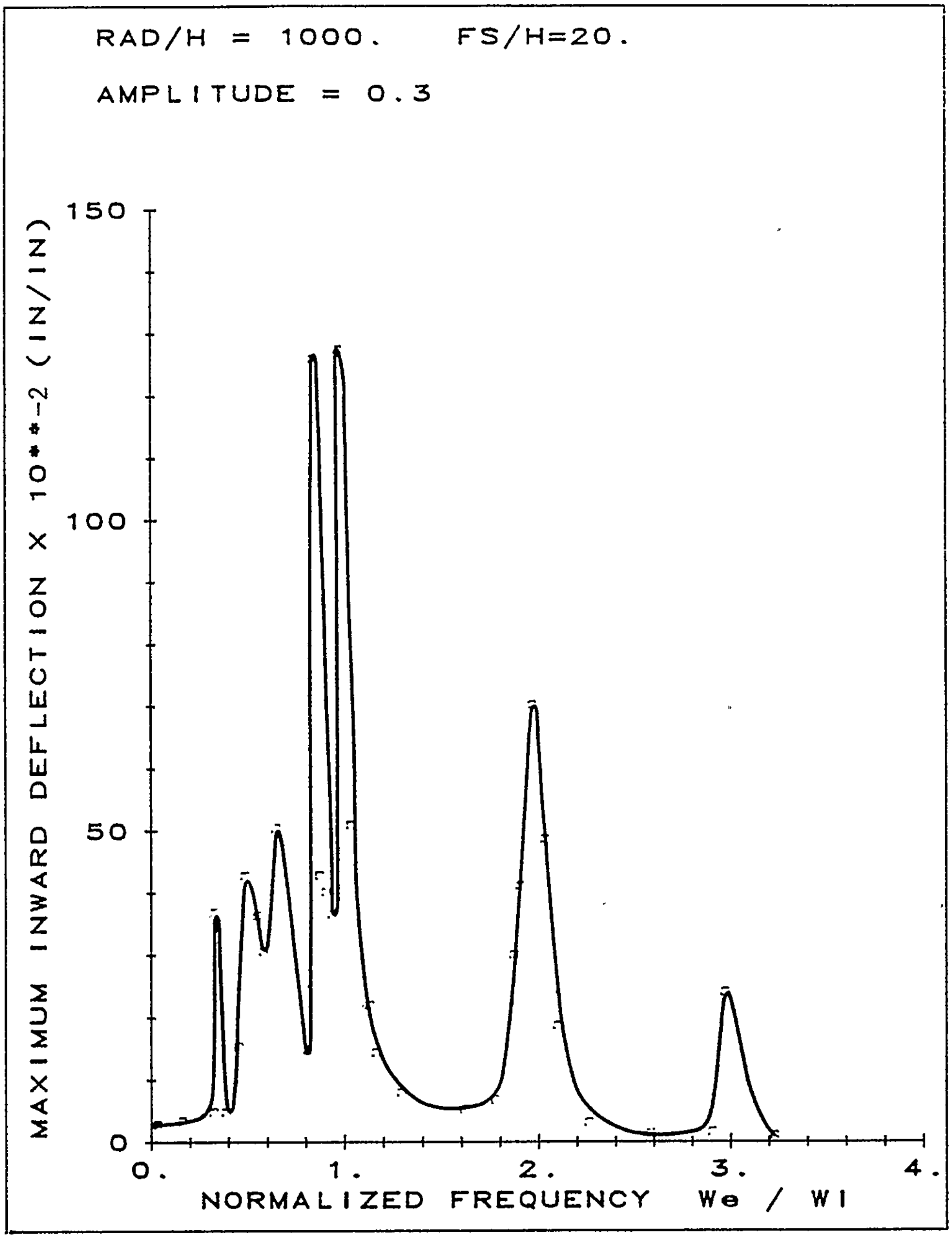

Figure 5.57 Response Curve Showing the Amplitude of Maximum Inward Deflection of Spherical Shells with Excitation of Constant Amplitude $\alpha = 0.3$

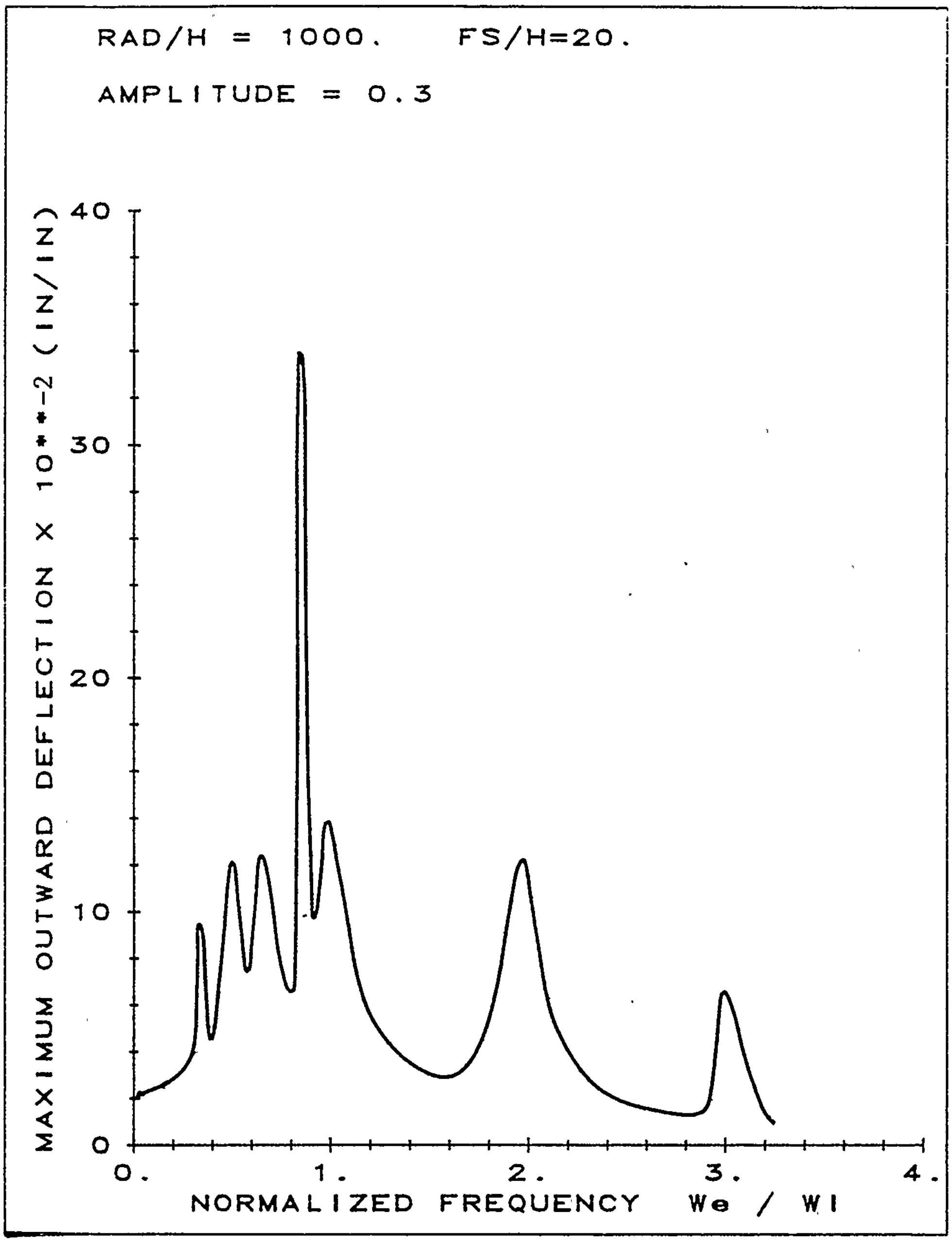

Figure 5.58 Response Curve Showing the Amplitude of Maximum Outward Deflection of Spherical Shells with Excitation of Constant Amplitude $\alpha = 0.3$

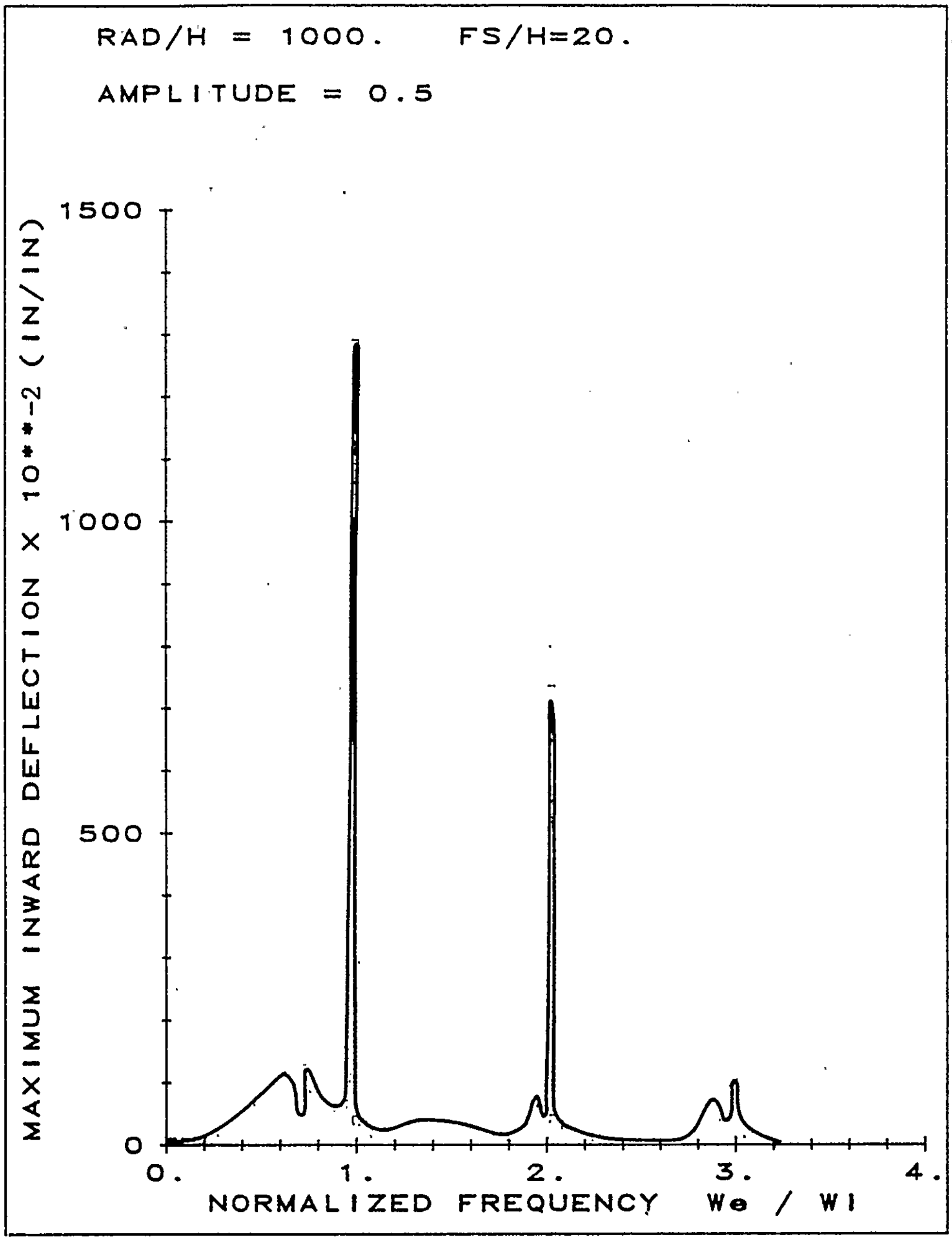

Figure 5.59 Response Curve Showing the Amplitude of Maximum Inward Deflection of Spherical Shells with Excitation of Constant Amplitude = 0.5

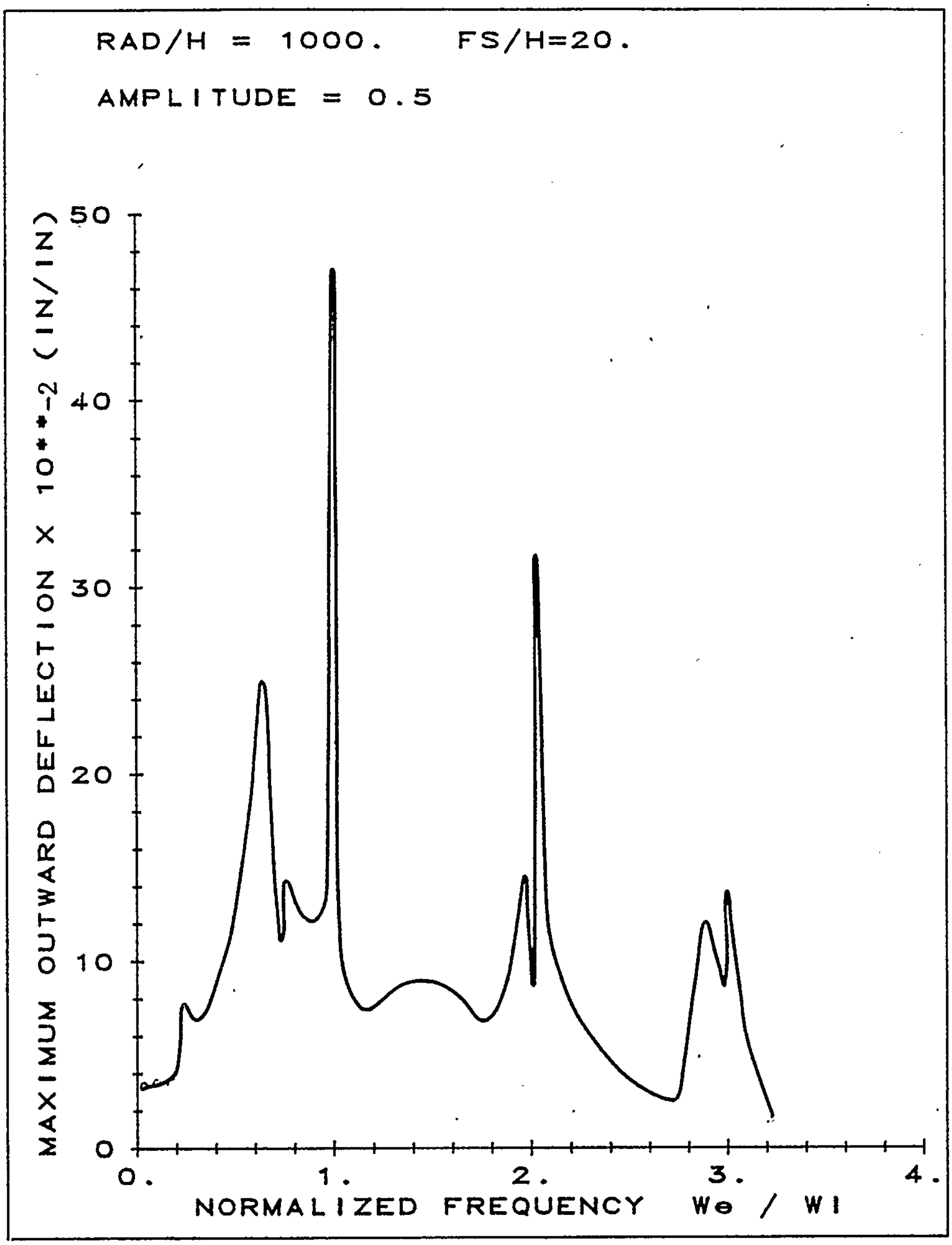

Figure 5.60 Response Curve Showing the Amplitude of Maximum Outward Deflection of Spherical Shells with Excitation of Constant Amplitude $\alpha = 0.5$

CHAPTER 6

REMARKS AND SUMMARY

6.1 REMARKS AND LIMITATIONS

This thesis has presented a simple analysis of the dynamic response of spherical shells, subjected to inward concentrated loads. The most important feature of Pogorelov's approach is that it can be applied to very large deflections. The mirror reflection of an initial surface is the most simple form of isometric transformation of the surface. In case of large deformations, the principal curvatures of the isometrically deformed surface undergo changes, and only the bending energy occurs. In the ridge region, the quasi-isometric deformations are imposed by the conditions of continuity of deformations, existing between the isometrically deformed region and the external undeformed region. The conditions must be satisfied in the transition region B-C-D, as shown in Figure 3.1, where the shell undergoes severe bending. The strain in the radial direction is very small. However, the only significant strain in the middle surface is the circumferential strain caused by the deflection W. Therefore, the total strain energy in this region consists of the bending energy and the membrane energy. The area outside the ridge undergoes small curvature change. This region is assumed to be rigid.

When the shell structure is subjected to large deflections, the final mechanism of deformation can be described by several different non-isometrically deformed surfaces as shown in Figure 6.1. It is noticed that the shell deforms isometrically in the region A-B and quasi- isometrically in the region B-C-D. For regions D-E-F and F-G-H, the shell deforms in a non-isometric manner. This mechanism of deformation is possible if the inertia of the shell is very large as compared to that of the applied mass M at the apex. In this case, the presented theoretical model is applicable to the region A-B-C-D. For the other regions, the total strain energy for each of the non-isometrically deformed surfaces must be calculated. The deformation of the surfaces is required to satisfy the conditions of continuity of displacements imposed between the transition regions.

6.2 SUMMARY

A theoretical nonlinear model relating the geometrical parameters and the applied load has been formulated using Hamilton's variational principle. An attempt has been made to solve analytically [6.1] the obtained governing equation of motion (3.25). It is believed that a closed form solution of the equation is too complex, and thus exceeding the scope of this work. However, in order to obtain a closed form solution, a linearization of the nonlinear problem has been performed. Two different numerical

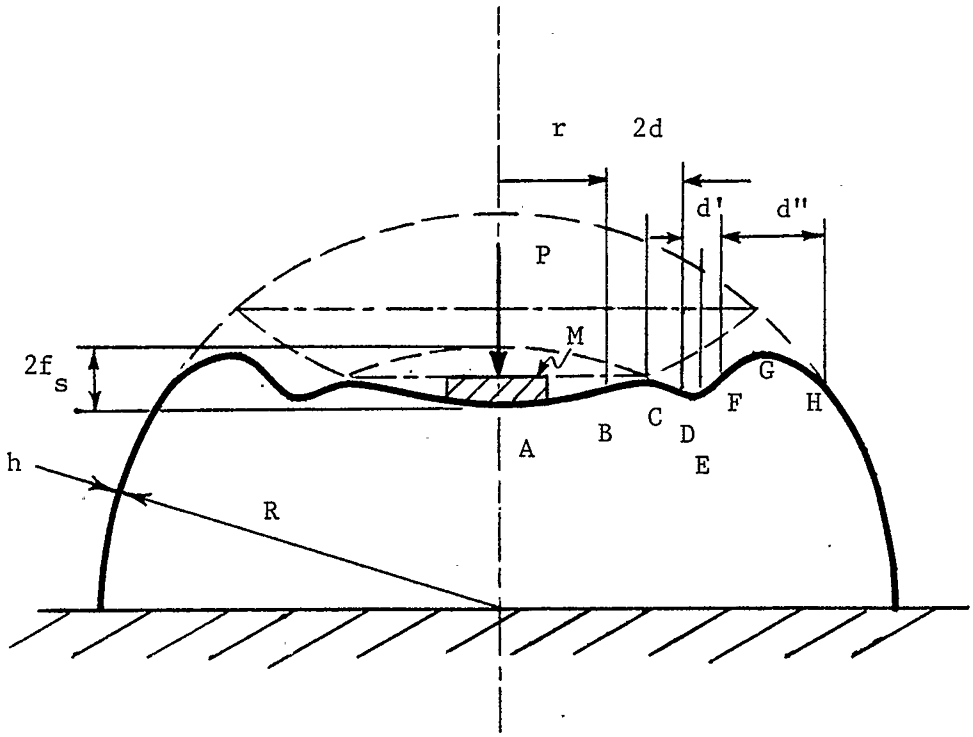

Figure 6.1 Higher Modes of Deformation of Spherical Shells under Concentrated Load at the Apex

methods are used to assess the inaccuracies. The results of nonlinear analysis are also compared with the results of the linearized equations.

The linear mathematical model, assuming that nonlinear effects are negligible, has been found satisfactory when compared with the results obtained from the nonlinear system. A typical linearized result is shown in Figure 5.28; its comparison with the result from Figure 5.25 indicates that the damping effect of the system is very small. The natural linear frequencies obtained in Table 5.5 adequately predict the frequencies of the nonlinear system in free vibration.

It has been found that the frequency of vibration is inversely proportional to the applied load as shown in Figure 5.34. Similar results were obtained in the nonlinear vibration of columns and circular cylindrical shells [5.13-5.14, 6.2]. The results of the analysis indicate that nonlinear effects depend inversely on the square of the linear frequency. With the increase of the compressive load, the linear frequency decreases to zero. The system is no longer vibrating and becomes unstable.

The principle of superposition states that the response to the simultaneous application of two different forcing inputs is the sum of two individual responses. However, in a nonlinear vibration system, the principle of the superposition is not applicable. The sum of a response due to the initial conditions and a response due to the forcing input cannot respresent the total response of the system.

The free response is related only to the system equations and is studied here to obtain a basic understanding of the dynamic behaviour of the system under various initial conditions. The frequency of vibration is no longer constant.

The dynamic jump phenomena occur in the forced response with an excitation of constant amplitude at varying frequencies. The dynamic response to a sinusoidal force shows the characteristics of a nonlinear softening system. The results show that the harmonic components increase as the forcing frequency is close to the dynamic jump and that the harmonics may contribute to the instability of the shell.

CHAPTER 7

RECOMMENDATIONS AND CONCLUSION

7.1 RECOMMENDATIONS

Although the comparison of the results obtained by two different numerical methods shows a good agreement, the methods applied to the solution of differential equations are less effective than expected. The convergence of the solutions is slow in the Runge-Kutta method, but the average computing time is about 1.75 times shorter than that in the Adam-Moulton method. However, an average of 1100 time steps is required for the Runge-Kutta method to satisfy the accuracy requirement. In order to obtain a higher accuracy of the results in a shorter time, certain adaptive control procedures for a greatly time varying system, such as the variable-step and variable-order method, using the predictor and corrector and backward differentiation formula [5.2, 5.5], can be applied.

Further studies of random load responses and other related problems may provide important information in the field of the stability of spherical shells. The presence of higher harmonics in the responses should be further investigated.

7.2 CONCLUSION

The solution for the nonlinear vibrations of spherical shells subjected to very large deformation was analysed and obtained. These results are based on the simplified assumption of isometric deformation of the shell. The total strain energy in Eq. (3.12) is only an approximation under the assumption that the ridge region is very small and that the local deflections at the point of the applied load in the central region are not taken into account. These approximations may cause certain inaccuracies of the results. Recently, finite element methods have been applied to the analysis of nonlinear vibrations of beams and plates. Similar techniques can be used to obtain a solution for the simplified theoretical model presented here for the shell. Further experiments are necessary to improve the response description. It would be interesting to compare the current results with experimental data. However, there is no comparable result available in the literature, and the present analysis provides a basis for future theoretical and experimental research on the dynamic response of vibrating spherical shells.

REFERENCES

1.1 Pogorelov, A.W., 1967: Geometrical Methods in Nonlinear Theory of Shells (In Russian), Moscow.

1.2 Love, A.E.H., 1944: A Treatise on the Mathematical Theory of Elasticity, 4th edition. Dover Publications, New York.

1.3 Reissner, E., 1946: Stresses and Small Displacements of Shallow Spherical Shells, II, Journal of Mathematics and Physics, 25, pp. 279.

1.4 Flügge, W. and Conrad, D.A., 1956: Singular Solutions in the Theory of Shallow Shells, Standard University Division of Engineering Mechanics, Technical Report No. 101, 10.

1.5 Kalnins, A. and Nahdi, P.M., 1960: Propagation of Axisymmetric Waves in an Unlimited Elastic Shell, Journal of Applied Mechanics, 27, Trans. ASME 82, Ser. E., pp. 690-695.

1.6 Leckie, F.A., 1961: Localized Loads Applied to Spherical Shells, Journal of Mechanical Engineering and Sciences, 3, 2, pp. 111-118.

1.7 Lukasiewicz, S.A., 1979: Local Loads in Plates and Shells. Fridjhoff and Nordhoff, Netherlands.

1.8 Biezeno, C.B., 1935: Uber die Bestimmung der "Durchschlagkraft" einer schwachgerummten, Kreisformigen Platle. ZAMM Bd. 15: 10-22. Repeated in Biezeno, C.B., Grammel, R., 1956: Engineering Dynamics - Vol.II, Elastic Problems of Single Machine Elements. Van Nostrand Rinchold, New York, pp. 484-496.

1.9 Chien, W.Z., Hu, H.C., 1957: On the Snapping of a Thin Spherical Cap. Ninth Intern. Congr. Appl. Mech., Univ. of Brussels, 6: pp. 309-337.

1.10 Ashwell, D.G., 1959: On the Large Deflection of a Spherical Shell With an Inward Point Load. In W.T. Koiter (ed.): Proc. IUTAM Symp. on the Theory of Thin Elastic Shells, Delft, Netherlands, pp. 43-64.

1.11 Archer, R.R., 1962: On the Numerical Solution of the Nonlinear Equations for Shells of Revolution. Journal of Math. Phys. 41, pp. 165-178.

1.12 Fitch, J.R., 1968: The Buckling and Post Buckling Behaviour of Spherical Caps Under Concentrated Load. Intern. J. Solids Structures 4: pp. 421-446.

1.13 Mescall, J.F., 1965: Large Deflections of Spherical Shells Under Concentrated Loads. Journal of Applied Mechanics. 32: pp. 936-938.

1.14 Evan-Iwanowski, R.M., Loo, T.C., 1962: Deformations and Stability of Spherical Shells Subjected to the Action of the Systems of Line Loads and Concentrated Loads. Syracuse University, Research Inst. (SURI) Report pp. 834-835.

1.15 Bushnell, D., 1967: Bifurcation Phenomena in Spherical Shells Under Concentrated and Ring Loads. AIAA J. 5: pp. 2034-2040.

1.16 Penning, F.A., Thurston, G.A., 1965: The Stability of Shallow Spherical Shells Under Concentrated Load. NASA Cr-256, Washington, D.C.

1.17 Penning, F.A., 1966: Nonaxisymmetric Behaviour of Shallow Shells Loaded at the Apex. Journal of Applied Mechanics. 33: pp. 699-700.

1.18 Penning, F.A., 1966: Experimental Buckling Modes of Clamped Shallow Shells Under Concentrated Load. Journal of Applied Mechanics. 33: pp. 297-304.

1.19 von Kármán, T., Tsien, H.S., 1939: The Buckling of Spherical Shells by External Pressure. Journal of Aeronautics Science, 7: pp. 43-50.

1.20 Budiansky, B., 1960: Buckling of Clamped Shallow Spherical Shells. In. W.T. Koiter (ed.): Proc. Symp. on the Theory of Thin Elastic Shells. North-Holland, Amsterdam, pp. 64-94.

1.21 Thurston, G.A., 1961: A Numerical Solution of the Nonlinear Equations for Axisymmetric Bending of Shallow Spherical Shell. Journal of Applied Mechanics, 28: pp. 557-562.

1.22 Weinitschke, H.J., 1958: On the Nonlinear Theory of Shallow Spherical Shells. Journal of the Society for Industrial and Applied Mathematics, Vol. 6, pp. 209.

1.23 Parmerter, R.R., 1963: The Buckling of Clamped Shallow Spherical Shells Under Uniform Pressure. (Ph.D. thesis, California Institute of Technology, Report AFOSR5362.

1.24 Huang, N.C., 1964: Unsymmetrical Buckling of Thin Shallow Spherical Shells. Journal of Applied Mechanics, 30: pp. 447-457.

1.25 Weinitschke, H.J., 1965: On Asymmetric Buckling of Shallow Spherical Shells. Journal of Math. Phys. 44: pp. 141-163.

1.26 Evan-Iwanowski, R.M., Loo, T.C., Chia, Y.C., 1965: Influence of Imperfections on Mechanism of Buckling of Shallow Spherical Shells. Technical Report AFFDL-TR-65-8. Syracuse Univ. Research Institute.

1.27 Gol'denveizer, A.L., 1983: Geometrical Theory of Stability of Shells. Mechanics of Solids. Vol. 18, No. 1, pp. 135-145.

1.28 Federhofer, K., 1937: Zur Berechnung der Eigenschwingungen der Kugelschale, Sitzungberichte der Akademic der Wissenschaften in Wien, Mathematischnaturwissenschaftliche Klasse, No. 2A, 146: pp. 57-69, 505-514.

1.29 Naghdi, P.M., Kalnins, A., 1962: On Vibrations of Elastic Spherical Shells. Journal of Applied Mechanics, TRANS. ASME Vol. 28, Series E, pp. 65-72.

1.30 Reissner, E., 1946: On Vibrations of Shallow Spherical Shells. Journal of Applied Physics. 17: pp. 1038-1042.

1.31 Naghdi, P.M., 1959: On the General Problem of Elastokinetics in the Theory of Shallow Shells. Proc. IUTAM Symposium on Theory of Thin Elastic Shells, Delft.

1.32 Naghdi, P.M., Kalnins, A., 1960: Axisymmetric Vibrations of Shallow Elastic Spherical Shells. Journal of Acoustic Society of America. 32, No. 3: pp. 342-347.

1.33 Kalnins, A., 1964: Effects of Bending on Vibrations of Spherical Shells. Journal of Acoustic Society of America, 36, No. 1: pp. 74-81.

1.34 Conner, J., 1960: Nonlinear Transverse Axisymmetric Vibrations of Shallow Spherical Shells. Watertown Arsenal Laboratories Report.

1.35 Grigolink, E.I., 1955: Nonlinear Vibrations and Stability of Shallow Shells. Inst. Engr. Research, Univ. of Calif., Berkeley, Applied Mech. Series 131, No. 7, (in Russian).

1.36 Ho, F.H.H., 1965: Dynamic Instability of a Deep Spherical Shell. Am. Soc. Civil Engr., 91, No. EM3: pp. 233-248.

1.37 Archer, R.R., Fanieli, J., 1965: On the Vibration and Stability of Finitely Deformed Shallow Spherical Shells. Journal of Applied Mechanics 32: pp. 116-120.

2.1 Kraus, H., 1967: Thin Elastic Shells. John Wiley & Sons Inc., New York.

2.2 Gould, P.L., 1977: Static Analysis of Shells. D.C. Heath and Company, Toronto.

2.3 Novozhilov, V.V., 1959: The Theory of Thin Shells. P. Noordhoff Ltd., The Netherlands.

2.4 Lipschutz, M.M., 1969: Theory and Problems of Differential Geometry. McGraw-Hill Book Company, New York.

2.5 Niordson, F.I., 1985: Shell Theory. Elsevier Science Publishers B.V., The Netherlands.

3.1 Bushnell, D., 1979: Control of Surface Configuration by Application of Concentrated Loads. AIAA Journal, Vol. 17, No. 1, pp. 71-77.

3.2 Meirovitch, L., 1967: Analytical Methods in Vibrations. The Macmillan Company, New York.

3.3 Dym, C.L. and Shames, I.H., 1973: Solid Mechanics: A Variational Approach. McGraw-Hill, Inc. New York.

3.4 Fung, Y.C., 1965: Foundations of Solid Mechanics. Prentice-Hall, Inc., New Jersey.

3.5 Timoshenko, S., 1955: Vibration Problems in Engineering, Von Nostrand Co.

3.6 Wells, D.A., 1967: Theory and Problems of Lagrangian Dynamics. Schaum's Outline Series, McGraw-Hill Inc., New York.

3.7 Elsgolc, L.E., 1961: Calculus of Variations, Addison-Wesley Book Co.

3.8 Yu, Y.Y., 1963: Application of Variational Equation of Motion to the Nonlinear Vibration Analysis of Homogeneous and Layered Plates and Shells. Journal of Applied Mechanics. Vol. 30, No. 1, Trans. ASME. Vol. 85, Series E, pp. 79-86.

3.9 Koplik, B. and Yu, Y.Y., 1967: Axisymmetric Vibrations of Homogeneous and Sandwich Spherical Caps. Journal of Applied Mechanics. Vol. 34, Trans. ASME, Vol. 89, Series E, pp. 667-673.

3.10 Boyce, W.E. and DiPrima, R.C., 1977: Elementary Differential Equations and Boundary Value Problems. Third Edition. John Wiley and Sons, Inc., New York.

3.11 Simitses, G.J., 1976: An Introduction to the Elastic Stability of Structures, Prentice-Hall, Inc., Englewood Cliffs, New Jersey.

3.12 Brush, D.O., Almroth, B.O., 1975: Buckling of Bars, Plates and Shells. McGraw-Hill Inc., New York.

3.13 Lukasiewicz, S., 1967: Concentrated Loads on Shallow Spherical Shells. Quarterly Journal of Mechanical Applied Mathematics. Vol. 20, No. 3, pp. 293-305.

4.1 Cunningham, W.J., 1958: Introduction to Nonlinear Analysis. McGraw-Hill Inc., New York.

4.2 Meirovitch, L, 1970: Methods of Analytical Dynamics. McGraw-Hill, Inc., New York.

4.3 Ogata, K., 1970: Modern Control Engineering. Prentice-Hall Inc., Englewood Cliffs, New Jersey.

4.4 Minorisky, N., 1962: Nonlinear Oscillations. D. Van Nostrand Co., Princeton, New Jersey.

4.5 Stoker, J.J., 1950: Nonlinear Vibrations, Interscience Publishers, Inc., New York.

4.6 Ku, Y.H., 1958: Analysis and Control of Nonlinear Systems. The Ronald Press Company, New York.

4.7 Tse, F.S., et al., 1978: Mechanical Vibrations Theory and Applications. Second Edition. Allyn and Bacon Inc., Boston.

5.1 Conte, S.D., 1965: Elementary Numerical Analysis, Second Edition, McGraw Hill, Inc., New York.

5.2 International Mathematical & Statistical Libraries (IMSL) Reference Manual, Edition 9, Revised June, 1982, IMSL-0009. Houston, Texas.

5.3 Hamming, R.W., 1973: Numerical Methods for Scientists and Engineers, Second Edition, McGraw-Hill Inc., New York.

5.4 Scheid, F., 1968: Theory and Problems of Numerical Analysis. McGraw-Hill Inc., New York.

5.5 Simulation Services, 1985: Continuous System Simulation Language - Version IV. User's Guide and Reference Manual.

5.6 Lukasiewicz, S.A., Glockner, P.G., 1983: Collapse by Ponding of Shells. International Journal of Solids Structures. Volume 19, No. 3, pp. 251-261.

5.7 Brigham, E.O., 1974: The Fast Fourier Transform. Prentice-Hall, Inc. Englewood Cliffs, New Jersey.

5.8 Bendat, J.S. and Piersol, A.G., 1971: Random Data: Analysis and Measurement Procedures, Wiley-Interscience, New York.

5.9 Newland, D.E., 1974: An Introduction to Random Vibrations and Spectral Analysis. McGraw-Hill Inc., New York.

5.10 Blakely, K.D. and Dobbs, W., 1982: System Identification Using Sinusoidal Test Data. Published by SAE Aerospace Congress and Exposition: Advances in Dynamic Analysis and Testing. SAE Technical Series Paper 821460.

5.11 Cooley, J.W. and Tukey, J.W., 1965: An Algorithm for the Machine Calculation of Complex Fourier Series, Mathematics for Computation, Vol. 19, pp. 297-301.

5.12 Evensen, D.A., 1963: Some Observations on the Nonlinear Vibration of Thin Cylindrical Shells. AIAA J. Vol. 1, pp. 2857-2858.

5.13 Evensen, D.A., 1968: The Influence of Initial Stresses and Boundary Restraints on the Nonlinear Vibrations of Cylindrical Shells. Unpublished manuscript.

5.14 Evensen, D.A., 1972: Nonlinear Vibration of Circular Cylindrical Shells. Published in Thin-Shell Structures Symposium, California Institute of Technology. Prentice-Hall Inc., Englewood Cliffs, New Jersey, pp. 133-155.

5.15 Vol'mir, A.S., 1966: Stability of Elastic Systems. Translated from Russian, Foreign Technology Division, Air Force Systems Command, Wright-Patterson Air Force Base, Ohio, pp. 65-68.

5.16 Chen, J.C., 1972: Nonlinear Vibration of Cylindrical Shells. Ph.D. Thesis, California Institute of Technology, Pasadena.

5.17 Grossman, P.L., Koplik, B., Yu, Y.Y., 1969: Nonlinear Vibrations of Shallow Spherical Shells. Journal of Applied Mechanics. Vol. 36, TRANS ASME. Vol. 36, Series E, pp. 448-451.

6.1 Kamke, E., 1959: Differentialgleichungen Lösungsmethoden Und Lösungen, Chelsea Publishing Company, New York.

6.2 Reissner, E., 1955: Nonlinear Effects in the Vibrations of Cylindrical Shells. Report No. Am5-6. Ramo-Wooldridge Corp.

APPENDIX A

EXAMPLES OF LAMÉ PARAMETERS

A. EXAMPLES OF LAMÉ PARAMETERS

The choice of curvilinear coordinate is rather arbitrary. It depends on how to simplify the problem and to obtain a concise mathematical expressions for the solution. There are three simple examples illustrating the calculations of Lamé parameters from the geometrical relationships.

Consider a circular arc of radius R in x - z plane as shown in Figure A.1. First, the polar angle is chosen as the curvilinear coordinate.

$$dS = R\, d\rho \;, \tag{A.1.1}$$

Then, the Lamé parameter is R.

Second, if the z coordinate is chosen, the equation of a circle is given by

$$x^2 + z^2 = R^2 \;,$$

$$2xdx = -2zdz \;,$$

$$dx^2 = \left(\frac{z}{x}\right)^2 dz^2 \;.$$

From Eq. (2.9a),

$$ds^2 = dx^2 + dz^2 \;,$$

$$ds^2 = \left(1 + \frac{z^2}{x^2}\right) dz^2 \;,$$

$$ds = \left(1 + \frac{z^2}{x^2}\right)^{\frac{1}{2}} dz^2 \;. \tag{A.1.2}$$

The Lamé parameter is

$$\left(1 + \frac{z^2}{x^2}\right)^{\frac{1}{2}} \;.$$

Finally, the arc length is chosen at the Curvilinear co-ordinate and the Lamé parameter is one,

$$ds = 1 \cdot ds \quad . \tag{A.1.3}$$

In most application in shells of revolution, the circumferential angle Θ is chosen as one of the curvilinear coordinates. For the other coordinate, there are at least three choices, namely the meridian angle ϕ, the axial coordinate z, and the arc length. The most common preference is the meridian angle ϕ with the Lamé parameter being constant.

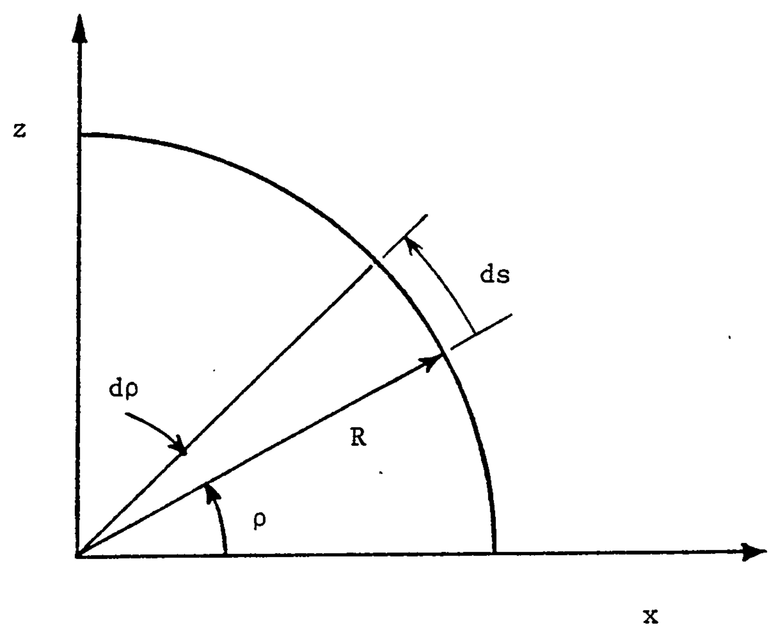

Figure A.1 A Circular Arc on x-z Plane

APPENDIX B

SUMMARY OF THE STRAIN ENERGY FOR THE INNER AND OUTER STRIPS OF THE RIDGE REGION [1.1]

B. SUMMARY OF THE STRAIN ENERGY FOR THE INNER AND OUTER STRIPS OF THE RIDGE REGION [1.1]

Consider the ridge region B-C-D as shown in Figure 3.1. Physically, the ridge is very small, and the strain in the meridian direction is negligible.

$$\varepsilon_r \cong 0 \quad . \tag{B.1.1}$$

The circumferential strain in the middle surface is obtained as

$$\varepsilon_\theta = \frac{2\pi(r_1 + u) - 2\pi\, r_1}{2\pi\, r_1} \cong \frac{u}{r_1} \quad . \tag{B.1.2}$$

The membrane strain energy is given by

$$U_m = \frac{Eh}{4} \iint_{s_{II}} \left(\frac{u}{r_1}\right)^2 ds_{II} \; . \tag{B.1.3}$$

The integration over the area of the inner or outer strip is

$$ds_{11} = 2\pi\, r_1\, dr_1 \quad . \tag{B.1.4}$$

From Eq. (B.1.4)

$$U_m = \frac{\pi E\, h\, r_1}{2} \int_o^d \left(\frac{u}{r_1}\right)^2 dr_1 \quad . \tag{B.1.5}$$

It is noted that the membrane strain energy in the inner strip is the same as that in the outer strip.

The bending energy in the outer strip is associated with the changes in curvatures.

$$\Delta\kappa_1 = \kappa_1{}' - \kappa_1 = \left(\frac{1}{R} + W''\right) - \frac{1}{R} = \frac{\partial^2 W}{\partial\, r^2} \quad . \tag{B.1.6}$$

$$\Delta\kappa_2 = \kappa_2{}' - \kappa_2 = \frac{1}{R}\left(1 + \frac{W'}{\Phi}\right) - \frac{1}{R} = \frac{1}{\Phi R}\frac{\partial\, W}{\partial\, r} \quad . \tag{B.1.7}$$

From Eq. (3.9), the bending energy can be calculated as

$$U_b' = \pi D \int_o^d r_1 \left[W''^2 + \left(\frac{W'}{\Phi R}\right)^2 + 2\nu W'' \frac{W'}{\Phi R}\right] dr_1 \quad .$$

The boundary conditions are given as

$$W' \ (r_1 = 0) = -\phi \quad , \tag{B.1.8a}$$

$$W' \ (r_1 = d) = 0 \quad . \tag{B.1.8b}$$

Hence, the bending energy in the outer strip is

$$U_b' = \pi D \int_o^d r_1 W''^2 \, dr_1 + \frac{2\pi D\nu}{\Phi R} \int_o^d r_1 W'' W' \, dr_1$$

$$= \pi D \int_o^d r_1 W''^2 \, dr_1 - \pi D\nu d \frac{\Phi}{R} \quad . \tag{B.1.9}$$

Similarly, the bending energy in the inner strip can also be calculated from the changes in curvatures. The changes of curvature are given as

$$\Delta\kappa_1 = \kappa_1' - \kappa_1 = \left(-\frac{1}{R} + W''\right) - \frac{1}{R} = W'' - \frac{2}{R} \quad . \tag{B.1.10}$$

$$\Delta\kappa_2 = \kappa_2' - \kappa_2 = -\frac{1}{R}\left(1 + \frac{W'}{\Phi}\right) - \frac{1}{R} = -\frac{W'}{\Phi R} - \frac{2}{R} \quad . \tag{B.1.11}$$

From Equ. (3.9), the bending energy is then calculated as

$$U_m = \frac{D}{2} \int_o^d \left[\left(W'' - \frac{2}{R}\right)^2 + \left(-\frac{W'}{\Phi R} - \frac{2}{R}\right)^2 + \right.$$

$$\left. 2\nu \left(W'' - \frac{2}{R}\right)\left(-\frac{W'}{\Phi R} - \frac{2}{R}\right)\right] 2\pi \, r_1 \, dr_1$$

$$= \pi D \, r_1 \int_o^d W''^2 \, dr_1 - 4(1+\nu) \, \pi D d \frac{\Phi}{R} + \pi D d\nu \frac{\Phi}{R} \; . \tag{B.1.12}$$

In order to calculate the total strain energy in Eq. (B.1.5), (B.1.9), and (B.1.12), the condition of continuity given by a displacement function for the deformation of the shell in the ridge must satisfy the boundary conditions Eq. (B.1.8). The displacement function is of the form

$$u' + \Phi W' + \frac{1}{2} W'^2 = 0 \quad . \tag{B.1.13}$$

An energy functional obtained from the total energy in the inner strip and outer strip is reduced to

$$J = \int_0^d D W''^2 + \frac{E h}{2} \left(\frac{u}{r_1}\right)^2 dr_1 \quad .$$

The application of the Lagrange multiplier method is then applied to the minimization of the functional, satisfying the constraint in Eq. (B.1.13) and the boundary conditions Eq. (B.1.8). The minimum of the functional is 1.15 obtained by Pogorelov, and the total strain energy of the shell is given by

$$U = \frac{2\pi c E h^{5/2} (2f)^{3/2}}{R} \quad , \tag{3.12}$$

where

$$c = \frac{J}{12^{3/4} (1 - \nu^2)} \cong 0.19 \quad .$$

APPENDIX C

DERIVATION OF THE ENERGY FUNCTIONAL EQ. (3.20) FOR THE GOVERNING EQUATION

C. DERIVATION OF THE ENERGY FUNCTIONAL EQ. (3.20) FOR THE GOVERNING EQUATION

The Lagrangian has been derived in Eq. (3.19) as

$$L = \pi R\gamma h(f_s + \frac{x}{2})\,\dot{x}^2 + \frac{M}{2}\,\dot{x}^2 - \frac{2\pi cE\ h^{5/2}}{R}[2(f_s + \frac{x}{2})]^{3/2}$$
$$+ 2P(f_s + \frac{x}{2}) \quad . \qquad (C.1.1)$$

Hamilton's principle then requires

$$\delta I = \delta \int_{t_1}^{t_2} L\ dt = 0 \quad . \qquad (C.1.2)$$

From (C.1.2),

$$\delta I = \int_{t_1}^{t_2} \pi R\gamma h\ \delta(f_s + \frac{x}{2})\dot{x}^2 + \frac{M}{2}\,\delta\dot{x}^2 - \frac{2\pi cE\ h^{5/2}}{R}\,\delta[2(f_s + \frac{x}{2})]^{3/2}$$
$$+ 2P\ \delta(f_s + \frac{x}{2})\ \ dt = 0 \quad . \qquad (C.1.3)$$

Carrying out the variation operation and integrating each term by parts with respect to time, the following results are obtained as:

For the first term,

$$\gamma h\pi R \int_{t_1}^{t_2} [2f_s\ \dot{x}\ \delta\dot{x} + \frac{1}{2}(\delta x\ \dot{x}^2 + x\ \delta\dot{x}^2)]\ dt$$

$$= \gamma h\pi R\ \{ \int_{t_1}^{t_2} -2f_s\ \ddot{x}\ \delta x\ dt + 2f_s\ \dot{x}\ \delta x\Big|_{t_1}^{t_2}$$

$$+ \frac{1}{2} \int_{t_1}^{t_2} (-\dot{x}^2 - 2x\ddot{x}) \; \delta x \; dt + (2f_s \; \dot{x} + x\dot{x}) \; \delta x \; \Big|_{t_1}^{t_2} \; \}$$

$$= \gamma h \pi R \; \{ \int_{t_1}^{t_2} (-2f_s \; \ddot{x} - \frac{1}{2} \dot{x}^2 - x\ddot{x}) \; \delta x \; dt$$

$$+ \; \delta x \; (2f_s \; \dot{x} + x\dot{x}) \; \Big|_{t_1}^{t_2} \; \} \quad . \tag{C.1.4}$$

For the second term,

$$\frac{M}{2} \int_{t_1}^{t_2} 2\dot{x} \; \delta\dot{x} \; dt = \int_{t_1}^{t_2} -M\ddot{x} \; \delta x \; dt + M\dot{x} \; \delta x \; \Big|_{t_1}^{t_2} \quad . \tag{C.1.5}$$

For the third term,

$$\frac{-2\pi cE \; h^{5/2}}{R} \int_{t_1}^{t_2} 3\sqrt{2} \; (f_s + \frac{x}{2})^{\frac{1}{2}} \cdot \frac{\delta x}{2} \; dt$$

$$= - \frac{3\sqrt{2} \; \pi cE \; h^{5/2}}{R} \int_{t_1}^{t_2} (f_s + \frac{x}{2})^{\frac{1}{2}} \; \delta x \; dt \quad . \tag{C.1.6}$$

And for the fourth term,

$$2P \int_{t_1}^{t_2} \delta (f_s + \frac{x}{2}) \; dt = P \int_{t_1}^{t_2} \delta x \; dt \quad . \tag{C.1.7}$$

Summing the terms from Eq. (C.1.4) to (C.1.7), Eq. (3.20) is then obtained.

APPENDIX D

COMPUTER PROGRAM FOR SOLVING THE EQUATIONS

OF MOTION OF SPHERICAL SHELLS

```
**************************************************************************
*
* PURPOSE    :  THE PROGRAM IS TO ANALYZE THE DYNAMIC RESPONSE OF
*               SPHERICAL SHELLS UNDER A CONCENTRATED LOAD.
*               THE EXCITATION FORCE IS A SINUSOIDAL FUNCTION.
*
* DESCRIPTION:  THE PROGRAM IS TO INPUT GEOMETRICAL AND MATERIAL
*               CONSTANTS AND INITIAL CONDITIONS FOR TIME, DISPLACEMENTS
*               AND VELOCITY EITHER BY CALLING SUBROUTINE readØ2 OR
*               BY OPENING DATA FILE inØ2.  THESE INPUT DATA WILL
*               PASS ON TO THE SUBROUTINE DVERK AND SUBROUTINE eqn2.
*               THE OUTPUT DATA IS STORED IN FILE outØ2.
*
*               THE SUBROUTINE DVERK IS A DIFFERENTIAL EQUATION SOLVER
*               USING THE RUNGE-KUTTA FIFTH AND SIXTH ORDER METHOD
*               DEVELOPED BY VERNER.  THE EQUATION OF MOTION IS
*               DIFFERENTIAL EQUATION  WITH INITIAL CONDITIONS.  DVERK
*               WILL THEN FIND APPROXIMATIONS TO THE SOLUTION OF THE
*               EQUATIONS AUTOMATICALLY BY SETTING THE INDICATOR, ind,
*               TO 1.  HOWEVER, MANY OPTIONS ARE PROVIDED TO INCLUDE
*               ERROR CONTROL, TO RESTRICT STEP SIZES, AND TO INTERRUPT
*               AND EXAMINE THE INTERMEDIATE STAGES OF CALCULATIONS.
*
*               THE SUBROUTINE eqn2 IS USED TO EVALUATE THE DISPLACEMENT
*               AND VELOCITY FOR THE EQUATIONS OF MOTION EVERYTIME
*               CALLED FROM THE MAIN PROGRAM.
*
**************************************************************************
*
* THE IMSL SUBROUTINE DVERK IS DESCRIBED AS FOLLOWS:
*
* PURPOSE:      TO SOLVE DIFFERENTIAL EQUATION USING RUNGE-KUTTA FIFTH
*               AND SIXTH ORDER METHOD
*
*
* TYPE:         IMSL SUBROUTINE (PLEASE REFER TO IMSL MANUAL FOR DETAIL)
*
* CALL FORMAT:
*
*     call imsl$dverk(n, eqn2, t, y, tend, tol, ind, c, nw, w, ier)
*
* ARGUMENTS:
*
*          Type     Description                                 Data Flow
*
*   n      integer  number of equations                         in
*   eqn2   ----     name of subroutine to evaluate              in
*                   the system equations
*   t      real     independent variable                        in/out
*   y      real     dependent variable                          in/out
*   tend   real     value of t at which solution is desired     in
*   tol    real     tolerance for error control                 in
*   ind    integer  indicator, 1 for default                    in
*                               2 for option                    in
*                               3 for return                    out
*                              -3 for tolerance too small       out
*                              -2 hmin > hmax (tol too small)   out
*                              -1 for exceeding max. no. of
*                                 eqn2 evaluation               out
*   c      real      communication vector,
```

```
*                        c(1) to c(9) input only for ind .ne. 1     in/out
*                        c(1Ø) to c(24)                             out
*   nw     integer       row dimension of matrix w  i.e.(nw.ge. n)  in
*   w      real          working area matrix, w(nw, 9)              in
*   ier    integer       error parameter,
*                               Ø for no terminal error             out
*                             129 for (nw .lt. n) or (tol .le. Ø)   out
*                             13Ø for ind not in range 1 to 6       out
*                             131 for tend is not changed           out
*                             132 for relative error control
*                                     selected c(1) = 2             out
*
*************************************************************************
*
* REAL VARIABLE DESCRIPTION
* h      =  thickness                      (in)
* rad    =  radius of curvature            (in)
* m      =  mass at the apex               (lbf.sec**2/in)
* mo     =  arbitrary mass                 (lbf.sec**2/in)
* fs     =  static deflection              (in)
* fo     =  fs/rad                         (in/in)
* v      =  Ø.3       Possion ratio
* g      =  386.4     gravitational constant (in/sec**2)
* pi     =  3.1416    constant
* cof    =  Ø.19      constant
* e      =  Young's modulus                (psi)
* r      =  unit mass of the shell         (lbm/in**3)
* acon   =  constant of system equations
* bcon   =  constant
* ccon   =  constant
* dcon   =  constant
* pm     =  static force due to mass at apex(lbf)
* p      =  excitation force of sinusoidal
*           function                       (lbf)
* ampl   =  amplitude factor for p         constant
* we     =  excitation frequency           (rad/sec)
* ptol   =  total applied force  p + pm    (lbf)
* pcon   =  (p + pm)/(mo *g)               (lbf/lbf)
*
* INTEGER VARIABLE DESCRIPTION
* tmax   =  total number of time intervals  (sec)
*
* INITIAL CONDITIONS (REAL VARIABLES)
* t      =  time                           (sec)
* x(1)   = deflection                      (in)
* x(2)   = velocity                        (in/sec)
* y(1)   = deflection (x(1)/rad)           (in/in)
* y(2)   = velocity (x(2)/rad)             (1/sec)
*
* REAL VARIABLES FOR PLOTTING
* time   =  vector for time intervals      (sec)
* y1     =  deflection                     (in/in)
* y2     =  velocity                       (1/sec)
*
* VARIABLES FOR FAST FOURIER TRANSFORM  (FFT)
*                                                   TYPE
* ns     =  number of samples to be transformed     integer
* nsp    =  vector for total sample points          real
* wf     =  frequency in rad/sec (2*pi*ij/ns)       real
* y1f    =  deflection output after FFT             complex
```

```
* ylre  =  real part of the complex ylf           real
* ylj   =  imaginary part of the complex ylf      real
* ylabs =  magnitude of the complex ylf           real
*
* INTEGER VARIABLES FOR DO LOOPS
* i     =  counter for inputting communication vectors
* j     =  counter for outputting communication vectors
* k     =  counter for integrating the system equations
* iset  =  counter for computting the other half of FFT
* ij    =  counter for outputting vector of length (ns/2 + 1)
*
* FILE NUMBERS AND NAMES
*      File number  Name     Description
*      15           inØ2     Input data for geometrical and material
*                            constants and initial conditions
*      16           outØ2    Output data including plotting
*      17           ylØ2     Output data t, yl, and y2 for IGP plotting
*      18           ylØf     Output data ij, ylre, ylj and ylabs for
*                            IGP plotting
*
*
* VARIABLE TYPES
*
      common h, rad, mo, fs, fo, e, r, acon, bcon, ccon, dcon, p,
     z ampl, we, pm, ptol, pcon
*
      real t, x(2), y(2), c(24), w(2,9), time(256), yl(256), y2(256)
     z, mo, m, ptol, e, r
*
      integer n, ind, nw, ier, k, tmax
*
      complex ylf(256)
      real nsp(256),  wf(256), ylre(256), ylj(256), ylabs(256), wk(1)
      integer ns, iwk(8), ij
      external eqn2, plotØ1, readØ2
*
      data v/Ø.3/, g/386.4/, pi/3.1416/, cof/Ø.19/
*
* OPEN DATA FILES
*
*     open(15, form = 'formatted', mode = 'in', file = 'inØ2'
*    z, carriage = .true., defer = .true.)
      open(16, form = 'formatted', mode = 'out', file = 'outØ2'
     z, carriage = .true., defer = .true.)
      open(17, form = 'formatted', mode = 'out', file = 'ylØ2')
      open(18, form = 'formatted', mode = 'out', file = 'ylØf')
*
* THERE ARE TWO WAYS OF INPUTTING DATA:
*                A.  OPENING FILE 15 (inØ2)
*             OR B.  CALLING SUBROUTINE readØ2
*
* A.  OPENING FILE 15
*     read(15,1ØØ) h, rad, fs, e, r, tmax, t, x(1), x(2)
*     format(5(f1Ø.5, /), /, i3, /, 3(f1Ø.5, /), /,i5, /, 9(f1Ø.5,/))
*     close (15)
*
* OR
* B.  CALLING SUBROUTINE TO INPUT DATA AND ECHØ PRINT CONSTANTS
*          1. GEOMETRICAL CONSTANTS
```

```
*          2. MATERIAL CONSTANTS
*          3. INITIAL CONSTANTS
*          4. COMMUNICATION VECTORS c(1) TO c(9)
*
      call readØ2(h, rad, fs, e, r, tmax, t, x, ind, c, ampl, we)
*
* INTRODUCE NON-DIMENSIONALIZED PARAMETERS
*
      y(1) = x(1)/rad
      y(2) = x(2)/rad
      fo = fs/rad
*
* CALCULATION OF MASS AT THE APEX FROM STATIC FORCE  pm
* ptol = p + pm
*
      pm = 3.Ø *1.414 *pi *cof *e *(h**2.5) *sqrt(fs) /rad
      m = pm/ g
      mo = m
*
* SET CONSTANTS FOR SUBROUTINE SUBPROGRAM
*
      acon = (3.Ø* 1.414* pi* cof* e* (h**2.5))/ (sqrt(rad)* mo* g)
      bcon = m* rad/ (mo* g)
      ccon = 2.Ø* pi* r* h* rad**3.Ø/ (mo* g)
      dcon = (4.Ø* e* h* h)/ (mo* g* sqrt(3.Ø* (1.Ø - v* v)))
*
* OUTPUT INITIAL CONDITIONS
*
      write(6,2ØØ)  t, y(1), y(2)
      write(16,2ØØ) t, y(1), y(2)

2ØØ   format(/, 1Øx, 'INITIAL CONDITIONS:  TIME t = ', f1Ø.6, 5x,
     z'(SEC)', /, 3Øx, ' DEFLECTION y(1) = ', f1Ø.6, 5x, '(IN/IN)',
     z/, 3Øx, ' VELOCITY y(2) = ', f1Ø.6, 5x, '(1/SEC)',//)
*
* OUTPUT HEADING
*
      write(6,215)
      write(16,215)
215   format(/, 11x, 'TIME t(SEC)', 11x, 'DEFLECTION y(1)', 8x,
     z'VELOCITY y(2)')
*
* SET PARAMETERS
*
      n = 2
      nw = 2
      tol = Ø.ØØ1
*
* LOOP TO SET COMMUNICATION VECTORS
*
*     do 5 i = 1, 9
*        c(i) = Ø.Ø
*5      continue
*     c(1) = 1.Ø
*
* LOOP TO EVALUATE SYSTEMS EQUATIONS BY IMSL SUBROUTINE
*
      do 1Ø k = 1,tmax
         tend = float(k)
         call imsl$dverk(n, eqn2, t, y, tend, tol, ind, c, nw, w, ier)
*
```

```
*        CHECK INDICATOR AND ERROR PARAMETER .
*
*        OUTPUT ERROR MESSAGE FOR INTERMEDIATE STAGE
*        IF
*
         if ((ind .lt. Ø) .or. (ier .gt. Ø)) then
            write(6,23Ø)  tol, ind, ier, t
            write(16,23Ø) tol, ind, ier, t
23Ø         format(//, 1Øx, 'ERROR IS FOUND IN INTERMEDIATE STAGES.', /
     z      , 1Øx, 'THE PROGRAM IS TERMINATED.  PLEASE CHECK FOR:', //
     z      , 15x, 'THE TOLERANCE FOR ERROR CONTROL  tol = ', f1Ø.6, /
     z      , 15x, 'THE INDICATOR ind = ', i5, /
     z      , 15x, 'THE ERROR PARAMETER  ier = ', i5, /
     z      , 15x, 'AT TIME  t = ', f1Ø.3)
*
*           EXAMINE COMMUNICATION VECTOR
*
            do 12 j = 1, 24
               write(6,231)  j, c(j)
               write(16,231) j, c(j)
231            format(15x, 'c(', i3, ')=', f1Ø.3)
12          continue
            stop
*
*        ELSE  OUTPUT CURRENT DATA
*
         else
            write(6,22Ø)  t, y(1), y(2)
            write(16,22Ø) t, y(1), y(2)
22Ø         format (1Øx, e12.5, 1Øx, e12.5, 1Øx, e12.5)
*
*           STORE DATA  t, y1 and y2 IN FILE 17 FOR IGP PLOTTING
*
            write(17,221) t, y(1), y(2)
221         format(e12.5, 5x, e12.5, 5x, e12.5)
*
            time(k) = t
            y1(k) = y(1)
            y2(k) = y(2)
         end if
1Ø    continue
*
*     END LOOP
*
* OUTPUT FINAL ERROR PARAMETER AND INDICATOR
*
      write(6,235)  tol, ier, ind, t
      write(16,235) tol, ier, ind, t
235   format(//, 1Øx, 'THE TOLERANCE FOR ERROR CONTROL  tol = ', f1Ø.6,
     z/, 1Øx, 'THE ERROR PARAMETER  ier = ', i5,
     z/, 1Øx, 'THE INDICATOR  ind = ', i5,
     z/, 1Øx, 'AT TIME  t = ', f1Ø.3)
*
* OUTPUT GEOMETRICAL AND MATERIAL CONSTANTS
*
      write(16,24Ø)
24Ø   format(//, 1Øx, 'GEOMETRICAL AND MATERIAL CONSTANTS ARE:')
*
      write(6,25Ø)  h, rad, fs, fo, e, r, acon, bcon, ccon, dcon
     z, pm, m, p, ampl, we, ptol, pcon
```

```
      write(16,250) h, rad, fs, fo, e, r, acon, bcon, ccon, dcon
     z, pm, m, p, ampl, we, ptol, pcon
250   format(/, 15x, 'THICKNESS                h (in) = ', f10.4,/
     z, 15x, 'RADIUS OF CURVATURE rad (in) = ', f10.4, /
     z, 15x, 'STATIC DEFLECTION    fs (in) = ', f10.4, /
     z, 15x, '                  fo (in/in) = ', f10.4, /
     z, 15x, 'YOUNG`S MODULUS      e (psi) = ', e12.5, /
     z, 15x, 'UNIT MASS r  (lbm/in**3)     = ', f10.4, //
     z, 15x, 'CONSTANTS               acon = ', e12.5, /
     z, 15x, '                        bcon = ', e12.5, /
     z, 15x, '                        ccon = ', e12.5, /
     z, 15x, '                        dcon = ', e12.5, //
     z, 15x, 'STATIC LOAD         pm (lbf) =     ', e12.5, /
     z, 15x, 'MASS      m  (lbf.sec**2/in) =     ', f10.4, //
     z, 15x, 'EXCITATION FORCE     p (lbf) =     ', e12.5, /
     z, 15x, 'AMPLITUDE FACTOR     ampl    = ', f10.4, /
     z, 15x, 'EXCITATION FREQ.  we (rad/sec) = ', f10.4, /
     z, 15x, 'TOTAL FORCE       ptol (lbf) = ', e12.5, /
     z, 15x, '              pcon (lbf/lbf) = ', e12.5, /)
*
* EXAMINE COMMUNICATION VECTOR
*
      write(16,255)
255   format(/, 10x, 'COMMUNICATION VECTORS ARE:', /)
      do 15 j = 1, 24
        write(6,260)  j, c(j)
        write(16,260) j, c(j)
260     format(15x, 'c(', i3, ') = ', f10.3)
15    continue
*
* OUTPUT HEADING AND PLOT DEFLECTION VERSUS TIME (y1 vs. time)
* (IN FILE 16)
*

      call plot01(k, time, y1, 16)
      write(16,270)
270   format(/, ' DEFLECTION  y1 (IN/IN) VS. TIME  t (SEC)')
*
* OUTPUT HEADING AND PLOT PHASE PLANE DIAGRAM (y2 vs. y1)
* (IN FILE 16)
*
      call plot01(k, y1, y2, 16)
      write(16,280)
280   format(/, ' PHASE PLANE PLOT  y2 (1/SEC) VS. y1 (IN/IN)')
*
* CALCULATE DISCRETE FOURIER TRANSFORM (DFT)
* BY METHOD OF FAST FOURIER TRANSFORM (FFT)
*
*     COMPUTE FFT OF REAL VALUED SEQUENCE BY IMSL SUBROUTINE FFTRC
*
*     SET PARAMETER AND EVALUATE FFT FROM 0 TO ( ns/2 + 1 )
*
      ns = tmax
      call imsl$fftrc(y1, ns, y1f, iwk, wk)
*
*     COMPUTE THE REMAINING VALUES FROM ( ns/2 + 1 ) TO ns
*     nsd2 = ns/2
*     do 20 iset = 2, nsd2
*        y1f(ns + 2 - iset) = conjg( y1f(iset) )
*20   continue
*
```

```
*
* OUTPUT HEADING AND FFT
*
      write(16,29Ø)
29Ø   format(1h1, /, ' FAST FOURIER TRANSFORM OF y1 :', //
     z, ' SAMPLE NO.', 5x, 'FREQUENCY (rad/sec)', 5x
     z, 'REAL', 11x, 'IMAGINARY', 11x, 'MAGNITUDE', //)
*
* LOOP TO CALCULATE REAL, IMAGINARY AND MAGNITUDE OF THE COMPLEX y1f
*
      do 25 ij = 1, (ns/2.Ø + 1.Ø)
         nsp(ij) = float(ij)
         wf(ij) = 2.Ø * pi * ij/ns
         ylre(ij) = real( y1f(ij) )
         y1j(ij) = aimag( y1f(ij) )
         ylabs(ij) = cabs( y1f(ij) )
*
*        OUTPUT FFT
*
         write(16,3ØØ) nsp(ij), wf(ij), y1f(ij), ylabs(ij)
*        write(6,3ØØ)  nsp(ij), wf(ij), y1f(ij), ylabs(ij)
*3ØØ     format(f7.1, 7x, f8.4, 12x, f1Ø.6, 5x, f1Ø.6, 5x, f1Ø.6)
3ØØ      format (f7.1, 7x, f8.4, 12x, e12.5, 5x, e12.5, 5x, e12.5)
*
*        STORE FFT DATA wf , ylre, y1j, ylabs FOR IGP PLOTTING
*        (IN FILE 18)
*
         write(18,3Ø5)  wf(ij), ylre(ij), y1j(ij), ylabs(ij)
3Ø5      format(f1Ø.5, 5x, e12.5, 5x, e12.5, 5x, e12.5)
*
25    continue
*
* PLOT AMPLITUDE VS. NUMBER OF SAMPLES (nsp)
* (IN FILE 16)
*     call plotØ1(ij, nsp, ylre, 16)
*     write(16,31Ø)
*31Ø  format(/,' FFT:  REAL PART  VS. NUMBER OF SAMPLES')
*
*     call plotØ1(ij, nsp, y1j, 16)
*     write(16,32Ø)
* 2Ø  format(/,' FFT:  IMAGINARY PART  VS. NUMBER OF SAMPLES')
*
      call plotØ1(ij, nsp, ylabs, 16)
      write(16,33Ø)
33Ø   format(/,' FFT:  MAGNITUDE  VS. NUMBER OF SAMPLES')
*
* CLOSE ALL FILES
*
      close(16)
      close(17)
      close(18)
*
* END MAIN PROGRAM
*
      stop
      end
*
*
*
*
```

```
************************************************************************
*
* PROGRAM:      SUBROUTINE FOR DYNAMIC RESPONSE OF SPHERICAL SHELLS
*               eqn2.fortran
*
* PURPOSE:      TO SET INITIAL CONSTANTS AND EVALUATE SYSTEM EQUATIONS
*
* TYPE:         SUBROUTINE
*
* CALL FORMAT:
*
*       call imsl$dverk(n, eqn2, t, y, tend, tol, ind, c, nw, w, ier)
*                          ====
* ARGUMENTS:
*          Type      Description                                Data Flow
*   eqn2   ----      name of subroutine                         in
*   n      integer   number of equations                        in
*   t      real      independent variable                       in/out
*   y      real      dependent variable                         in/out
*   yd     real      dependent variable                         in/out
*
*
************************************************************************
*
* REAL VARIABLE DESCRIPTION
*
* h     = thickness                                  (in)
* rad   = radius of curvature                        (in)
* mo    = arbitrary mass                             (lbf.sec**2/in)
* m     = mass at the apex                           (lbf.sec**2/in)
* fs    = static deflection                          (in)
* fo    = fs/rad                                     (in/in)
* v     = Ø.3          Poisson ratio
* g     = 386.4        gravitational constant        (in/sec**2)
* pi    = 3.14159      constant
* c     = Ø.19         constant
* e     = Young's modulus                            (psi)
* r     = unit mass of the shell                     (lbm/in**3)
* acon  = constant of system equations
* bcon  = constant
* ccon  = constant
* dcon  = constant
* f     = half of the total deflection               (in/in)
* pm    = static force due to mass at the apex       (lbf)
* p     = excitation force of sinusoidal
*         function                                   (lbf)
* ampl  = amplitude factor for p                     constant
* we    = excitation frequency                       (rad/sec)
* ptol  = total force (p + pm)                       (lbf)
* pcon  = (p + pm)/(mo * g)                          (lbf/lbf)
* y(1)  = current value of deflection at time t      (in/in)
* y(2)  = current value of velocity at time t        (1/sec)
* yd(1) = evaluated value of velocity                (1/sec)
* yd(2) = evaluated value of acceleration            (1/sec**2)
*
* VARIABLE TYPES
*
      subroutine eqn2(n, t, y, yd)
      common h, rad, mo, fs, fo, e, r, acon, bcon, ccon, dcon, p,
     z ampl, we, pm, ptol, pcon
```

```
      real y(n), yd(n), t, mo, p, pm, ptol, pcon
      integer n
      data g/386.4/
*
* SET CONSTANT
*
*     acon = (3.Ø *1.414 *pi*cof *e *h**(5.Ø/2.Ø))/(sqrt(rad) *mo *g)
*     bcon = m *rad/(mo *g)
*     ccon = 2.Ø *pi *r *h *rad**3.Ø/(mo *g)
*     dcon = (4.Ø *e *h *h)/(mo *g *sqrt(3.Ø *(1.Ø - v *v)))
*
      p  = ampl *pm *sin(we *t)
      ptol = p + pm
      pcon = ptol/(mo *g)
*
* MAXIMUM DEFLECTION FROM THE APEX  Wmax = 2* f
* HALF OF THE TOTAL DEFLECTION  f
*
      f = fo + y(1)/2.Ø
*
* CHECK IF DEFLECTION y(1) EXCEEDS TWICE OF STATIC DEFLECTION fo
*
*     CLASSIFY DEFLECTION y(1) GREATER THAN -(2. *fo)
*     (i. e.  y(1) + 2 fo > Ø )
*     IF:
*
      if (y(1) .ge. (-2.Ø *fo)) then
         yd(2) = (pcon - acon *sqrt(f) - ccon *y(2) *y(2)/4.Ø)/
     z   (bcon + ccon *f)
         yd(1) = y(2)
*
*        CLASSIFY DEFLECTION y(1) LESS THAN -(2.Ø *fo)
*        (i. e.  y(1) + 2 fo < Ø )
*     ELSE:
*
      else
         yd(2) = (pcon - 2.Ø *dcon *f)/bcon
         yd(1) = y(2)
      end if
*
* RETURN
*
      return
*
* END SUBROUTINE
*
      end
```